PERFORMANCE-BASED CAPACITY AND DEMAND ESTIMATE AND FRAGILITY ANALYSIS OF PRESTRESSED CONCRETE AND REINFORCED CONCRETE NUCLEAR CONTAINMENT PANELS SUBJECT TO MISSILE IMPACT

A Thesis Submitted

In Partial Fulfilment of the Requirements

for the Degree of

DOCTOR OF PHILOSOPHY

by

Jaswanth Gangolu

DEPARTMENT OF CIVIL ENGINEERING

INDIAN INSTITUTE OF TECHNOLOGY GUWAHATI

GUWAHATI – 781039

May 2020

DECLARATION

I hereby declare that work which is being presented in the thesis titled "**Performance-Based Capacity and Demand Estimate and Fragility Analysis of Prestressed Concrete and Reinforced Concrete Nuclear Containment Panels Subject To Missile Impact**", submitted in the fulfilment of the requirements for the award of the degree of DOCTOR OF PHILOSOPHY in CIVIL ENGINEERING, with specialization in STRUCTURAL ENGINEERING, is an authentic record of my own work carried out in the Department of Civil Engineering, Indian Institute of Technology Guwahati under the supervision of Dr. Hrishikesh Sharma, Assistant Professor, Department of Civil Engineering, IIT Guwahati.

The matter embodied in this thesis work has not been submitted by me for the award of any other degree or diploma of this Institute or any other University/Institute.

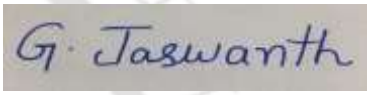

Date: 19/05/2020

Jaswanth Gangolu

CERTIFICATE

It is certified that the work contained in the thesis entitled "**Performance-Based Capacity and Demand Estimate and Fragility Analysis of Prestressed Concrete and Reinforced Concrete Nuclear Containment Panels Subject to Missile Impact**", by **Jaswanth Gangolu** (146104042) has been carried out under my supervision and that this work has not been submitted elsewhere for the award of a degree or diploma.

Date: 19/05/2020

Dr. Hrishikesh Sharma
Assistant Professor
Department of Civil Engineering
Indian Institute of Technology Guwahati

ACKNOWLEDGEMENTS

The satisfaction and euphoria on the successful completion of any task would be incomplete without mentioning the people who made it possible and; whose constant guidance and encouragement crowned my effort with success.

First of all, I would like to express my sincere thanks and heart full gratitude towards my LORD & SAVIOR JESUS CHRIST who died for me on the cross and redeemed me and gave New Life of Salvation. Because of HIS loving-kindness, grace and mercy could able to attain eternal life, freely. He is the one who upholds, encourages, motivates, endorses me every time, even in troubles and difficulties.

Glory to God for giving me such a good, helpful and very talented project guide Dr. Hrishikesh Sharma. Without his co-operation, suggestions and esteemed guidance throughout my project could not be able to execute correctly and may I will be faithful to him throughout my life.

Submitting this thesis would have been an arduous job, without the encouragement, support and suggestions from my mentors and friends. I want to thank them for their wholehearted help in personal and professional life. I want to thank my mentors and supporters, Palathinkal and family, Prakash and family, Sivaram, Venkat, Didi, Reuben, Chandaluri Brother's, Bala. I would also like to deliver my thanks and gratitude to my friends who are like my family members AU Friends, IITG Friends, NGA buddies, Priya, Raji Matha, Tharun Masteru, Mahesh Macha, Pradeep Pedha Siru, Anitha (: P Sneha), Febro, Barri, Saki the cool, Anil Jntuk (=D), Sunil Mama, Kiran J, Sunil JC, Banda Ramana (Sorry Bonu Ramana), Bhagath anna and family, and to my colleagues Suman, Bharath, Anjani, Jhuma, Umesh, Narayana Reddy, for their valuable support.

Especially I sincerely appreciate and share my whole heart thanks to my friends and colleagues Kasturi and Ajay. I'm very grateful to you for your sacrificial help in my research career. Really I didn't expect this much help from you guys. Finally, one word I would like to say, I'll never forget your great help and return you back when the time comes.

At last, I would like to thank my parents, who taught me the value of hard work and moral values. Without them, I'm like chaff. And my younger brother who looks elder than me (: P), and stood by me every time. They have consistently given me enormous support throughout the tenure of my stay at IIT Guwahati.

JASWANTH GANGOLU

ABSTRACT

In the modern world, the majority of structures mainly made up of concrete due to its inexpensiveness and excellent stability. Due to hike in civil engineering structures globally over the years, natural and human-made offensive events increased eventually on these structures. Projectile impacts are one of them and seen in the case of the 9/11 attacks, World war – II, Persian – Gulf war, etc. These attacks greatly affected in the failure of structures, economic decline, nations nobility, losing many human lives, including soldiers and, etc. One of the majorly considered sources for electricity is nuclear power plants. The outer casing of power plants called Nuclear containment structures is primarily made of the two-layered wall structure. Many of the structures are made up of reinforced concrete (RC) wall without rear side steel liner as outer case, and prestressed concrete comprises reinforcement (PC) with a rear side steel liner. Based on past attacks, there is a chance of missile attacks on these structures in the coming days due to anti-social activities. The existing codal provisions are not accurate enough to account for local damage effects due to high dynamic load imposed due to missile impact on Nuclear containment structure. Therefore, there is a need to assess the vulnerability of the structure against such impacts.

This present research aim is to develop a framework for the performance-based analysis and design of the nuclear containment structures subject to missile impact. Current research helps to diminish the damage and provide economical design guidelines. The present study considers into account performance-based analysis and design as opposed to only collapse prevention design. Proposed performance levels are tied to impact levels to estimate the reliability of the containment structure for the desired performance objectives. The performance-based probabilistic models for estimating the capacity of containment structure and demand on containment structure are developed. The fragility (vulnerability) of the

containment structure subject for selected performance levels is evaluated. In addition to performance-based analysis and design, probabilistic formulations are developed for local missile impact effects on containment structures.

Table of Contents

List of Figures

LIST OF TABLES

Chapter 1. INTRODUCTION

1.1. General

Due to efficacy and economic cost, concrete has been extensively used universally by civil engineers and military people for construction purposes (Li *et al.*, 2005). During extreme loading conditions such as collision, the structures are subjected to the very high intensity of loading in a short duration. A collision of two or more bodies in a short duration with high force or shock is defined as impact load. Intentional and unintentional impact collisions on structures have accelerated from the past few decades due to a rapid hike in infrastructure projects (Sharma and Hurlebaus, 2012). Such events are becoming more and more noticeable by the day such as automobile collisions towards barriers and plane crashes and hard impacts like missiles, rockfalls, and debris hitting buildings because of tornadoes (Asplund and Steckmest, 2014) (Daudeville and Malécot, 2011), as shown in Figure 1.1 and Figure 1.2. Crash on easily accessible parts of a structure might drive to damage, and failure of the structure is observed frequently. The response of structures for such extreme loadings differs from static to dynamic due to the inertia effect, change in material behaviour when subject to rapid loading. This phenomenon is noted as the dynamic behaviour of the material under impact loading. The critical parameter is the rapid change in strain, which leads to a significant change in material behaviour. Classification of loadings on engineering structures can be based on the strain rate parameter. Strain rate plays a vital role, mainly in high strain loadings like earthquake, impact, and blast loadings due to their short time interval. The strain rate of impact loading usually varies in between 10^{-4} to 10^{2} per second (Daudeville and Malécot, 2011)(Bischoff and Perry, 1991), as shown in Figure 1.3.

Figure 1.1 (a) Scenario after a missile hit in World War – 2 (b) Iraq Scud Missile impact on Burma Embassy in Israel, 2004 (c) 9/11 aircraft attacks on twin towers (d) Gaza rockets attacks on Israel, 2019

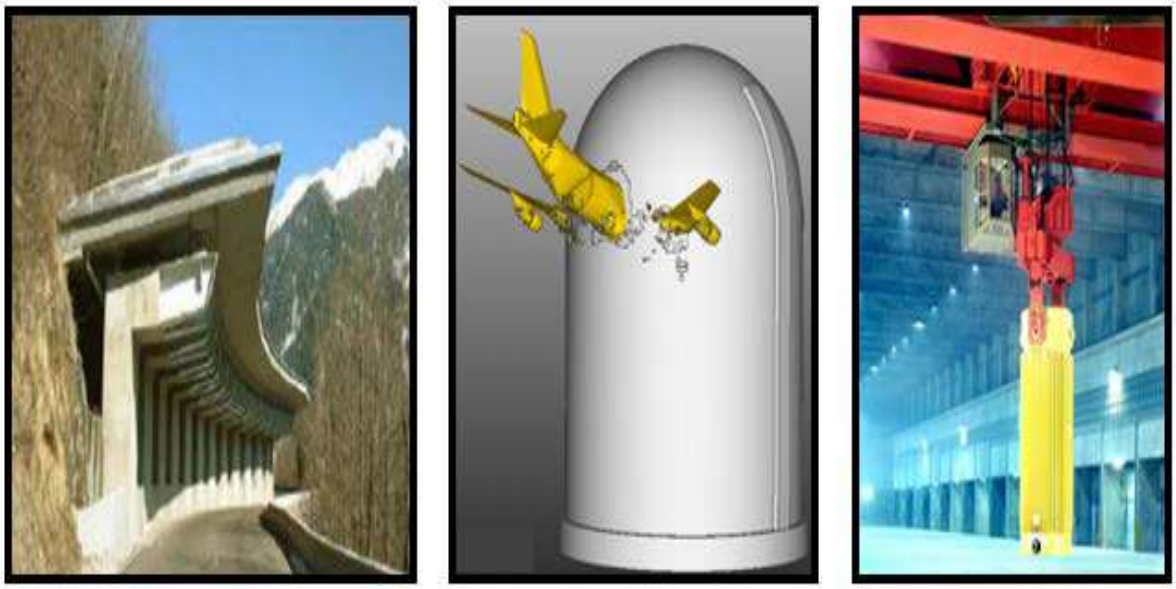

Figure 1.2 Examples of impact loadings on engineering structures (Kaseem 2015)

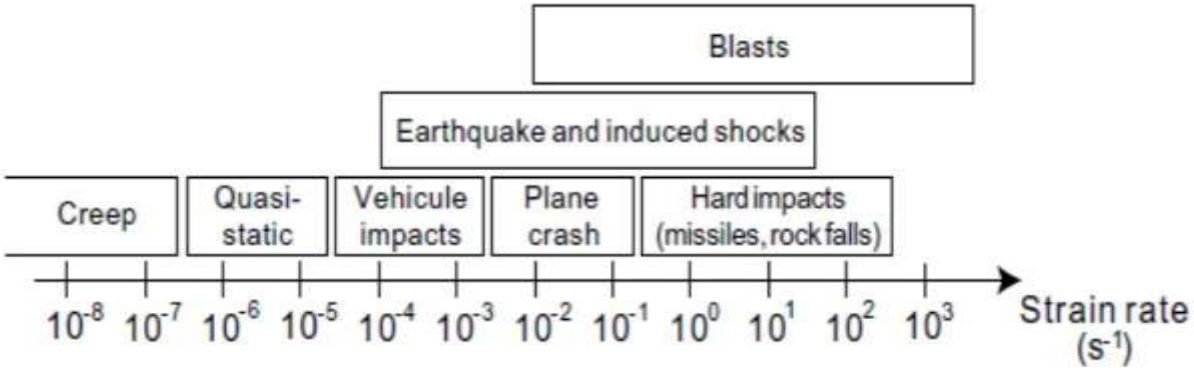

Figure 1.3 Strain rate of various loadings (Bischoff and Perry, 1991)

The structures are being subjected to impact loading due to extreme loading conditions which are human-made as well as natural in nature. Some countries are prone to hefty winds and tornadoes, which result in vehicles falling on the roof of the buildings and generating impact loading. Rockfall impact is often seen, especially at the landslides area, and is one of the significant threats, especially to humankind and defence-related protective structures. Nazi Germany in World War II for the first time, operated a sequence of missiles. September 11 aircraft attacks in USA and Scud (Al Hussein) missile attacks in Iran – Iraq war (1980 – 88) & Persian – Gulf war (1991) marked the extensive use of human-made threats. All these events result in colossal loss of humankind, and damage to buildings like the Pentagon, WTC tower, and US army barracks in Dhahran, Saudi Arabia (1991) (Khaji et al., 2012). These assaults are eye-opening to all the world and attracted research in the area of protective technology extensively. Bridges, skyscrapers, protective structures like Nuclear Power Plant (NPP) containment, bunkers, etc, are some structural members who are most vulnerable to impact loading of missile due to their importance as a paramount target (Sharma et al., 2012) (Zhang et al., 2018). The consequences of a failure of these structures lead to extensive loss of human life as well as maximum disruption. Figure 1.4 details the occurrence of events across the globe.

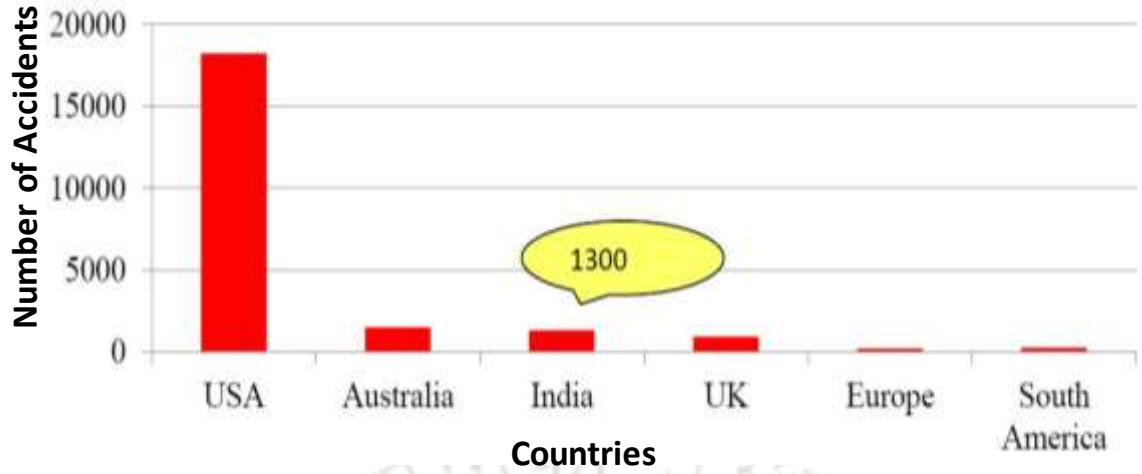

Figure 1.4 Impact and succeeding blast occurrences (1999-2005) (Bangash, 2006)

1.2. Motivation

Based on the severity of a disaster, which results from the damage to protective structures when subject to impact loading, there is an impending need to assess the fragility of structures subject to impact loading. Prediction of effect of missile impact on concrete structures like nuclear containment structures, LNG storage tanks and hardened aircraft shelters, bunkers, etc., becomes of paramount importance when analysed from the backdrop of Section 1.1.

In today's world, with the ever-growing demand for power and ever-decreasing resources, the focus on nuclear energy has increased throughout the world. The number of Nuclear power plants is increasing across the globe. In this context, keeping in view the vulnerability of Nuclear containment structures to missile impact and the disaster that is caused in the aftermath, the current research focuses on studying the effects of missile impact on Nuclear Containment structures and develop design basis provisions for protection against missile impact. This has been kept as a central aim because the loss of precious human lives, uneconomical renovation seriously hampers the functioning capacity of the nation where such catastrophic events occur (Daudeville and Malécot, 2011).

1.3. Existing Studies

Current codal provisions such as illustrated in ASME BPV III and ACI 349-06 literature (Ashar et al., 2013), focusses on static loading only. The impetus to the change in material behaviour due to high strain rate is also restricted in the current design guidelines. The effect of localized damage and thereby adequate design and detailing needs refined analysis which is not dealt with the fullest in the existing design methodologies. The treatment of the existing design guidelines for accounting the inherent uncertainty associated with the missile impact loading, geometric and material uncertainty of concrete structure, and the uncertainty in the interaction of impact loading with the concrete structure is restricted. The design philosophy does not account for the different performance-level associated with the structure and most of the times designed for a single limiting scenario. The details related to Reinforced Concrete (RC) panels and Prestressed Concrete (PC) panels are as follows:

1.3.1. Reinforced Concrete (RC) Panels

- For the design of RC panels, existing empirical formulae for predicting the structural capacity and demand do not conform well with experimental results since the uncertainties involved in the interaction, structural configuration and range of dimensions used for calibration of the many empirical formulae do not conform to realistic scenarios (Reid and Wen, 2001; Wen and Xian, 2015; Kojima 1991).
- Most of the existing formulation is based on laboratory experiments in which due to the inherent restrictions, either lower velocity missile impact with greater missile mass or higher missile velocity with lesser mass was used for the development of formulations. Thereby, the worst-case scenario of hard missile impact on RC structures often does not accurately estimate the performance quantities (Li et al., 2005; Kojima 1991; Kumar et al., 2017; Rajput and Iqbal 2016).

1.3.2. Prestressed Concrete (PC) Panels

- Majority research till now was carried out on thin flat RC panels subject to a hard missile with different nose shapes, but the research on PC panels is minimal.
- Research on PC nuclear containments and LNG storage tanks are almost negligible because of large and complicated configuration with curvature, steel liner at the rear side, and post-tensioning effects, etc., as shown in Figure 1.5.
- Effect of steel liner has not much studied in the literature, (except in Kojima, 1991) which is also on an RC slab.
- Jung et al., 2015 reported that curvature and post-tensioning effect reduces the penetration depth and maximum central displacement by almost 10 % - 30 % which is not accurately accounted in current provisions.

Performance-based design of RC and PC structures which takes into consideration the energy imparted to the system by missile impact and energy absorbed and dissipated by the structural system is not well addressed in any literature on Nuclear containment structures when subject to missile impact. So, the necessity of further research on the development of an accurate formulation for performance-based analysis and design which accounts for local missile impact effects on RC and PC panels subject to missile impact loading becomes imperative.

Figure 1.5 (a) Nuclear Containment Structure, Shin-Wolsong Nuclear Power Unit 2 (b) LNG storage tank

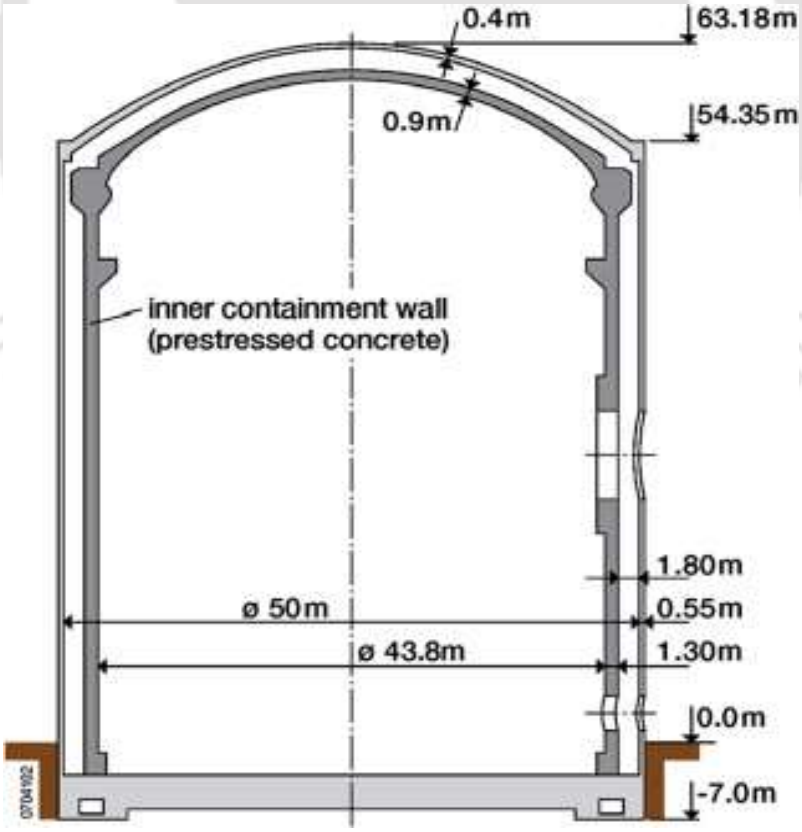

Figure 1.6 Double Layered Containment Wall of Nuclear Power Plants (Sehgal 2011)

1.4. Objectives

The research objective is to develop a framework for performance-based analysis and design of Nuclear Containment Structures subject (Figure 1.6) to missile impact which takes into the inherent uncertainty in the system properties, material and geometric configurations, as well as the interaction of the structure and the missile. The outer wall of Nuclear containment structure is made up of reinforced concrete and the inner wall is made up of reinforced post-tensioning prestress concrete with a steel liner. This framework development will be achieved in the following way:

First of all, three different performance level of the structure will be identified and quantified based on the damage occurring in the RC and PC panels subject to missile impact. These three performance levels will be tied up with four damage states. These performance levels will be deformation based, viz. penetration depth of missile into the target, the residual velocity of a missile, perforation limit of the target. Probabilistic models will be developed to accurately quantify these performance levels, so that the structure can be analysed and as well as designed based on these different performance levels.

After obtaining the performance levels for RC and PC panels, probabilistic capacity models will be developed corresponding to each performance levels. The developed probabilistic capacity models will accurately estimate the capacity of RC or PC panel at the given performance level. The developed capacity models will be based on Energy-based formulation.

Moving ahead with the same approach, the probabilistic demand model will be developed to estimate the demand imposed on RC and PC panel subject to missile impact. The developed demand models will be based on Energy-based formulation.

The developed Performance-based capacity and demand model will have the following advantages, accounting for:

- The multi-modal response of the structure,
- The transition of failure modes and their interaction
- Inherent uncertainty associated with the modelling, configuration and material properties
- The model will be easy to use.
- The model will incorporate the uncertainty in modelling, material properties and configuration.
- The model will account for the increase in strength of material due to the strain rate.
- The model will account for the effect of inertia due to dynamic loading.
- The dynamic capacity of different modes of failure and the interaction will be estimated.

These developed capacity and demand model will be used to analyse the fragility (vulnerability) of any given Nuclear Containment structure subject to missile impact. The same formulation can also be used to designing Nuclear Containment structures made of RC and PC panels subject to missile impact. This procedure provides a performance-based framework for analysis and design of RC and PC panels of Nuclear containment structures subject to missile impact.

The organization of the thesis is presented in the following section.

1.5. Organisation of the Thesis

This thesis is organized into twelve individual chapters. The first chapter gives an introduction to the need of the research, the overview of the current state of the art, objectives to be achieved and their uses. The second chapter presents the state of practice of missile and the effect of impact loading that it causes on concrete structures. The third chapter presents an overview of the Nuclear Power Plant. The fourth chapter illustrates the detailed procedure to

formulate the three different performance levels of the Nuclear Containment Structure and quantify it based on the damage occurring in the RC and PC panels subject to missile impact. The fifth chapter discusses on modelling of RC panels subject to missile impact loading based on Finite element technique and obtains the desired results. The sixth chapter discusses on modelling of PC panels subject to missile impact loading based on Finite element technique and obtains the desired results. The seventh chapter provides experimental design for conducting Finite element analysis. The eighth chapter presents the development of the deformation based probabilistic performance levels, viz. penetration depth of missile into the target, residual velocity of a missile, perforation limit of the target. The ninth chapter details development of probabilistic capacity models for three performance levels of RC panels subject to missile impact. The tenth chapter details the development of probabilistic demand model for missile impact on RC structures and assesses the vulnerability of a given RC structure subject to missile impact. The eleventh chapter details the development of probabilistic capacity models for three performance levels of PC panels subject to missile impact. The twelfth chapter details the development of a probabilistic demand model for missile impact on PC structures and assesses the vulnerability of a given PC structure subject to missile impact. Finally, the thesis ends with conclusions and suggestions on the future scope of research.

Chapter 2. STATE OF PRACTICE FOR MISSILE IMPACT

In this chapter, the definition of impact, missile, types of missile, its interaction with structure, a manifestation of the impact of the missile on a structure in terms of a quantifiable phenomenon is presented.

2.1. Impact Loading

A collision of two or more bodies in a brief moment with high force or shock is traditionally defined as impact (Figure 2.1). Possibilities of missile impact loading on structures are numerous. For example, intentional or unintentional use of aircraft, rockets, jets, and missiles on structures due to technical hurdles or warfare (Findlay and Harrison, 2002), failure of crane cable while lifting massive loads and failure of a reactor pressure vessel and fragments generated, fragments collision in premeditated terrorist bomb blasts and particles hitting due to unexpected detonations, are amongst some of the known events.

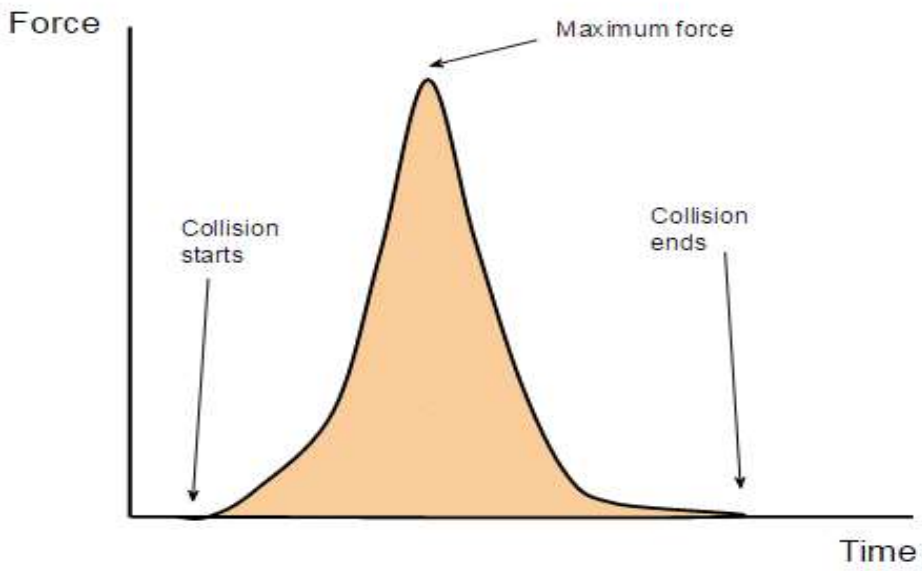

Figure 2.1 Impact Loading, Force vs Time (Jasawanth *et al.*, 2017)

2.2. Configuration of the Missile

A weapon which is self-propelling or guided by remote control, and with or without carrying a nuclear explosive or conventional explosive, is defined as a Missile. Possible missile impact scenarios observed till now are airborne missiles, flying fragments due to tornadoes, fragments due to explosions and debris of pressure vessels due to detonations, etc.

Mach number of a single projectile is classified based on its velocity. Nose cone shape plays a very significant role while a missile is flying in the atmosphere or above. Minimal drag coefficient cone shape is a prime choice for aviation and missile technology. The majority of subsonic aircraft, projectiles, etc. adopt parabolic shape, for example, Boeing 777, Tomahawk missile, and Nirbhay missile. Ogive shape has been adopted by supersonic aircraft, rockets, missiles, etc. such as BrahMos missile, F-15 Eagle fighter, Phoenix missile. In supersonic flow due to the high velocity of a projectile, atmospheric air does not have any prior clue of the approaching vehicle. Shock is resulted due to the first contact of a missile, and pointy tip empowers a decline in shock, which subsequently reduces the drag. Greater penetration could be attained with sharper nose shape due to a pointed tip. Missile velocities are classified into three categories,

- Subsonic Missile: A missile whose Mach number is less than 1
- Supersonic Missile: A missile whose Mach number is between 1 – 5
- Hypersonic Missile: A missile whose Mach number is greater than 5

Nose shape plays a very crucial role while missile travelling in space. Drag depends on the size, nose shape and body shape, and velocity of the object and also on fluid properties. Drag equation given below is used to find drag force. Lesser the drag coefficient is higher the missile velocity of the alike mass.

$$F = C_d \times A \times 0.5 \times r \times V^2 \qquad (2.1)$$

F is a drag force, C_d is the drag coefficient, A is the cross-sectional area of a missile, r is the fluid density, V is the velocity of the missile, given in Figure 2.2 and Figure 2.3.

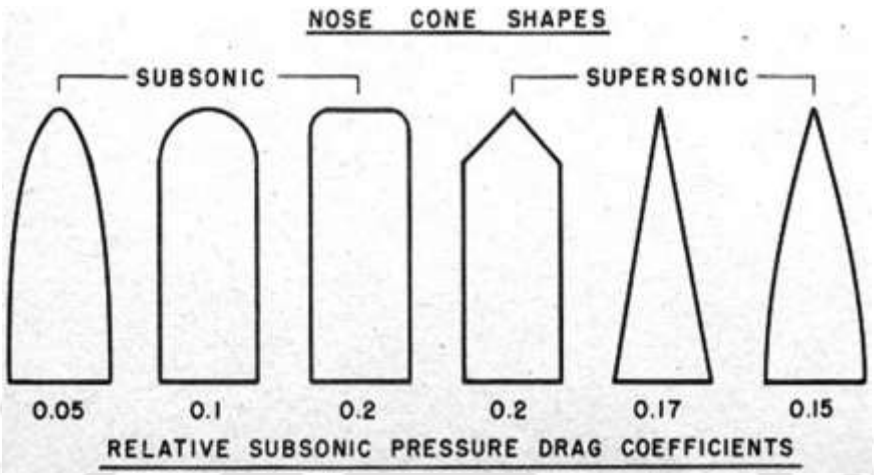

Figure 2.2 Drag coefficients of Missile nose shapes

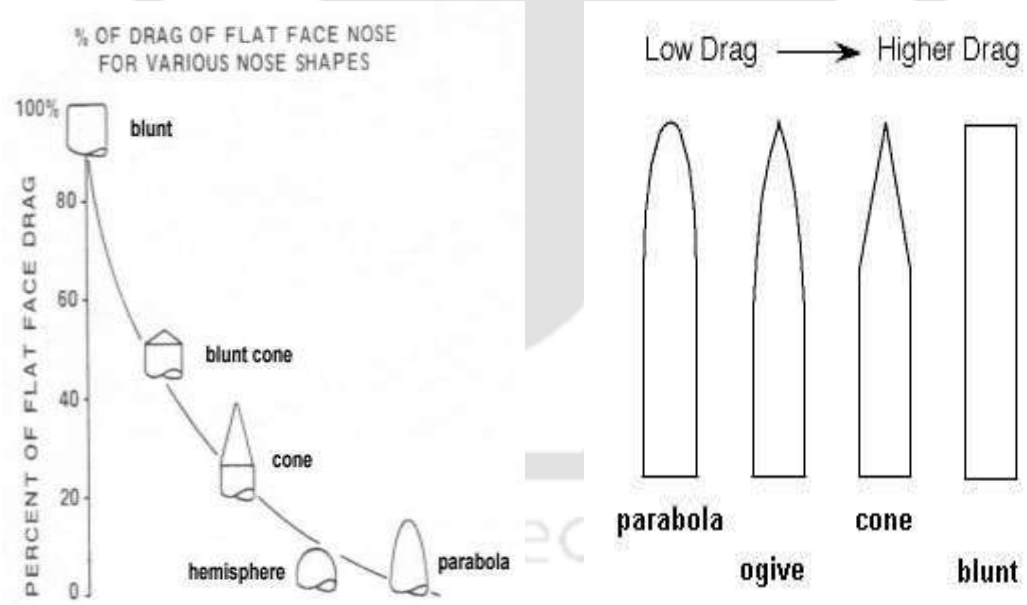

Figure 2.3 Nose Cone Shapes of Missiles

2.3. Types of Missile Impact on Structures

The missile impact on the concrete structure is categorized into hard and soft impact based on the structural configuration of missile and target, interaction amongst each other. This key phenomenon further manifests into a different type of structural behavior which will be discussed in this section.

2.3.1. Classification of Missile Impact Loading

The missile impact loading is classified into two categories based on the stiffness of impactor (Eibl, 1987) (CEB, 1988). *Hard missile impact* is defined as a scenario in which little damage to impactor occurs due to its high rigidity than the target structure. *Soft missile impact* is defined as a scenario in which significant wear and tear of impactor occur than panel structure because of higher target stiffness in comparison to the missile (Daudeville and Malécot, 2011) (Kœchlin and Potapov, 2009) (Figure 2.4). The rigidity aspect of the impactor is a crucial aspect in case of a concrete target subject to impact loading. Impact manifests its effect on the concrete structure in the form of observable phenomenon like penetration, scabbing, and perforation. These phenomena are mostly restricted for hard missile impact because of high impactor rigidity and are called as local missile impact effects. Studies on local missile impact effects on concrete structures have been carried out from the mid of the 1700s (Li *et al.*, 2005). Global displacement of the target occurs in case of soft missile impact and is titled as non-local missile impact effects. Aircraft impact on structures is a classic example of this phenomenon (Li *et al.*, 2005) (Kœchlin and Potapov, 2009) (Daudeville and Malécot, 2011).

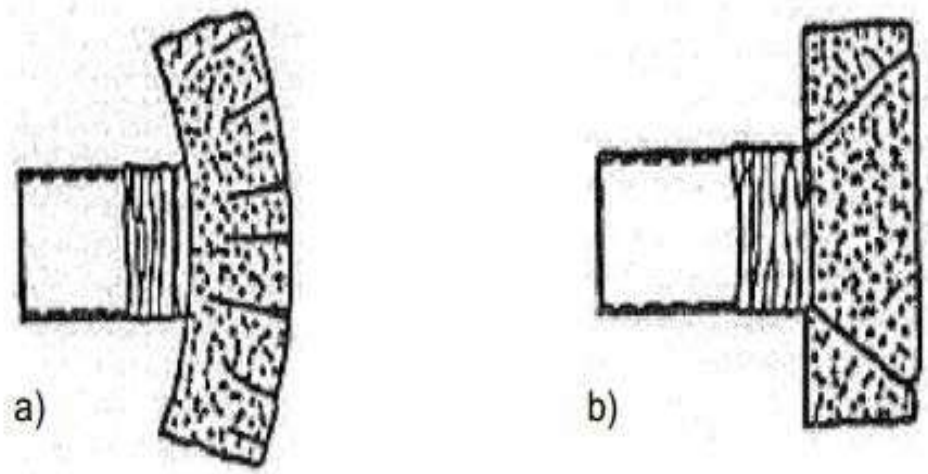

Figure 2.4 (a) Soft Impact of Missile (b) Hard Impact of Missile (Martin, 2010)

2.3.2. Existing Studies of Hard Missile Impact

Most of the current empirical formulae based on experimental and numerical analysis of local impact effects (non-deformable missile effects) on reinforced concrete (RC) panels are well-reviewed and presented in (Kennedy, 1976, Ranjan *et al.*, 2014, Orbovic *et al.*, 2015, Wen and Yang, 2014; Wen and Xian, 2015, Li and Reid, 2004, Forrestal and Hanchak, 2002, Chen and Li, 2002). Experimentation and analysis of hard missile on prestressed concrete (RC) members are presented in (Kumar *et al.*, 2017; Rajput and Iqbal, 2017; Kumar and Mittal, 2018; Iqbal *et al.*, Jiang and Chorzepa, 2015; Johansson and Fredberg, 2015; Schwer, 2016, Sagals *et al.*, 2015; Thai and Kim, 2017). The prestressing effect plays a very crucial role in PC members, the introduction of axial force to tendons leads to lesser displacement, lesser failure cracks and more impact force (Kumar and Mittal, 2018)(Johansson and Fredberg, 2015).

2.3.3. Local Missile Impact Effects on Panels

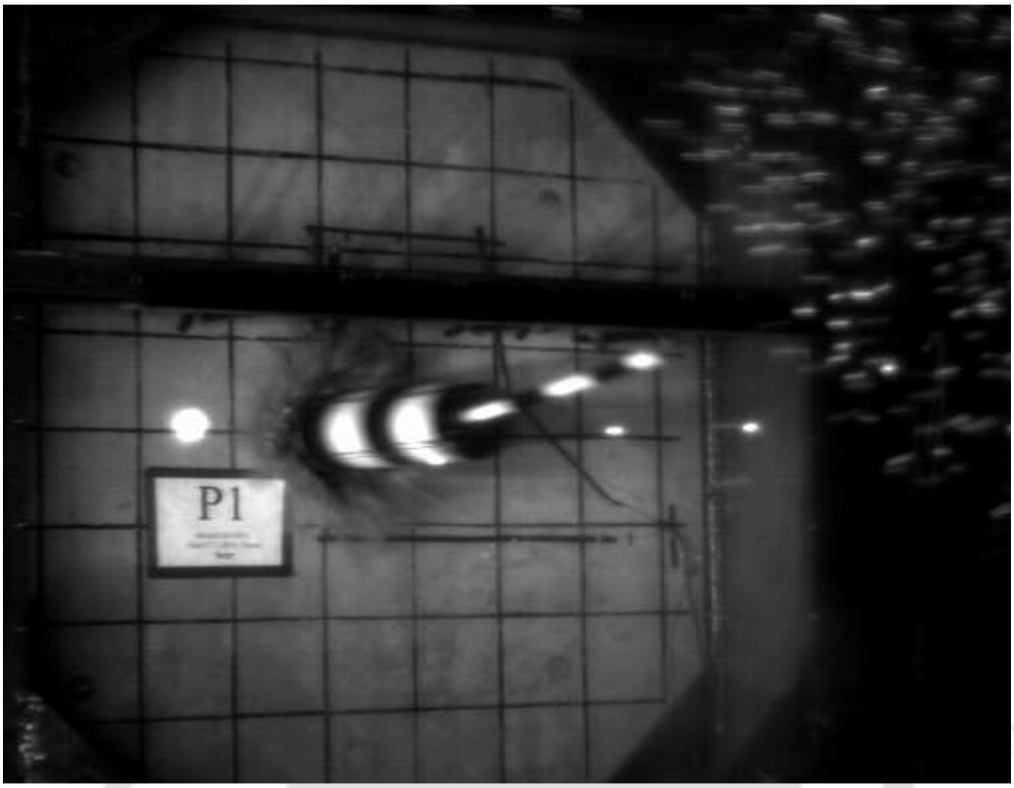

Figure 2.5 Hard Missile Impact upon RC Panel (Orbovic et al., 2015)

The manifestation of the effect of local missile effect (Figure 2.5) on concrete panels is summarized into a quantifiable phenomenon (Figure 2.6) as follows (Li *et al.*, 2005) (Kennedy 1976) (Ranjan *et al.*, 2014) (Fang and Wu, 2017):

- Penetration Depth (x): The depth of missile pierced into a target panel
- Scabbing Limit (h_s): Rear side abrasion of a target due to missile hit upon a panel
- Spalling: Erosion of target on the front side because of projectile impact on the target
- Perforation Limit (h_{per}): Minimum requirement target thickness to cease missile to perforate completely
- Residual Velocity (V_r): Entire piercing of projectile inside the target with or without net velocity
- Deformation of target: Displacement of panel structure with or without minimal erosion, or minor cracks on front face due to projectile impact

- Ballistic Limit (V_{bl}): Least velocity required to penetrate fully into the panel

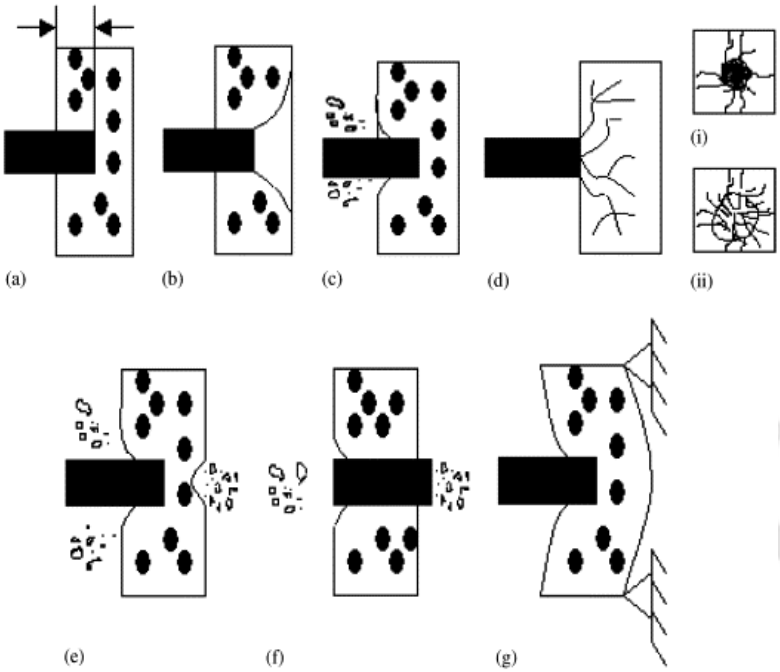

(a) Penetration

(b) Cone cracking

(c) Spalling

(d) Cracks on

(i) proximal face and

(ii) distal face

(e) Scabbing

(f) Perforation

(g) Overall response

Figure 2.6 Local Missile Impact Effects on Concrete Panels (Li *et al.*, 2005)

2.3.4. Existing Studies of Soft Missile Impact

Theoretical derivation of aircraft impact force (deformable missile) is presented in Kar, 1979, Riera, 1980, Bahar and Rice, 1978, Riera, 1968. The experimental analysis is detailed in (Nachtsheim and Stangenberg, 1983; Sugano *et al.*, 1993). The effect of aircraft impacts on prestressed nuclear containments and LNG storage tanks are presented in (Frano and Forasassi 2011; Lee *et al.*, 2013; Zhang *et al.*, 2017). The work is carried out numerically to analyse the phenomenon. In order to understand the effect of projectile impact upon structures, experimental and empirical research is carried on concrete panels by (Orbovic et al., 2015; Nachtsheim and Stangenberg, 1983; Sugano *et al.*, 1993) (Figure 2.7).

Figure 2.7 Aircraft Impact Test on Thick RC Panel (Sugano et al., 1993)

2.4. Empirical Formulation of Effect of Missile Impact on Structures

The following section presents the details of the different empirical formulation for the observed effect on the concrete structure caused by missile impact.

2.4.1. Empirical Formulae of Hard Missile for Penetration Depth and Perforation Limit

1. **Modified Petry formula (1910)** (Samuely and Hamann, 1939)

$$\frac{x}{d} = k.\frac{M}{d^3}.\log_{10}(1+\frac{V_0^2}{19,974}) \quad (2.2)$$

In the former petry formula, k is considered as 6.36E-04 for normal concrete, 3.39E-04 for concrete with reinforcement, and 2.26E-04 for any special type of reinforced concrete. In the modified petry formula, $k = 0.0795k_p$ and k_p is suggested by (Walter and Wolde-Tinsae, 1984) as

$$k_p = 6.34 \text{ X } 10^{-3} \exp(-0.2973 \text{ X } 10^{-7} f_c) \quad (2.3)$$

Amirikian (1950) proposed further for

$$\frac{h_{per}}{d} = 2\frac{x}{d} \quad (2.4)$$

x – Penetration Depth in the Concrete due to Missile Impact, d – Diameter of the Missile, M – Mass of the Missile, V_0 – Velocity of the Missile, f_c – concrete panel's unconfined compressive strength, h_{per} – Perforation Limit of the Concrete Target.

2. **Ballistic Research Laboratory's (BRL) formula (1941)** (Chelapati, Kennedy and Wall, 1972)

$$\frac{x}{d} = \frac{1.33 \text{ X } 10^{-3}}{\sqrt{f_c}} \cdot \left(\frac{M}{d^3}\right) \cdot d^{0.2} \cdot V_0^{1.33} \quad (2.5)$$

$$\frac{h_{per}}{d} = 1.3\frac{x}{d} \quad (2.6)$$

x – Penetration Depth in the Concrete due to Missile Impact, d – Diameter of the Missile, f_c – concrete panel's unconfined compressive strength, M – Mass of the Missile, V_0 – Velocity of the Missile, h_{per} – Perforation Limit of the Concrete Target.

3. **Army corps of engineer formula (ACE) (1946)** (Chelapati, Kennedy and Wall, 1972)

$$\frac{x}{d} = \frac{3.5 \text{ X } 10^{-4}}{\sqrt{f_c}} \cdot \left(\frac{M}{d^3}\right) \cdot d^{0.215} \cdot V_0^{1.5} + 0.5 \quad (2.7)$$

$$\frac{h_{per}}{d} = 1.32 + 1.24\frac{x}{d} \text{ for } 1.35 < \frac{x}{d} < 13.5 \text{ or } 3.0 < \frac{h_{per}}{d} < 18.0 \quad (2.8)$$

For 12.7 mm dia caliber bullets were attained and the perforation for the identical range of validity is modified as

$$\frac{h_{per}}{d} = 1.23 + 1.07\frac{x}{d} \tag{2.9}$$

x – Penetration Depth in the Concrete due to Missile Impact, d – Diameter of the Missile, f_c – concrete panel's unconfined compressive strength, M – Mass of the Missile, V_0 – Velocity of the Missile, h_{per} – Perforation Limit of the Concrete Target.

4. **Modified NDRC formula (1946)** (Kennedy 1976)

$$\begin{cases} \frac{x}{d} = 2.G^{0.5} \text{ for } G \leq 1, \\ \frac{x}{d} = G + 1 \text{ for } G > 1 \end{cases} \tag{2.10}$$

In which,

$$G = 3.8\ X\ 10^{-5}\frac{N\,.\,M}{d\sqrt{f_c}}\left(\frac{V_0}{d}\right)^{1.8} \tag{2.11}$$

Projectile nose shape factor, N for flat – 0.72, hemispherical – 0.84, blunt – 1.0 and very sharp projectile nose – 1.14, respectively

$$\frac{h_{per}}{d} = 1.32 + 1.24\frac{x}{d} \quad \text{for } 1.35 < \frac{x}{d} < 13.5 \text{ or } 3.0 < \frac{h_{per}}{d} < 18.0 \tag{2.12}$$

$$\frac{h_{per}}{d} = 3.19\frac{x}{d} - 0.718\left(\frac{x}{d}\right)^2 \text{ for } \frac{x}{d} \leq 1.35 \text{ or } \frac{h_{per}}{d} < 3 \tag{2.13}$$

x – Penetration Depth in the Concrete due to Missile Impact, d – Diameter of the Missile, f_c – concrete panel's unconfined compressive strength, M – Mass of the Missile, V_0 – Velocity of the Missile, h_{per} – Perforation Limit of the Concrete Target.

5. **Ammann and Whitney formula (1976)** (Kennedy 1976)

Penetration due to high-velocity fragments due to explosions (V_0> 300 $^{m}/_{s}$)

$$\frac{x}{d} = \frac{6\ X\ 10^{-4}}{\sqrt{f_c}}.N.\left(\frac{M}{d^3}\right).d^{0.2}.V_0^{1.8} \tag{2.14}$$

x – Penetration Depth in the Concrete due to Missile Impact, d – Diameter of the Missile, f_c – concrete panel's unconfined compressive strength, N – Projectile Nose Geometry Factor, M – Mass of the Missile, V_0 – Velocity of the Missile, h_{per} – Perforation Limit of the Concrete Target.

6. **Whiffen formula (1943)**

This formula is proposed by British Road Research Laboratory as

$$\frac{x}{d} = \left(\frac{2.61}{\sqrt{f_c}}\right).\left(\frac{M}{d^3}\right).\left(\frac{d}{a}\right)^{0.1}.\left(\frac{V_0}{533.4}\right)^{n} \text{ with } n = \frac{97.51}{\sqrt[4]{f_c}} \tag{2.15}$$

The range of application for this formula is $12.7 < d < 965.2$ mm, $0.136 < M < 9979.2$ kg, $5.52 < f_c < 68.95$ MPa, $0 < V_0 < 1127.8$ m/s, $0.5 < d/a < 50$. where 'a' is the coarse aggregate maximum size in concrete.

x – Penetration Depth in the Concrete due to Missile Impact, d – Diameter of the Missile, f_c – concrete panel's unconfined compressive strength, M – Mass of the Missile, V_0 – Velocity of the Missile, h_{per} – Perforation Limit of the Concrete Target.

7. **Kar formula (1978)**

The motive of Kar formula is to protect nuclear power plants subject to projectile with various materials. NDRC formula is based for the proposal of Kar formula

$$\begin{cases} \frac{x}{d} = 2.G^{0.5} \text{ for } G \leq 1 \text{ and} \\ \frac{x}{d} = G + 1 \text{ for } G > 1 \end{cases} \tag{2.16}$$

Where,

$$G = \frac{3.8\,X10^{-5}.N.M}{d.\sqrt{f_c}}.\left(\frac{V_0}{d}\right)^{1.8}.\left(\frac{E}{E_s}\right)^{1.25} \tag{2.17}$$

$$\begin{cases} h_{per} - a_d = 1.32d + 1.24x \text{ for } 1.35 < \frac{x}{d} \leq 13.5 \\ \frac{h_{per} - a_d}{d} = 3.19\left(\frac{x}{d}\right) - 0.718\left(\frac{x}{d}\right)^2 \text{ for } \frac{x}{d} \leq 1.35 \end{cases} \quad (2.18)$$

where a_d represents 50% of the size of coarse aggregate, E and E_s are projectile's young's modulus and steel's young's modulus, respectively. x – Penetration Depth in the Concrete due to Missile Impact, d – Diameter of the Missile, N – Projectile Nose Geometry Factor, f_c – concrete panel's unconfined compressive strength, M – Mass of the Missile, V_0 – Velocity of the Missile, h_{per} – Perforation Limit of the Concrete Target.

8. **CEA–EDF perforation formula (1974)**

Commissariat àl' Enerfie Atomoque-Electricité de France (CEA-EDF) given that

$$\frac{h_{per}}{d} = 0.82 \frac{M^{0.5} {V_0}^{0.75}}{\rho_0^{0.125} f_c^{0.375} d^{1.5}} \quad (2.19)$$

The application ranges are V_0< 200m/s, 23 MPa<f_c<46 MPa; 20 kg<M<300 kg, 0.35 < H/d < 4.17, ρ_0 is targets density in kg/m^3, h_{per} – Perforation Limit of the Concrete Target, d – Diameter of the Missile, f_c – concrete panel's unconfined compressive strength, M – Mass of the Missile, V_0 – Velocity of the Missile.

9. **UKAEA formula (1990)**

$$\begin{cases} \frac{x}{d} = 0.275 - [0.0756 - G]^2 \text{ for } G \leq 0.0726 \\ \frac{x}{d} = [4G - 0.242]^{0.5} \; for \; 0.0726 < G < 1.065 \\ \frac{x}{d} = G + 0.9395 \text{ for } G \geq 1.065 \end{cases} \quad (2.20)$$

$$\text{where } G = 3.8 \text{ X } 10^{-5} \frac{N.M}{d.\sqrt{f_c}} . \left(\frac{V_0}{d}\right)^{1.8} \quad (2.21)$$

This application ranges in between 29m/s<V_0<238m/s, 26MPa<f_c<44MPa, 3000 kg/m^3 <M/d^3< 222,200 kg/m^3.

x – Penetration Depth in the Concrete due to Missile Impact, d – Diameter of the Missile, f_c – concrete panel's unconfined compressive strength, M – Mass of the Missile, V_0 – Velocity of the Missile, h_{per} – Perforation Limit of the Concrete Target.

10. **Haldar–Hamieh formula (1984)**

$$\begin{cases} \frac{x}{d} = -0.0308 + 0.225I \text{ when } 0.3 \leq I \leq 4.0 \\ \frac{x}{d} = 0.6740 + 0.0567I \text{ when } 4 \leq I \leq 21 \\ \frac{x}{d} = 1.1875 + 0.0299I \; 21 \leq I \leq 455 \end{cases} \quad (2.22)$$

Where impact factor I_a,

$$I_a = \frac{N.M.V_0^2}{d^3.f_c} \quad (2.23)$$

x – Penetration Depth in the Concrete due to Missile Impact, d – Diameter of the Missile, N – Projectile Nose Geometry Factor, f_c – concrete panel's unconfined compressive strength, M – Mass of the Missile, V_0 – Velocity of the Missile, h_{per} – Perforation Limit of the Concrete Target.

11. **Adeli–Amin formula (1985)**

Haldar and Hamieh defined impact factor I_a and was adopted by this formula to fit the data collections on penetration, perforation, and scabbing.

$$\begin{cases} \frac{x}{d} = 0.0416 + 0.1698I - 0.0045I^2 \text{ for } 0.3 \leq I \leq 4 \\ \frac{x}{d} = 0.0123 + 0.1960I - 0.008I^2 + 0.001I^3 \text{ for } 4 \leq I \leq 21 \end{cases} \quad (2.24)$$

$$\frac{h_{per}}{d} = 1.8685 + 0.4035I - 0.0114I^2 \text{ for } 0.3 \leq I \leq 21 \quad (2.25)$$

The range of application for Adeli–Amin formula is: 0.7 < H/d < 18, 0.11 < M < 343 kg, 27 < V_0 < 312 m/s and $\frac{x}{d} < 2$

x – Penetration Depth in the Concrete due to Missile Impact, d – Diameter of the Missile, N – Projectile Nose Geometry Factor, f_c – concrete panel's unconfined compressive strength, M – Mass of the Missile, V_0 – Velocity of the Missile, h_{per} – Perforation Limit of the Concrete Target, H – Thickness of the Target.

12. **Hughes formula (1984)**

$$\frac{x}{d} = 0.19 \frac{N_h . I_h}{S_h} \tag{2.26}$$

Where N_h is a missile nose shape factor, i.e. for flat – 1.0, blunt – 1.12, spherical – 1.26 and very sharp noses – 1.39, respectively. Similarly like Haldar–Hamieh formula, by introducing an impact factor I_h as,

$$I_h = \frac{M . V_0^2}{d^3 f_t} \tag{2.27}$$

$$S_h = 1.0 + 12.3 \ln(1 + 0.03 I_h) \tag{2.28}$$

Where, f_t is the tensile strength of a concrete target

And the perforation limit is predicted as

$$\begin{cases} \frac{h_{per}}{d} = 3.6 \frac{x}{d} \text{ for } \frac{x}{d} < 0.7, \\ \frac{h_{per}}{d} = 1.58 d + 1.4 \text{ for } \frac{x}{d} \geq 0.7 \end{cases} \tag{2.29}$$

x – Penetration Depth in the Concrete due to Missile Impact, d – Diameter of the Missile, N – Projectile Nose Geometry Factor, f_t – Concrete Panel's Tensile strength, M – Mass of the Missile, V_0 – Velocity of the Missile, h_{per} – Perforation Limit of the Concrete Target, H – Thickness of the Target.

13. **Healey and Weissman formula** (Bangash 1989)

This formula is more likely as NDRC formula and Kar formula and proposed as

$$\begin{cases} \frac{x}{d} = 2G^{0.5} \text{ for } G \leq 1 \\ \frac{x}{d} = G + 1 \text{ for } G > 1 \end{cases} \quad (2.30)$$

Where,

$$G = 4.36 \times 10^{-5}.\left(\frac{E}{E_S}\right).\frac{N.M}{d.\sqrt{f_c}}.\left(\frac{V_0}{d}\right)^{1.8} \quad (2.31)$$

x – Penetration Depth in the Concrete due to Missile Impact, d – Diameter of the Missile, N – Projectile Nose Geometry Factor, f_c – Concrete Panel's Unconfined Compressive strength, M – Mass of the Missile, V_0 – Velocity of the Missile, h_{per} – Perforation Limit of the Concrete Target, H – Thickness of the Target, E and E_s are projectile's young's modulus and steel's young's modulus.

14. **IRS Formula** (Bangash 1993)

$$x = 3703.376f_c^{-0.5} + 82.15f_c^{-0.18}\exp(-0.104f_c^{0.18}) \quad (2.32)$$

Minimum shield thickness is given for complete protection of target for penetration, perforation, and scabbing is

$$H_{min} = 3913.119.f_c^{-0.5} + 132.409.f_c^{-0.18}\exp(-0.104f_c^{0.18}) \quad (2.33)$$

x – Penetration Depth in the Concrete due to Missile Impact, f_c – Concrete Panel's Unconfined Compressive strength, H_{min} – Minimum Thickness of the Target.

15. **CRIEPI Formula** (Kojima, 1991)

The Central Research Institute of Electric Power Industry (CRIEPI) proposed as

$$\frac{x}{d} = \frac{0.0265.N.M.d^{0.2}.V_0^2(114 - 6.83 \times 10^{-4}.f_c^{2/3})}{f_c^{2/3}}.\frac{(d + 1.25H_r)H_r}{(d + 1.25H)H} \quad (2.34)$$

$$\frac{h_{per}}{d} = 0.9\left(\frac{61}{V_0}\right)^{0.13}\left(\frac{M.V_0^2}{d^3.f_c}\right)^{0.5} \quad (2.35)$$

where H_r = 0.2 m is the reference thickness of the concrete slab, x – Penetration Depth in the Concrete due to Missile Impact, d – Diameter of the Missile, N – Projectile Nose Geometry Factor, f_c – Concrete Panel's Unconfined Compressive strength, M – Mass of the Missile, V_0 – Velocity of the Missile, h_{per} – Perforation Limit of the Concrete Target, H – Thickness of the Target.

16. **TM 5-855-1 Formula (TM 5-855-1 1986)**

Fragment formation due to explosion, the depth of penetration is given as

$$x = \begin{cases} \dfrac{0.027.M^{0.37}.V_0^{0.9}}{f_c^{0.25}} & \text{for } V_0 \le V_0^* \\ \dfrac{0.004.M^{0.4}.V_0^{1.8}}{f_c^{0.5}} + 0.395.M^{0.33} & \text{for } V_0 > V_0^* \end{cases} \quad (2.36)$$

$$h_{per} = 0.0311.M^{0.033} + 2.95.M^{0.33} \quad (2.37)$$

x – Penetration Depth in the Concrete due to Missile Impact, f_c – Concrete Panel's Unconfined Compressive strength, M – Mass of the Missile, V_0 – Velocity of the Missile, h_{per} – Perforation Limit of the Concrete Target, H – Thickness of the Target.

17. **UMIST Formula** (Li *et al.*, 2005)

$$\frac{x}{d} = \left(\frac{2}{\pi}\right)\frac{N.M.V_0^2}{0.72.\sigma_t.d^3} \quad (2.38)$$

$$\sigma_t(MPa) = 4.2f_c(MPa) + 135 + [0.014f_c(MPa) + 0.45]V_0\left(\frac{m}{s}\right) \quad (2.39)$$

where the application ranges are $50mm < d \le 600mm, 35kg \le M \le 2500kg, x/d \le 2.5$ and $3m/s < V_0 < 66.2m/s$

(i) For, $H/d < 5$

$$\begin{cases} \dfrac{h_{per}}{£\sigma_t d^3} = -0.00506\left(\dfrac{H}{d}\right) + 0.01506\left(\dfrac{H}{d}\right)^2 & \text{for } 0 < \dfrac{H}{d} \leq 1 \\ \dfrac{h_{per}}{£\sigma_t d^3} = -0.01\left(\dfrac{H}{d}\right) + 0.02\left(\dfrac{H}{d}\right)^3 & \text{for } 1 \leq \dfrac{H}{d} \leq 5 \end{cases} \quad (2.40)$$

$$£ = \begin{cases} 0.5 + \dfrac{3}{8}\left(\dfrac{d}{c_r}\right).r_t \text{ for } \dfrac{d}{c_r} < \sqrt{\dfrac{d}{d_r}} \\ 0.5 + \dfrac{3}{8}\sqrt{\dfrac{d}{d_r}}.r_t \text{ for } \dfrac{d}{c_r} \geq \sqrt{\dfrac{d}{d_r}} \end{cases} \quad (2.41)$$

However, the total bending rebar ratio is $r_t = 4r$ and $r = \dfrac{\pi {d_r}^2}{4Hc_r}$

(ii) For $^{H}/_{d} \geq 5$

$$\frac{h_{per}}{\sigma_t d^3} = \frac{\pi}{4}\left[\frac{H}{d} - 3.0\right] \quad (2.42)$$

c_r, and d_r represent the spacing between reinforcement and diameter of reinforcement, respectively. x – Penetration Depth in the Concrete due to Missile Impact, d – Diameter of the Missile, N – Projectile Nose Geometry Factor, f_c – Concrete Panel's Unconfined Compressive strength, M – Mass of the Missile, V_0 – Velocity of the Missile, h_{per} – Perforation Limit of the Concrete Target, H – Thickness of the Target.

18. **Wen Formula**

Based on the UMIST formula, (Wen & Xian, 2015; Wen & Yang, 2014) expressed a unified approach for determining the terminal ballistic performance of missiles as

$$\frac{x}{d} = \left(\frac{2}{\pi}\right)\frac{M.V_0^2}{\sigma.d^3} \quad (2.43)$$

$$\sigma = \left(\alpha' + \beta'\sqrt{\frac{\rho_0}{Y}}V_0\right)Y \quad (2.44)$$

$$Y = \begin{cases} 1.4f_c + 45 \ \text{ for } \ f_c \leq 75\text{MPa} \\ 150 \ \text{ for } \ 75\text{MPa} < f_c < 150\text{MPa} \\ f_c \ \text{for} \ f_c \geq 150\text{MPa} \end{cases} \quad (2.45)$$

(i) For the thin target

$$\begin{cases} \frac{h_{per}}{\emptyset' £ \sigma d^3} = 0.0048\left(\frac{H}{d}\right) + 0.0018\left(\frac{H}{d}\right)^2 \ \text{for} \ 0 < \frac{H}{d} \leq 1.3 \\ \frac{h_{per}}{\emptyset' £ \sigma d^3} = 0.0048\left(\frac{H}{d}\right) + 0.0018\left(\frac{H}{d}\right)^2 \ \text{for} \ 1.3 < \frac{H}{d} < 4 \end{cases} \quad (2.46)$$

(ii) For the thick target

$$\frac{h_{per}}{\sigma d^3} = \begin{cases} \frac{\pi}{4}\left(\frac{H}{d} - 3.0\right) \ \text{for} \ \frac{H}{d} \geq 4, V_0 < 300\text{m/s} \\ \frac{\pi}{4}\left(\frac{H}{d} - 2.0\right) \ \text{for} \ \frac{H}{d} \geq 4, V_0 < 300\text{m/s} \end{cases} \quad (2.47)$$

where α', β' and $\emptyset'$ are dependent on missile nose shape. £ is related to projectile-nose geometry and the arrangement of reinforcement. x – Penetration Depth in the Concrete due to Missile Impact, d – Diameter of the Missile, f_c – Concrete Panel's Unconfined Compressive strength, M – Mass of the Missile, V_0 – Velocity of the Missile, h_{per} – Perforation Limit of the Concrete Target, H – Thickness of the Target. The detailed expressions of parameters are given in (Wen & Xian, 2015; Wen & Yang, 2014).

19. **Berezan Formula**

$$\frac{x}{d} = \lambda . \frac{M}{10^5 . d^3} . V_0 . \cos\alpha \quad (2.48)$$

Where λ is the resistance coefficient (Gabi, Tov and Anatoly, 2013) for various targets, and α is the angle between the normal to the target surface and the impact direction. . x – Penetration Depth in the Concrete due to Missile Impact, d – Diameter of the Missile, M – Mass of the Missile, V_0 – Velocity of the Missile.

2.4.2. Empirical Formulae for Residual velocity (V_r) and Ballistic Limit (V_{bl})

1. Chen's Model

(Chen *et al.*, 2008) gave the formula to forecast the projectile's residual velocity V_r as

$$V_r = (V_o - V_{bl}), \text{for } \frac{H}{d} \leq \chi_c \tag{2.49}$$

$$V_r = \sqrt{V_o^2 - V_{bl}{}^2}, \text{for } \frac{H}{d} > \chi_c$$

where V_o is velocity of the missile, V_{bl} is the ballistic limit of a missile, H is the thickness of concrete targets, d is the diameter of projectile, and χ_c is a dimensionless critical thickness of concrete slabs with the following expression as,

$$\chi_c = \frac{\sqrt{1 + S.\tan\emptyset * \sqrt{3}} - 1}{2.\tan\emptyset} + k \tag{2.50}$$

$$S = 72.\left(\frac{f_c}{10^6}\right)^{-0.5} \text{ or } S = 82.6.\left(\frac{f_c}{10^6}\right)^{-0.544} \tag{2.51}$$

where $k = 0.707 + l_0/d$ is a dimensionless parameter, l_0 is the length of the missile nose, and f_c is the compressive strength of concrete targets, $\emptyset$ - cone slope angle of the rear crater and Ballistic limit (V_{bl}) is calculated as,

$$V_{bl} = \left(\frac{H}{d} - H_{cr}\right) * \sqrt{\frac{\pi * S * d^3 * f_c}{4.k.M}}, \text{for } \frac{H}{d} \leq \chi_c \tag{2.52}$$

$$V_{bl} = \left(\frac{H}{d} - \chi_c + \frac{k}{2}\right) * \sqrt{\frac{\pi * S * d^3 * f_c}{2M}}, \text{for } \frac{H}{d} > \chi_c \tag{2.53}$$

where H – Thickness of the Target, M – the mass of the projectile and H_{cr} – the height of the rear crater.

$$H_{cr} = \frac{\left(\sqrt{(1+(\frac{S\sqrt{3}}{4k}))^2 + (\frac{\sqrt{3}SH\tan\emptyset}{kd})}\right) - (1+\frac{S\sqrt{3}}{4k})}{2\tan\emptyset} \text{ for } \frac{H}{d} \leq \chi_c \quad (2.54)$$

$$H_{cr} = \frac{\sqrt{1+\sqrt{3}S\tan\emptyset} - 1}{2\tan\emptyset} \text{ for } \frac{H}{d} > \chi_c \quad (2.55)$$

2. Grisaro and Dancygier's model

(Grisaro and Dancygier, 2014) residual velocity is obtained using an energy balance approach (Fang and Wu, 2017).

$$\frac{V_r}{V_o} = \sqrt{1 - \left(\frac{V_{bl}}{V_o}\right)^2 - \left(\frac{V_{bl}}{V_o}\right)^{2\propto_1} - \left(\frac{V_{bl}}{V_o}\right)^{2\beta_1}} \quad (2.56)$$

Where, $\propto_1$ = 0.9 and β_1 = 1.6 and these coefficients are obtained empirically by fitting the obtained experimental results by (Hanchak *et al.*, 1992).

Ballistic limit V_{bl} is determined according to the NDRC model is (NDRC 1946)

$$V_{bl} = 59.53 \text{ X } 1000.\, d.\left(\frac{d.\, G(H)}{K.\, N.\, M}\right)^{\frac{1}{1.8}} \quad (2.57)$$

$$K = \frac{14.95}{\sqrt{\frac{f_c}{10^6}}} \quad (2.58)$$

where projectile nose geometry factor, N for flat – 0.72, hemispherical – 0.84, blunt – 1.0 and very sharp projectile nose – 1.14, respectively

$$G(H) = 0.25 * \left(\frac{h_{per}}{d}\right)^2, \text{for} \frac{h_{per}}{d} \leq 2 \quad (2.59)$$

$$G(H) = \frac{h_{per}}{d} - 1, \text{for} \frac{h_{per}}{d} > 2 \quad (2.60)$$

Where

$$\frac{h_{per}}{d} = 2.214 - \sqrt{4.9348 - 1.3928\frac{H}{d}}, \text{for } \frac{H}{d} \leq 3 \tag{2.61}$$

$$\frac{h_{per}}{d} = 0.8065\frac{H}{d} - 1.0645, \text{for } 3 < \frac{H}{d} < 18.06 \tag{2.62}$$

V_r – Residual Velocity of the Missile, V_0 - Velocity of the Missile, V_{bl} – Ballistic Limit of the Missile, d – diameter of the missile, h_{per} – Perforation Limit of the Target, H – Thickness of the Target, f_c – Unconfined Compressive of Concrete.

3. Fang and Wu Model (2017)

A very recent formula for residual velocity published in (Fang and Wu, 2017)

$$V_r = \sqrt{\frac{Sf_c d^3 I_r}{M}} \tag{2.63}$$

$$I_r = \frac{I_o - I_{BL}}{1 + \frac{\eta^2 \rho_o \Omega}{M}} \tag{2.64}$$

$$\Omega = \frac{\pi H_{cr}}{12}(4\tan^2 \emptyset H_{cr}^2 + 6d\tan\emptyset H_{cr} + 3d^2) \tag{2.65}$$

$\emptyset = 65.3^o, \eta = 0.2$

$$I_o = \frac{MV_o^2}{Sf_c d^3}, S = 82.6 * (\frac{f_c}{10^6})^{-0.544} \tag{2.66}$$

$$I_{BL} = \frac{\pi d}{4l_o}(\frac{H}{2d} + \frac{l_0}{2d}\frac{H}{5d})^2, \text{for } H \leq \frac{10l_0}{5d + l_0} \tag{2.67}$$

$$I_{BL} = \frac{\pi}{2}\left(\frac{H}{2d} - \frac{l_0}{2d} + \frac{l_0}{2d}\frac{H}{5d}\right) \text{for } \frac{10l_0}{5d + l_0} < \frac{H}{d} \leq 5 \tag{2.68}$$

$$H_{cr} = 0.5H \text{ for } H \leq 5d \tag{2.69}$$

$$H_{cr} = 2.5d \text{ for } H > 5d \tag{2.70}$$

Where lo = Projectile nose length. V_r – Residual Velocity of the Missile, V_0 - Velocity of the Missile, d – diameter of the missile, h_{per} – Perforation Limit of the Target, H – Thickness of the Target, f_c – Unconfined Compressive of Concrete.

4. Amde's Model (Amde *et al.*, 1997)

$$V_r = V_0\sqrt{1 - (0.5\,{}^{H}/_{x})} \tag{2.71}$$

where H is the thickness of the concrete target, respectively, x is obtained from the modified petry formula.

5. CEA-EDF Formula

Ballistic limit of CEA – EDF formula for circular cross-section is given as

$$V_{bl} = 1.3\rho_0^{1/6} f_c^{0.5} \left(\frac{d.H^2}{M}\right)^{2/3} \tag{2.72}$$

For non-circular cross sections and reinforced concrete targets proposed as,

$$V_{bl} = 1.3\rho_0^{1/6} f_c^{0.5} \left(\frac{pH^2}{\pi M}\right)^{2/3} (r + 0.3)^{0.5} \tag{2.73}$$

where p is the perimeter of the missile cross-section, and r represents the rebar ratio. V_r – Residual Velocity of the Missile, V_0 - Velocity of the Missile, d – diameter of the missile, h_{per} – Perforation Limit of the Target, H – Thickness of the Target, f_c – Unconfined Compressive of Concrete, M – Mass of the Missile.

6. UK Atomic Energy Authority (UKAEA) Formula

$$V_{bl} = V_a \quad \text{for } V_a < 70\frac{m}{s} \tag{2.74}$$

$$V_{bl} = V_a \left[1 + \left(\frac{V_a}{500}\right)^2\right] \text{ for } V_a > 70\frac{m}{s} \tag{2.75}$$

in which,

$$V_a = 1.3\rho_0^{1/6}.k_c^{0.5}.\left(\frac{p.H^2}{\pi.M}\right)^{2/3}(r+0.3)^{0.5}\,(1.2-0.6\left(\frac{c_r}{H}\right)) \tag{2.76}$$

where c_r is the spacing of rebar, r is rebar ratio % (each-way-each-face, EWEF), and k_c = f_c for f_c < 37 MPa, and k_c = 37 MPa for f_c > 37 MPa. The application ranges are 11 m/s <V_{bl} < 300 m/s, 22MPa < f_c <52MPa, 0.33 < H/(p/π) < 5, 0 < r < 0.75%, 0.12 < c_r/H < 0.49, 150 kg/m^3 < M/p^{2}H < 10^4 kg/m^3. When c_r/H=0.49 ballistic formula for a non-circular cross-section can be used. V_r – Residual Velocity of the Missile, V_0 - Velocity of the Missile, V_{bl} – Ballistic Limit of the Missile, d – diameter of the missile, h_{per} – Perforation Limit of the Target, H – Thickness of the Target, f_c – Unconfined Compressive of Concrete, p is the perimeter of the missile cross-section, ρ_0 – Density of the Target.

Due to the heightened probability of terrorist attacks events across the globe, there is mandatory need to ensure the safety of the buildings, structures, military storages, official government structures, etc, against such events. Since there is a significant increment in Nuclear power plants (NPP) all over the globe, protection of Nuclear containment structures due to missile attacks is of paramount concern due to the severity of the disaster it can create. The following section explains the statistics of NPP and their calamities.

Chapter 3. NUCLEAR POWER PLANT

The current chapter presents the details about the usage of Nuclear Power Plant (NPP) in the world, types of NPP, structural configuration of NPP and disasters that have occurred in NPP. It also details the human-made threats such as missile attack that the NPP's might be vulnerable too.

3.1. Nuclear Energy

Nuclear energy produces 11% of world's electricity next to coal, gas, and hydro sources. Developed countries like USA and France produce one – fifth and three – fourth of their electricity with the help of nuclear power plants. There are 452 units in operation and 55 units of Nuclear Power Plant (NPP) under construction by February 2019 (https:/pris.iaea.org/pris/) (Figure 3.1). Increment of 17% in nuclear power share is predicted by the International Energy Agency (IEA) by the year, 2050 (Houssin *et al.*, 2015) (Gu, 2018). Tremendous increment in statistics of nuclear power plants is predicted by 2050. Table 3.1 presents the details of different types of NPP. In general, nuclear power plants last at least 30 years and 80 years could be maximum termination. The protective safety barrier is mandatory and is strongly recommended by (International Atomic Energy Agency, 2004) since the construction of first NPP in the 1950s. Unfortunate internal accidents and external attacks on NPP's gives preeminence to terrible disasters as a result of hazardous gases released into the environment and other nuclear contaminants and harmful radiation.

Table 3.1 Percentage of Worldwide Reactor Types

Type	Number of Reactors	Percentage (%)
PWR (Pressurized Water Reactor)	298	65.78
BWR (Boiling Light-Water Cooled and Moderated Reactor)	75	16.55
PHWR (Pressurized Heavy-Water Moderated and Cooled Reactor)	49	10.81
LWGR (Light-Water Cooled, Graphite Moderated Reactor)	15	3.31
GCR (Gas Cooled, Graphite Moderated Reactor)	14	3.09
FBR (Fast Breeder Reactor)	3	0.66

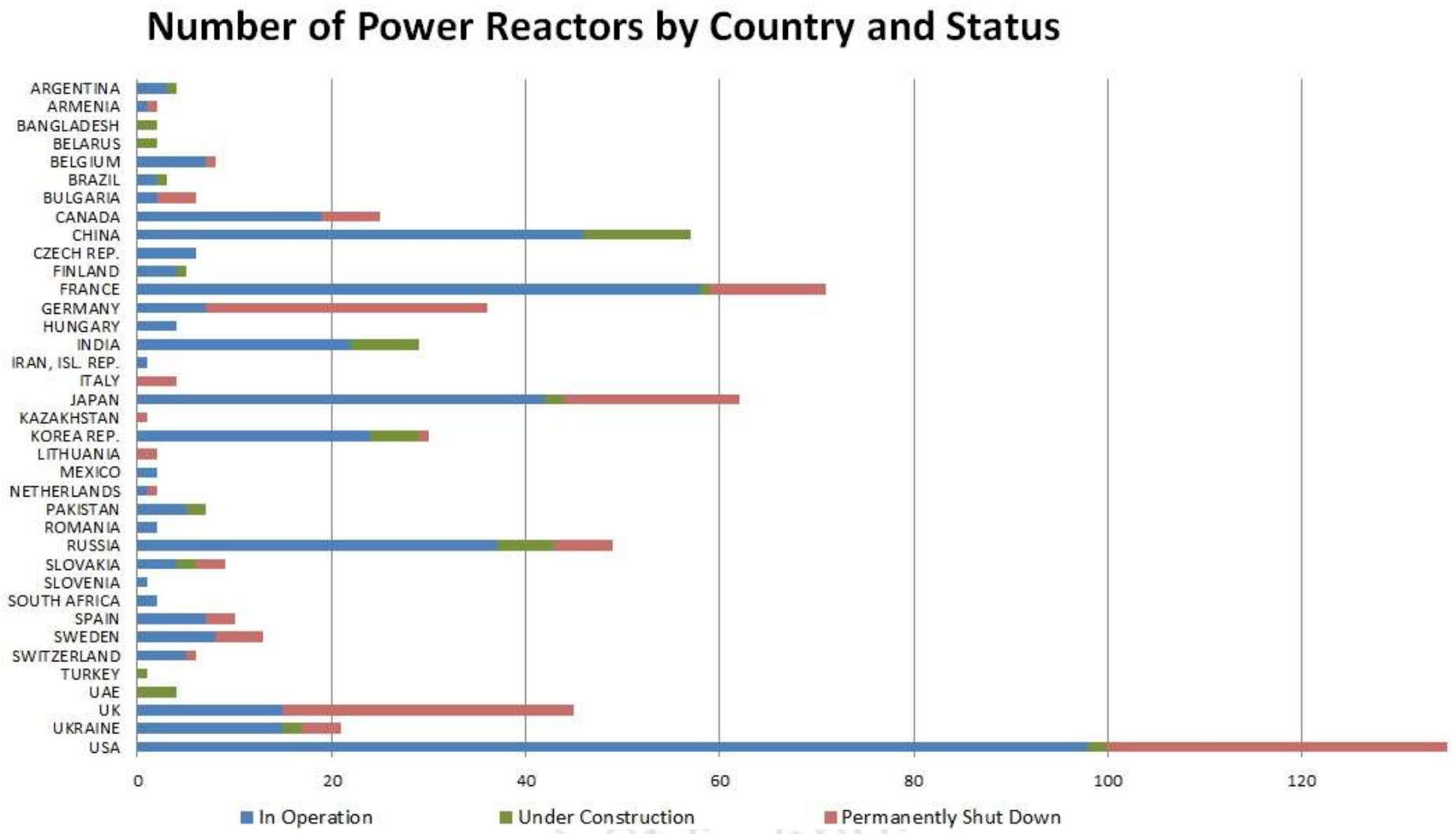

Figure 3.1 Nuclear Power Plants, World Wide (https:/pris.iaea.org/pris/)

3.2. Calamities of Nuclear Power Plants

Three large scale nuclear accidents have occurred in history which are: Three Mile Island (TMI) accident (March 28, 1979), Chernobyl accident (April 25-26, 1986) and Fukushima accident (March 11, 2011). Gu, 2018 reviewed these three disasters which sheds light into the distinct reasons behind each. This could be set as a warning and certainty for another catastrophic event in the upcoming years. The analogy of calamities shows vulnerability and accountability. One important information is drawn after the 9/11 attacks were that some resources said that it was initially planned on a nuclear power plant. In the wake of these attacks in the USA, Nuclear Regulatory Commission (NRC) revised the code of Federal Regulations 10 CFR part 50 for newly constructing containment structures after July 13, 2009 (Bangash, 2011). Fukushima accident is a prototype for an accident occurring due to a natural disaster in a recently manufactured Nuclear containment building (Zhou *et al.*, 2018). After these accidents, the terrible effect on people and resources surfaces with life marred with health disorders (IRSN, 2016). Based on this, it should be realized that the threat of conventional missile impacting a nuclear containment structure can be a reality in near future and effort should be made to design the Nuclear Containment structure to resist it if it could not be stopped at the onset (Figure 3.2).

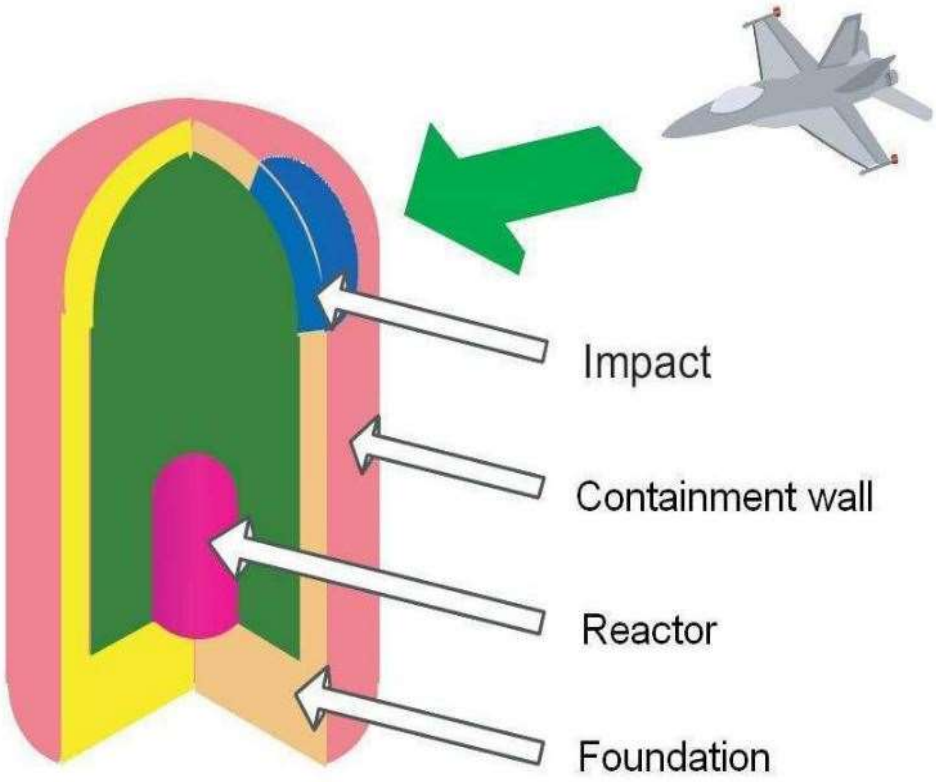

Figure 3.2 Containment building subject to Aircraft impact (Daudeville and Malécot, 2011)

3.3. Nuclear Containment Structures

A defensive barrier for NPP's is termed as nuclear containment structure, which is designed as a defensive barrier for NPP's, which is intended to be leak-proof to avoid or minimize toxic and virulent gases transmission due to close-in detonations (U.S. Department of Defense, 2008). Likewise, it protects from external hazards like aircraft impact loads, tornado wind and associated air-borne projectile loads, hurricane loads, tsunami loads, conventional missile impact loads, human-induced disasters, etc. (Bangash, 2011).

Most of the existing nuclear containment structures are made up of concrete material. Typical containment structures are made with a single-walled structure with a metallic liner,

double-wall structure with or without metallic liner, steel containment structure, etc,. with various dome shapes like hemispherical, oval, flat, etc.,. as shown in Figure 1.6 and Figure 3.3. In case of double-wall structure, the outer layer is made up of reinforced concrete and the inner layer is made up of post-tensioned concrete with a rear side steel liner as shown in Figure 3.4, Figure 3.5 and Figure 3.6.

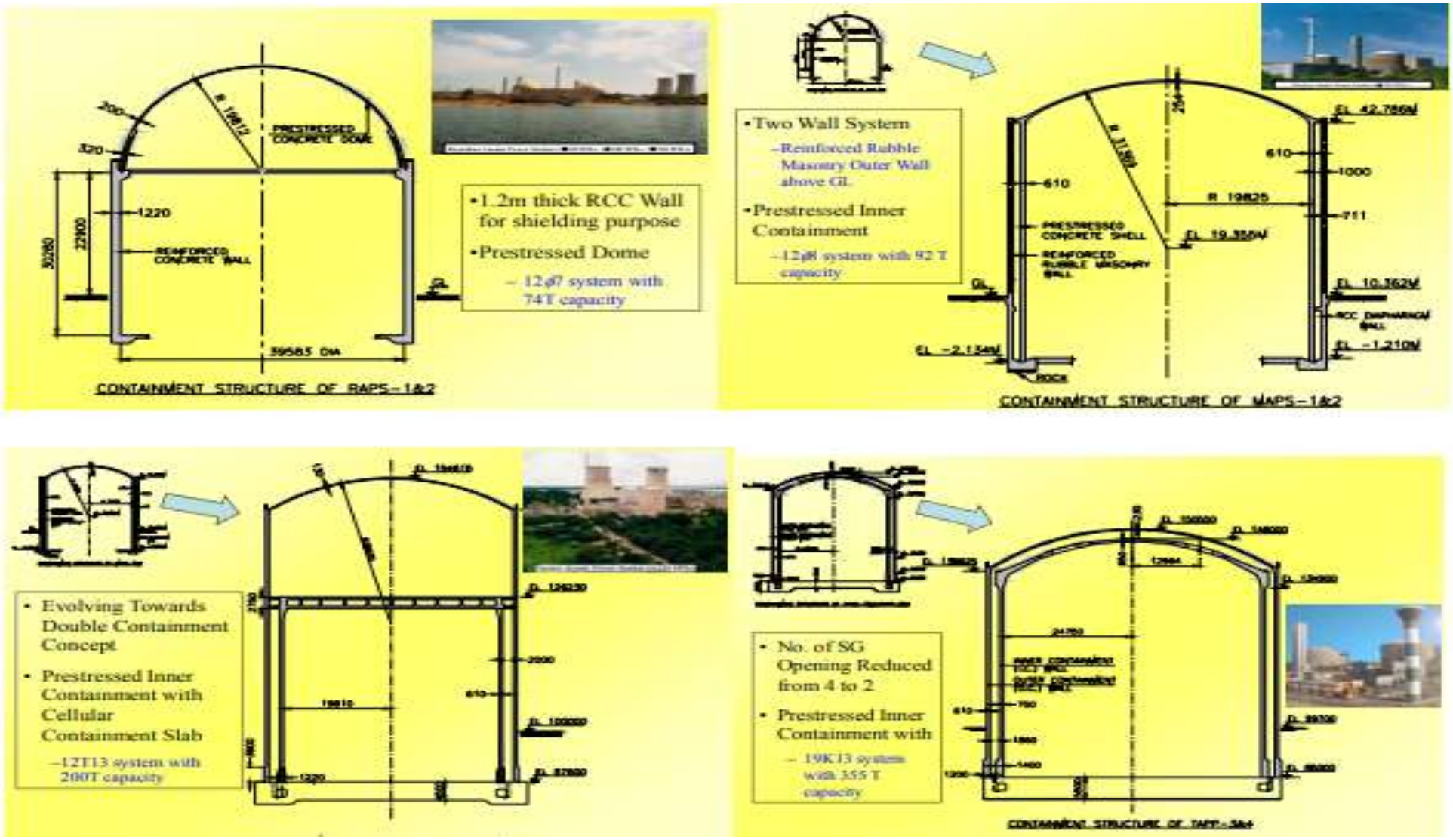

Figure 3.3 Types of Containment Structures in existence

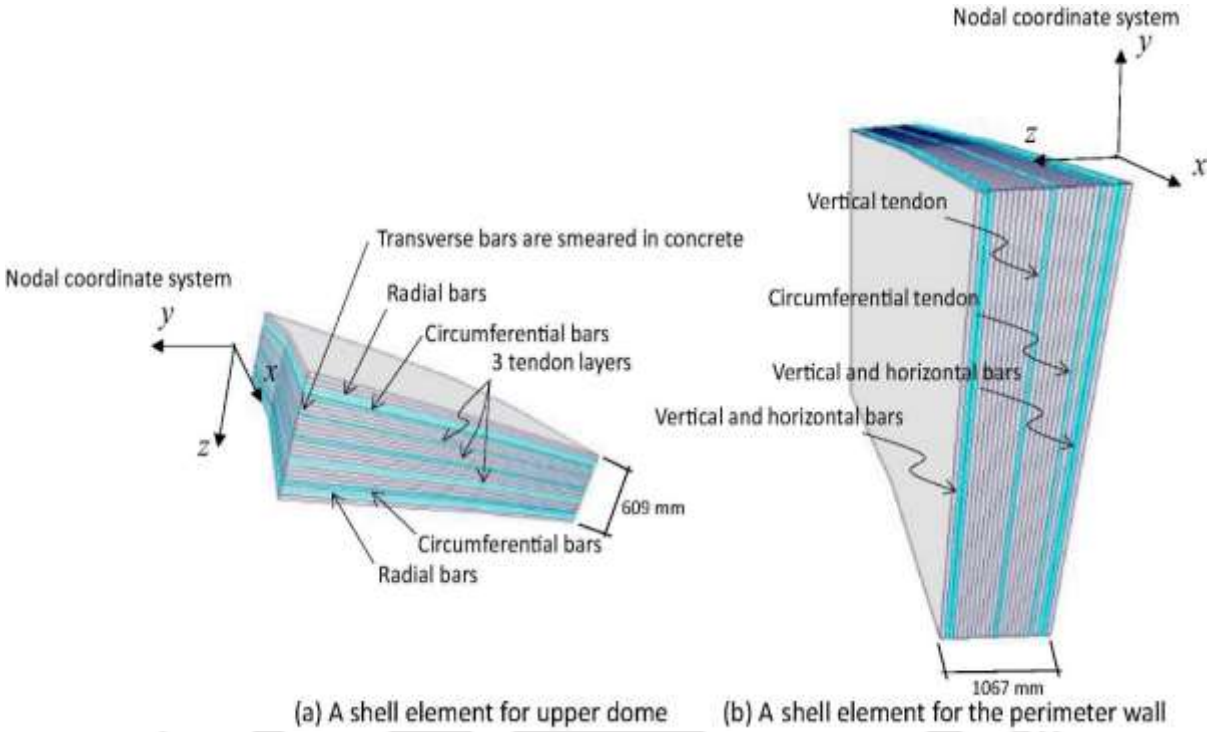

Figure 3.4 Typical layout of Dome and Wall of Nuclear Containment (Huang *et al.*, 2017)

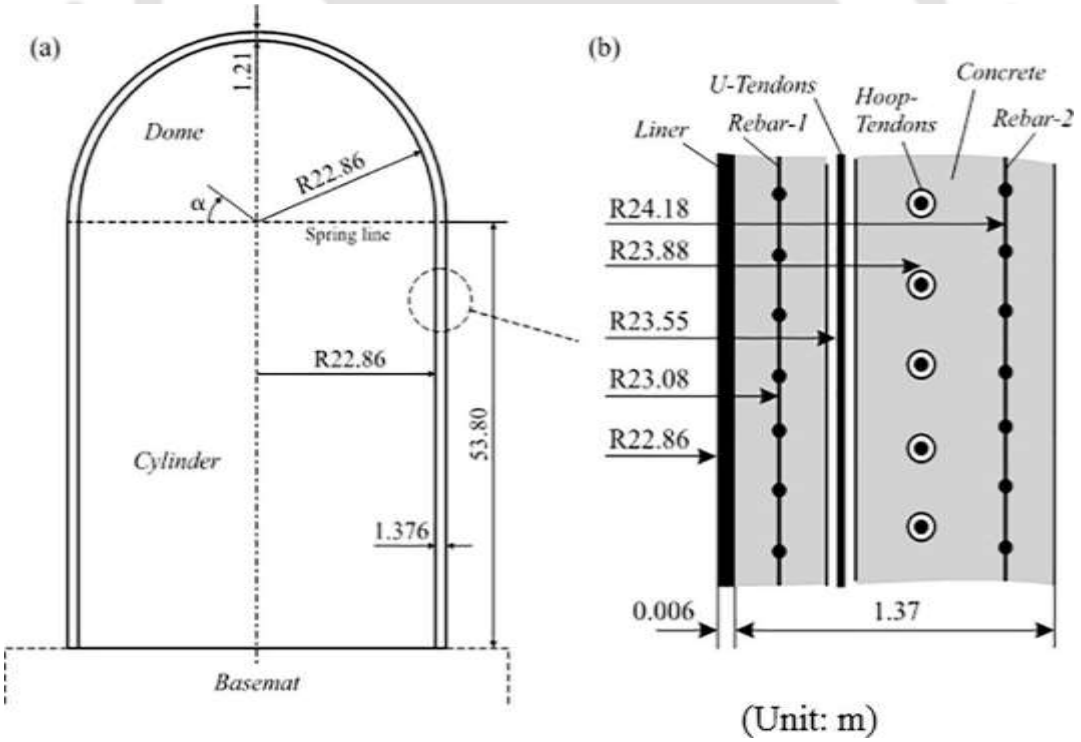

Figure 3.5 (a) Nuclear Containment Layout (b) Section of containment structure (Choun and Park, 2015)

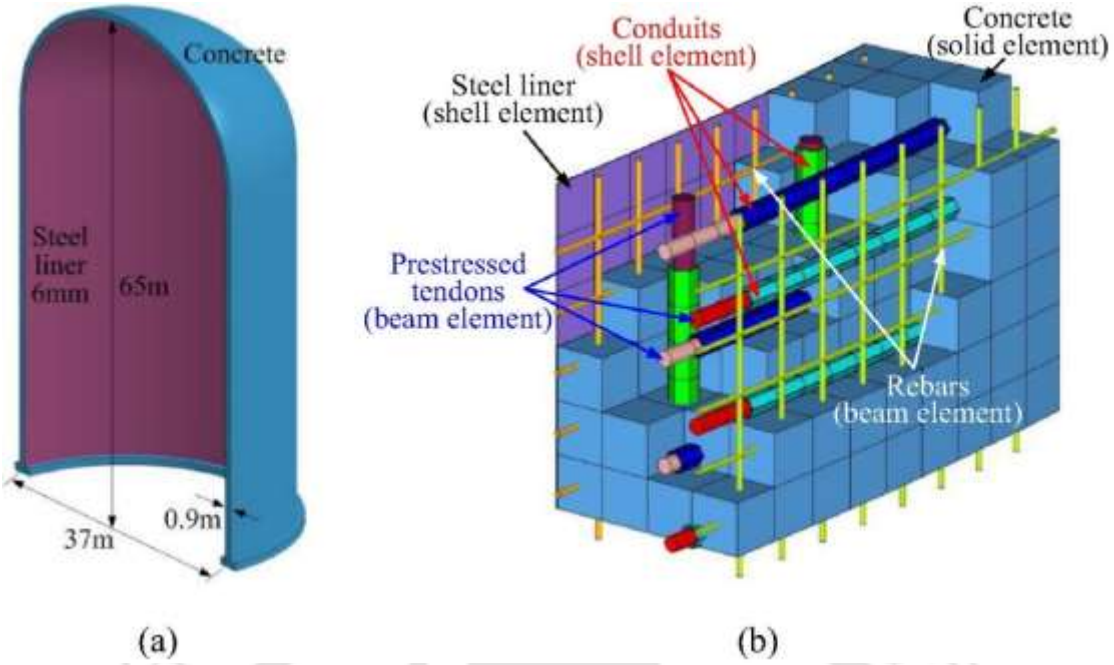

Figure 3.6 Typical cross of Nuclear containment (Zhang et al. 2017)

The occurrence of missile impact scenario upon containment structure is becoming a horrifying possibility in coming days due to very large increment of nuclear power plants globally. So there is a great need of impact analysis to mitigate the failure of the structure. A performance-based analysis and design with desired performance levels tied with damage states could be the possible solution to prevent damage and develop economical design guidelines which are explained in the following section.

Chapter 4. PERFORMANCE LEVELS OF NUCLEAR CONTAINMENT STRUCTURES

4.1. Performance-Based Design (PBD)

The concept of performance-based design is not a recent invention but was centuries ago, i.e. 1955 BC to 1913 BC in the reign of the Babylonian king Hammurabi. The code is entitled as 'Code of Hammurabi' (Gross, 1996) and motto is stated as '*a house should not collapse and kill anybody*', and it is a performance statement. This statement mainly focusses on structural safety rather than user performance requirements. However, it talks about the result than structural dimensions, spacing, size and thickness of walls, material, etc. Later in 1982 by the CIB W60 Commission (Gibson 1982) stated that "*first and foremost, the performance approach is [...] the practice of thinking and working in terms of ends rather than means. [...] It is concerned with what a building or building product is required to do, and not with prescribing how it is to be constructed*" (Becker 2008).

Definition: PBD is a process that facilitates the progress of structures that will have predictable performance when subjected to defined loading.

For the specific hazard, the designer goal is to achieve various expected performance scenarios is by considering past data or predictions. PBD is validated through analysis, simulation, experimental or a combination. PBD is based on the argument of satisfying the defined performance objectives of the structural system as well as supporting nonstructural systems. The basic procedure to evaluate PBD is as follows,

1. Defining Performance Objectives
2. Range of Initial Design

3. Validating performance through FE simulation, experimentation, or a combination of

In case of any loading, defining performance objectives are very crucial because they establish the design. A client or stakeholder with a certain requirement is involved, and this requirement is termed as Demand (Becker 2008). The structural capacity should always be greater than the demand of the client to avoid collapse prevention. Performance objectives are quantitative in traditional codal approach but qualitative in PBD to meet clients demand i.e. low probability of failure. General pattern of describing various performance objectives (Whittaker et al., 2003; Sharma and Hurlebaus, 2012) or different loadings is considered as follows,

- Fully Operational with No Damage
- Operational with a Damage
- Collapse Prevention

From recent decades the concept of PBD is majorly practiced in seismic design (Whittaker et al., 2003) of various structural constructions like buildings, bridges, nuclear containment structures, etc., (Yamawaki et al., 2000; Priestley 2000) as well as wind loadings especially on skyscrapers, buildings (Jeong and Tarrant 2018) and fire safety design (Nour 2018) of buildings as seen in 9/11 attacks on World Trade Centre (WTC). Currently PBD is extended to engineering fields with extreme loadings like vehicle collisions (Sharma and Hurlebaus, 2012), blast loadings (Whittaker et al., 2003) and so on.

4.1.1. **Advantages of PBD**

Various advantages can be drawn from the studies of PBD and research in this field is improving over last few centuries. Predominantly for any structural designer the main objective is reliability of the structure, due to established performance objectives desired performance is attainable in PBD. Secondly, the appropriate performance level can be chosen by client or designer to satisfy the required criteria. Thirdly for designers need not to be limit to prescriptive

solutions due to defined performance objectives and process is flexibility in allowing innovation and new design solutions like materials.

In general, limit state code provisions are used as a guideline for the construction of structural elements and buildings, materials, etc. These guidelines are capable of taking frequently expected loads due to inherent safety measures but may not serve enhanced performance when subject to non-design loadings i.e. extreme and unpredicted loadings (Easa & Yan, 2019; Aktan et al., 2007). Traditional codes are process-oriented method but performance based design is product oriented method (Aktan et al., 2007). In product oriented approach the ultimate goal is to ensure long-term performance-in-use of buildings as an explicit target (Becker 2008). Naturally there is expectation of structural serviceability for decades and centuries, the mitigation of small sampling problem requires a major effort by using extensive instrumentation and monitoring programs. So, performance based design is best suitable solution to enhance the serviceability and strength of the structure, economically.

4.2. Bayesian Approach

In engineering, based on the available data we need to formulate sound design approaches (Ang & Tang, 2007). A significant amount of data plays very crucial role to accurately implement the risk-based design concept (Haldar and Mahadevan, 2000). So it is always suggestable to estimate uncertainty using significant observations. In general, acquired data is from observations either from field as well as experiments, derived information from theoretical models and professional judgements based on experience (Ang & Tang, 2007). Nevertheless, the sources and type of information is often combination of various required qualities. However, available information need to updated into new form or data acquired. When the data available is having variability i.e. invariable with the engineering information, the proper tools for combining and updating the available data is embodied in Bayesian approach (Ang & Tang,

2007). Probabilistic analysis often considers two uncertainties i.e. aleotary uncertainty and epistemic uncertainty. The former is associated with the inherent variability of the information which is irreducible and the later with lack of our knowledge, ability to make predictions, measurement errors, statistical uncertainty, model inexactness, etc. (Gardoni et al., 2002; Ang & Tang, 2007). In this concern the uncertainties can be evaluated by Bayesian approach in two ways (1) the systematic update of existing uncertainties approach as new information or data for each type of uncertainty is available (2) to ensure an another approach to combine both the uncertainties for the purpose of design formulations (Ang & Tang, 2007). In the approach the required unknown parameters are assumed to be random variables. By this way, all the sources uncertainties can be combined to estimate the parameters. Detailed literature about Bayesain approach is given in (Gardoni et al., 2002; Ang & Tang, 2007) which is based on Bayes rule. The purpose of Bayesian analysis is to determine posterior probabilities based on prior probabilities and new information. Bayesian analysis can be used in the decision-making process whenever additional information is gathered. Based on the formulations obtained through Bayesian approach the fragility analysis is carryout.

4.3. Fragility Analysis

Fragility is defined as the conditional probability of failure of a structural member or system for a given set of demand variables (Gardoni et al., 2002). Demand variables are based upon the type of loading acting on the structure, for earthquake loading the ground motion is considered as demand variables, impactor hitting on the structure in impact loading, blast pressure in case of blast loading and so on. Probabilistic demand models are used to establish the fragility of the structural component by providing treatment to aleatory and epistemic uncertainties. Aleatory uncertainties are random in nature and also known as inherent variable and randomness. This uncertainty cannot be observed by the spectator or pattern of observation

and is available in the set of quantifiable variables like material property constants, structural member dimensions, and imposed boundary conditions and partly in error terms (Gardoni et al., 2002). The Epistemic uncertainties arose due to our lack of knowledge, from measurement errors, from limited observation samples. This kind of uncertainty are available in capacity, demand models and partially in error terms. Fragility plots are generated for each performance objectives defined in the research. Each performance level could generate particular fragility curve to show the vulnerability of the specimen. In this research the performance levels of containment structures are defined in the following section.

4.4. PBD of Nuclear Containment Structures

Nuclear containment structures made with either reinforced or prestressed concrete may undergo damage during missile impact because of massive force transfer over a short period. Due to a short period, the resistance mechanism of the panel is based on inertia effect and local impact effects than global displacement. In that case, the local effects caused by severe dynamic loading on the structure become the main quantities than the global mechanism which can be represented using an equivalent static quantity. Based upon type and severity of missile impact damage states are varying. There is a necessity of performance-based analysis and design to diminish the damage of structure and to ensure economical design. Performance levels of the target structure where the panel are subject to missile impact have been identified to define damage states.

4.5. Behaviour of Target During Missile Impact

Significant experimentation has been done for scenarios in which missile impacts upon concrete targets to determine the dynamic effects and failure mechanism. Some noticeable features can be encapsulated as follows:

- Concrete brittle behavior is proportional w.r.t the loading rate
- Reinforcement and tendons strength increases w.r.t loading rate
- At the point of contact, a plastic hinge is formed

The behavior of the target structure while missile impacting as follows. The missile impact process is classified into two phases. In the initial phase, a missile comes into contact with the target with an initial velocity. The initial phase is the time of missile contact upon the target to the time when part of the target and missile obtain the same velocity and move together. Enormous force is developed due to inertia in a short period. Due to the rest position of the target and colossal mass, a tremendous force develops to achieve an identical velocity of missile and target. The current phase is governed by the inertia of the target. Localized effects are observed in the target due to great force upon structure. The second phase is the duration when part of the target and missile attains common velocity and moves to the time when either partial local failure of the target or complete local failure of the target. There is a transformation of the kinetic energy of missile into the target. Local effects of the target are obtained due to the erosion of concrete. In this research, no deformation is observed in missile due to rigidity.

Missile force imparted on the target is the demand imposed on the structure. Demand varies with velocity and mass of missile as well as properties and structural configuration of the target structure. The target resistance mechanism is an indicator of targets strength also called the capacity of the structure which is a combination of damping resistance, inertial resistance and local stiffness resistance. In the event of an impact, target capacity increases because of the enhancement of the material properties due to an increase in the strain rate. Prevention of the failure or damage of the target structure is attainable when the demand of missile is lesser than the capacity of the target. The missiles kinetic energy is transferred upon the target structure while impacting.

4.6. Performance Levels for Missile Impact

Based on material properties, geometry, boundary constraints of the target and velocity, type of missile, various levels of damage are possible when impact with a missile. This research proposes four damage levels with increasing intensity. Three performance levels are considered based on four achievable damage levels of the target subject to missile impact, in the spirit of performance-based analysis and design, as given below in Table 4.1

Table 4.1 Performance Levels Of Target Structure Subject To Missile Impact

Damage Level	Damage Description	Performance Level	Performance Level Description
D1	Zero penetration		
		P1	Operation with Minimum Damage
D2	Penetration up to clear cover, spallation of concrete		
		P2	Operation with Damage
D3	Penetration up to mid-depth of the section		
D4		P3	Collapse Prevention
	Full penetration of missile in section		

The damage levels rise in intensity from minimal damage to total failure of the target structure. The corresponding three performance levels defined are operational with minimal damage (P1), operational with damage (P2), and collapse prevention of target structure (P3). Performance level one with operation with minimum damage is considering missile penetration up to clear cover of the target panel, as shown in Figure 4.1. Performance level two is considered operational with some damage of target subject missile penetration up to the mid-

depth of the target panel, as shown in Figure 4.2. Performance level three is considered collapse prevention of target subject missile penetration up to the full-depth of the target panel, as shown in Figure 4.3. It is observed that peak energy in probabilistic models are observed near the middle of the containment structure. Based on this three performance levels are considered for this thesis.

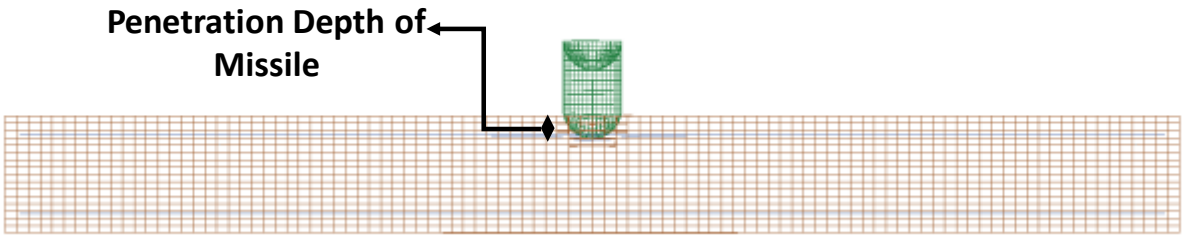

Figure 4.1 Penetration of Missile Up to Clear Cover in the Target, Performance Level 1

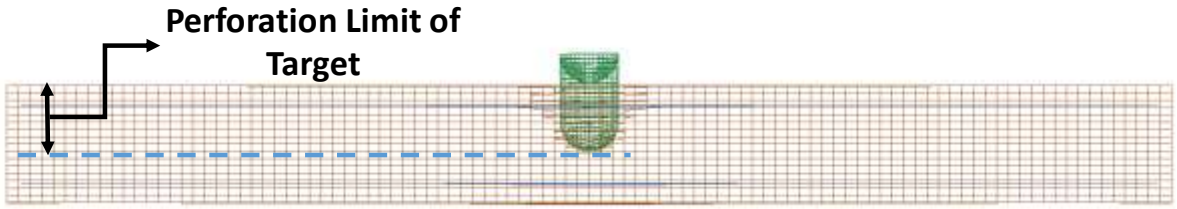

Figure 4.2 Penetration of Missile up to Mid-Depth in the Target, Performance Level 2

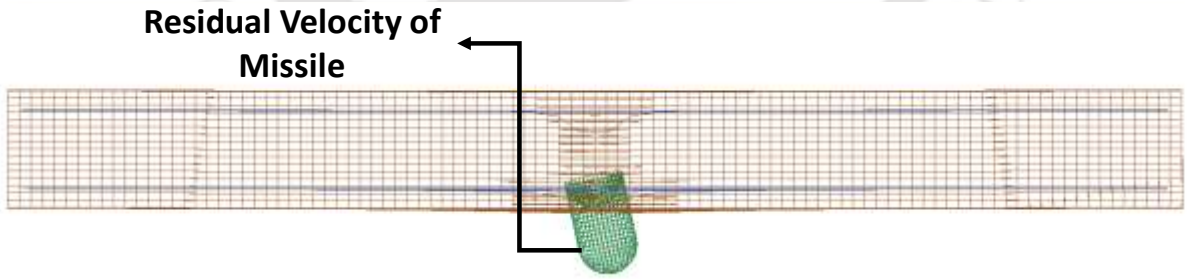

Figure 4.3 Penetration of Missile up to Full-Depth in the Target, Performance Level 3

4.7. Methodology for Estimating Probabilistic Models

To obtain the probabilistic models a series of experimental data is required. Experimentation in the realistic scenario is highly impossible due to many complications involved like the construction of massive thickness of the concrete, fixation of steel liner, post-tensioning of tendons in both directions, vast number of reinforcement bars in translational and longitudinal directions, equipment to initiate missile with a velocity, etc,. A requirement of skilled labour is needed for accomplishing this tedious job and is not economical. A performance-based analysis and design could help to mitigate the damage of the structure due to missile impact.

Due to constraints involved for experimentation, a finite element approach is used to get a large number of required data. In this research, the double-wall structure i.e. reinforced concrete structure which is the outer layer and reinforced post-tensioned prestress concrete with a metallic liner which in the inner layer is considered. A total of 50 RC panels, as shown in Figure 4.4 and 100 PC panels, as in Figure 4.5 of different sizes, reinforcement ratios, tendon ratios in realistic ranges are selected and are subjected to the flat nose-shaped hard missile of varying weight and velocity through finite element (FE) numerical analysis using LS-DYNA (Finite Element package), as detailed in Chapter 5, Chapter 6 and Chapter 7. In this research, PC panels mean prestressed concrete with reinforcement bars, post-tensioning tendons, a rear side steel liner and with curvature effect. RC panels comprise of reinforced concrete without steel liner, tendons and curvature. Based on the obtained FE results, the probabilistic models for various performance levels are estimated in Chapter 8. The performance-based capacity models for RC members are estimated in Chapter 9. The demand models for RC members subjected to missile impact loading is estimated in Chapter 10. The performance-based capacity models for PC members are estimated in Chapter 11. The demand models for PC members subjected to missile impact loading is estimated in Chapter 12. This performance-based

analysis and design approach comprises of probabilistic capacity and demand models for RC and PC panels using energy-based formulation.

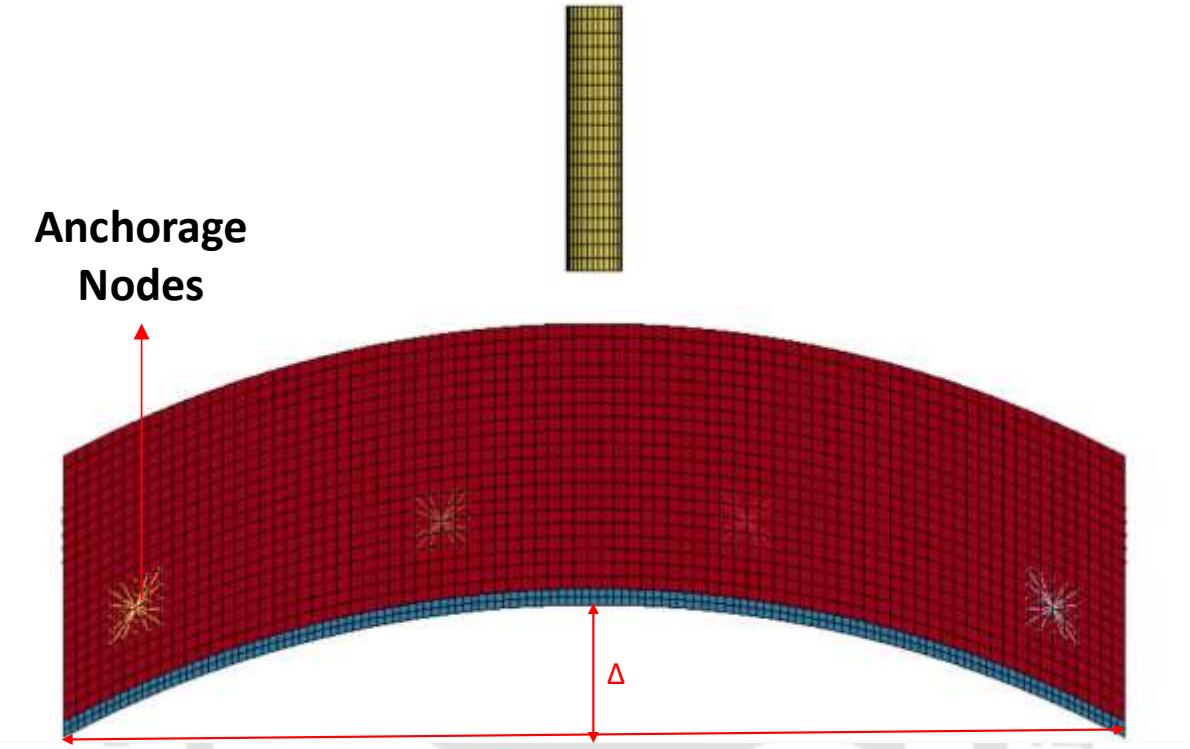

Figure 4.4 Prestressed Concrete Curved Panel with Steel Liner Subject to Flat Nose Missile

Figure 4.5 Reinforced Concrete Slab Subject to Flat Nose Shape Missile Impact

Achievement of accurate probabilistic models is possible with the advantage of a proper finite element validation which is explained in next Chapter 5 and Chapter 6.

Chapter 5. FINITE ELEMENT MODEL FOR RC MEMBERS SUBJECT TO MISSILE IMPACT

In the current chapter, a detailed analysis of Reinforced Concrete (RC) member subject to missile impact is presented. The material model, structural configuration, the element type is presented. Two sets of independent validation are carried out to establish the accuracy of the Finite element method in order to simulate the complex phenomenon.

5.1. Numerical Approach for RC Members

Intensification of numerical analysis is a considerable pedestal to the research world. Even though the experimental test approach which produces reliable data, numerical solutions are preferable for the sake of inexpensive cost and lesser time duration (Thai and Kim, 2017). The actual cost of concrete structures and performing realistic dynamic loadings is relatively unrealistic. So, Finite element (FE) codes which are capable of solving complex non-linear dynamics and quasi-static problems, especially those involving impact, shock, and highly discontinuous events is used. Finite element (FE) codes are the most valid accessible method for studying structural response subject to high strain loadings (Krauthammer, 1998). Finite element techniques are very much comfortable than experimentation because of the generation of realistic extreme loadings like high-velocity missile loadings and high-pressure blast loadings which are difficult to generate and control in a real-world than a simulated world. Local impact effects can accurately be captured using FE numerical methods and can be quickly validated with experimental data. FE based simulation techniques are the best solution for complex configurations with dynamic non-linear loadings, which cannot be easily solved analytically.

The use of FE techniques requires validation with experimental results. IRIS-2010/2012 benchmark project conducted some series of experiments with a hard and soft missile on RC slabs (Orbovic *et al.*, 2014). Twenty-eight teams from twenty different institutions and eleven different countries have participated in this workshop. Participants obtained desirable results using the hydrocodes that had integrated into software's like Abaqus, LS-DYNA, Europlexus, VecTor2 & VecTor3, SOFiSTiK Version 25, Ansys, Autodyn v13.0, Radioss V11, Simplified semi-analytical (Pentabloc), TeraGrande/Explicit, etc. Many of the numerical results made a desirable match with results obtained through experimentation with the same configuration. So, the numerical models are reliable to represent the behaviour of a structure when subject to impact by some simplified assumptions made for construction and material. (Iqbal *et al.*, 2019) analyzed the impact effects caused by impactor using the hycrocodes that are integrated into ABAQUS/Explicit finite element code. (Sharma and Hurlebaus, 2012; Thai & Kim, 2017; Do et al., 2018) well-validated and reviewed a few numerical techniques for various impact loadings through LS-DYNA finite element software. ABAQUS and LS-DYNA and are non-linear explicit transient dynamic finite element codes that are mostly used for extreme loadings. In this research, LS-DYNA is used for FE simulations.

5.2. Material Models

5.2.1. Concrete Modelling

There are various material models to represent concrete in Finite Element simulation. Out of those material models identifying suitable models could be based on the following criteria, like, least possible inputs, rate-dependent material, and capability to record concrete damage. Rate dependent behaviour is a significant factor in account rate effects, especially when subjecting to high strain and dynamic loadings like impact analysis, blast analysis, etc. (Winkelbauer, 2016). Many researchers based on this criteria used three material models are selected from the

repository of LS-DYNA (Finite Element Modeling Software), to study the response of concrete to high strain rate loading (Wu et al., 2012; Thai et al., 2019; Winkelbauer, 2016). Three constitutive models are Continuous Surface Cap Model (CSCM) Concrete, Winfrith Concrete, and Concrete Damage model. Formulations of these three constitutive models are well documented in Sharath et al. 2017; Wu *et al.*, 2012; Johansson and Fredberg, 2015).

5.2.2. CSCM Concrete Model

The development of the CSCM model was done in the 1990s by APTEK, Inc. mainly used for roadside safety analysis. This model requires a minimal number of inputs for analysis to be carried out. Concrete compressive strength, maximum aggregate size, and concrete erosion are sufficient and are user-friendly. One of the significant features of this model is a shear failure, and the compaction surface is mixed to form a smooth or continuous surface, as shown in Figure 5.1. CSCM model in LS-DYNA has two variants Mat-CSCM and Mat-CSCM Concrete; the first model has more inputs than the second model. The compressive strength range varies from 32 MPa to 58 MPa and aggregate size between 8 mm to 32 mm. Auto-generation capacity is high in this model. This model is more suitable for lower velocity impacts and shock pressure loadings, i.e., blast loadings.

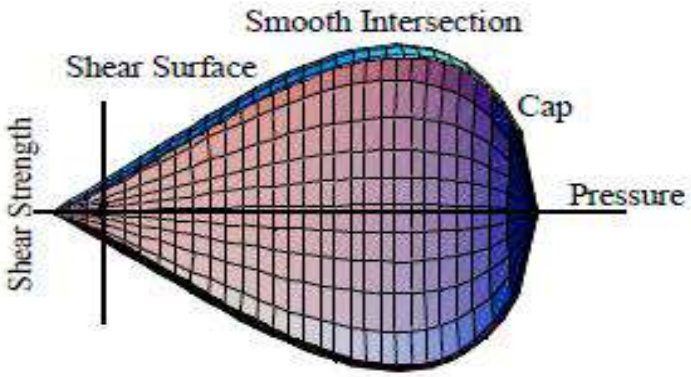

Figure 5.1 Failure surface and cap shape of CSCM

5.2.3. Winfrith Concrete Model

Winfrith Concrete constitutive model with material ID 84 is best suited in solving impact loads towards RC structures. This model was implemented into LS-DYNA in 1991 but has developed in the 1980s (Wu *et al.*, 2012), (*CEB-FIP MODEL CODE 1990*, 1993). Smeared reinforcement can directly be included in this model, which is not offered by other concrete models. The number of inputs is more than CSCM concrete, but this model is a basic plasticity model with Mohr coulomb behavior with third stress invariant to treat triaxial extension in compression and tension and strain-softening behavior in tension to make material regular via fracture energy, crack width, and aggregate size. Strain rate has ensured by the advantage of Mat_Add_Erosion (000). ('Ceb-Fip Model Code 1990', 1993) The code is used to give inputs for this model. Damage of both compression and tension has considered in two different variables. The study of Wu *et al.*, 2012 concluded that this model is best suitable for high strain impact loadings. Auto-generation capability is limited. Next section focuses on existing nuclear containment structures and predicts threats on those structures which are mainly made-up of concrete material.

5.3. Finite Element Configuration

In the present study, the commercial FE software LS-DYNA is used for the numerical FE analysis (Livermore Software Technology Corporation, 2006). HyperMesh (Altair Computing, 2006) is used to generate FE models which are considered in this study. Monitored quantities of interest are displacement, impact force, and reaction force. The explicit integration scheme is used for the analysis, which is based on the central difference method.

5.3.1. Material Models

All the considered materials are modelled as a rate dependent model due to the sensitivity of material properties with the loading rate. In this research, an available software material which

suits for impact loadings on concrete is used, i.e. winfrith concrete model. This model cannot take account of strain rate dependency of the concrete strength. Add erosion is used to ensure strain rate dependence. The elastoplastic material model is used for reinforcement bars and is also a strain rate dependent. High failure strain is allotted to missile material model due of rigidity. Velocity generation keyword for initiating missile velocity.

5.3.2. Structural Configuration

To model the impact of the missile with the RC member, a three-dimensional solid model is used. Concrete panel and missile are modelled by a constant stress solid element which is default element form. A one-dimensional component is used for reinforcement bars and is explicitly modelled. These one-dimensional beam elements grant both bending and axial stiffness of the beam. Lagrangian coupling method is used to fix contact between concrete and steel, as shown in Figure 5.2. This liberates the struggle of nodes matching of steel rebars & tendons and concrete, which is hard in a few instances like the modelling of nuclear containments, composite structures, etc. In Lagrangian models, the *CONSTRAINED LAGRANGE IN SOLID (CLIS) keyword is commonly used to couple reinforcement (modeled using beam elements) nodes to the concrete nodes. This is often the preferred method as compared to the shared-node approach, as it does not require the nodes for the concrete elements and the reinforcement elements to coincide in space i.e. they can be meshed independently (TAY et al., 2016). Rigid nodes are created to form anchorage plates (Johansson and Fredberg, 2015) well explained about creating anchorage. Contact between rigid nodes and tendon elements are established by merging the last node of tendon and one node in the respective node-set. Missile and concrete contact is guaranteed by eroding surface to surface contact and nodes to surface contact between missile and rebars. Mesh refinement achieves convergence, and hourglass energy is ensured.

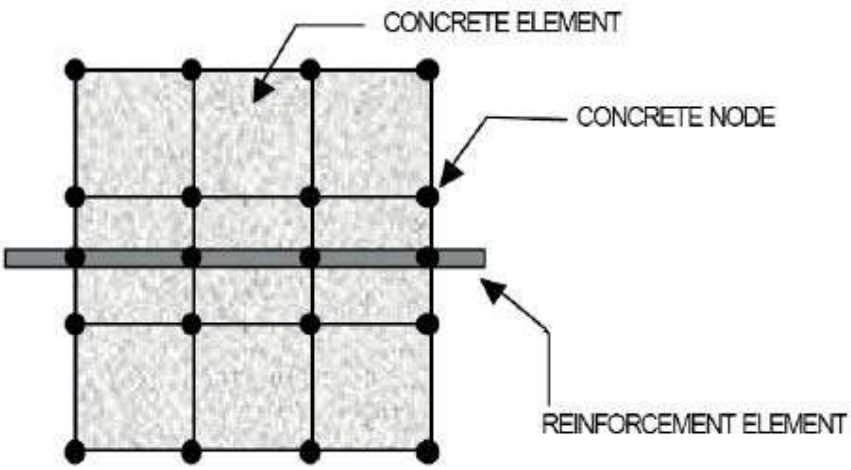

Figure 5.2 Reinforcement concrete contact share nodes (Johansson and Fredberg, 2015)

In case of non-linear loadings on concrete structures obtaining the parameters like displacements/deflections, stresses, natural frequencies, etc., with traditional procedures like hand calculations, simple equations are impossible to sort out. Alternatively, FEM and numerical methods provides an engineering analysis that takes into account much greater detail- which is impractical with hand calculations. In FE method the structure divides into smaller pieces enforcing continuity of displacements along these element boundaries. Generally, in FE analysis the term "convergence" is often used. Linear problems don't require iterations but non-linear problems do. In computational mechanics one of the overlooked factor is mesh convergence. If two refinements don't change much in results, then it can be assumed that the obtained results are converged. Mesh refinement of entire structural model may prolong in analysis time and is not suggestible. So based on the Saint-Venant's principle which states that the stresses in one region doesn't effect in another. Hence, from physical point of view fine refinement at required region and coarser mesh in another zone of the structure could validate the results appropriately. (Ranjan et al., 2014) through FE analysis validated experimental analysis of hard missile impact on concrete slab by (Kojima 1991). In this research convergence study is carried with various mesh sizes i.e. 8, 12 and 16 elements across

the depth of the slab have been studied. Likewise, in present analysis mesh convergence is taken care off and validated the results in following section.

The following section proposes a procedure to assess the proper validation of soft missile impact and hard missile impact upon RC structure (Orbovic et al., 2014), (Kojima, 1991).. A proper FE method is proposed in this chapter and the rest of the 50 RC FE simulations is followed with this procedure to obtain probabilistic models. All the keywords used in this analysis are given in Table 5.1. All the material models and structural configuration are as given in Section 5.3.1 and 5.3.2 are used for this FE analysis.

Table 5.1 Keywords used for FE analysis of RC members

Material	Keyword
Concrete	Winfrith Concrete MAT_084 with the erosion of 10 %
Rebar's & Tendons	Plastic Kinematic, MAT_003
Missile	Plastic Kinematic with infinity failure Strain, MAT_003
Contact between Missile and Concrete	Eroding Surface to Surface, Missile as Master & Concrete as Slave
Contact between Missile and Beam elements	Eroding Nodes to Surface, Missile as Master & Beam elements as Slave
Contact between Concrete and Steel Liner	Tied Surface to Surface, Steel Liner as Master & Concrete as Slave

5.4. Finite Element Validation

5.4.1. Validation – 1

A series of 12 experiments had been carried out in (Kojima, 1991), ten specimens with hard missile and two samples with the soft projectile. In this analysis, two experiments with a

hard missile are considered to validate with finite element modelling (Figure 5.3), as shown in Table 5.2

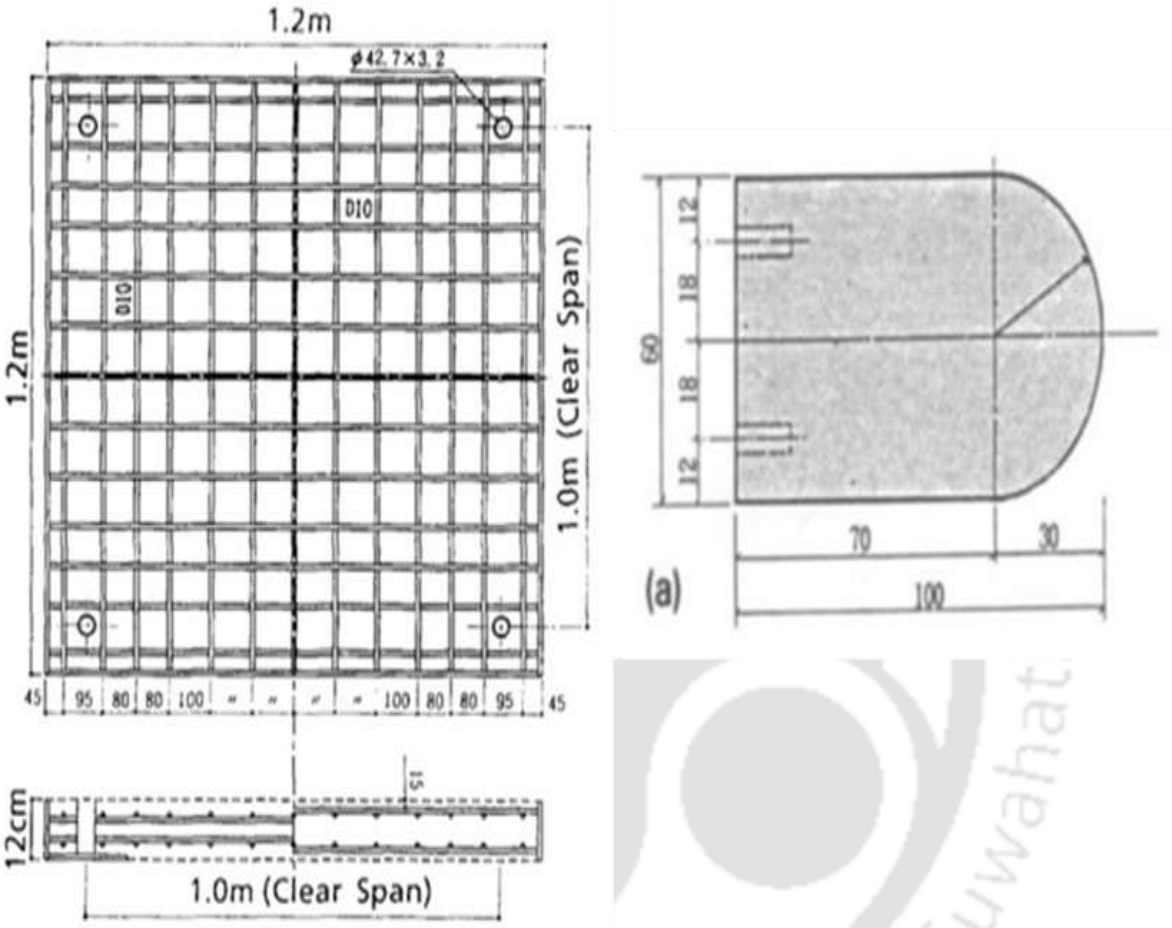

Figure 5.3 Layout of RC slab and Missile

The details of the experiment with the validation are presented in Table 5.2.

Table 5.2 Dimensions of RC slab, Missile and Obtained Results

Target Dimensions	Impactor			Penetration Depth, mm	
	Velocity	Weight	Shape and Type	Expt	FEM
1.2 m * 1.2 m* 0.12m	95 m/s	2 kg	Hemispherical and Hard	44	45
1.2 m * 1.2 m* 0.12m	164 m/s	2 kg	Hemispherical and Hard	100	108

Figure 5.4 and Figure 5.5 shows the evolution of the damage and penetration of the missile in the RC structure with varying loading. The penetration depth can be seen in the presented Finite Element simulation. It can be inferred that the present simulation captures the complex phenomenon well and is able to predict the damage accurately.

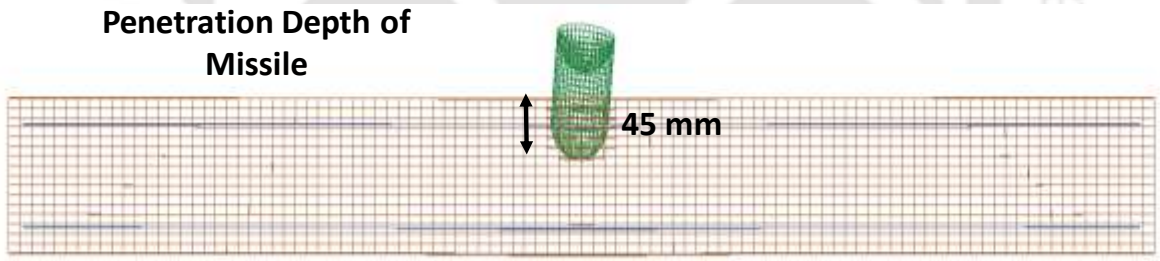

Figure 5.4 FE model of Missile Impacting RC Slab, 95 m/s

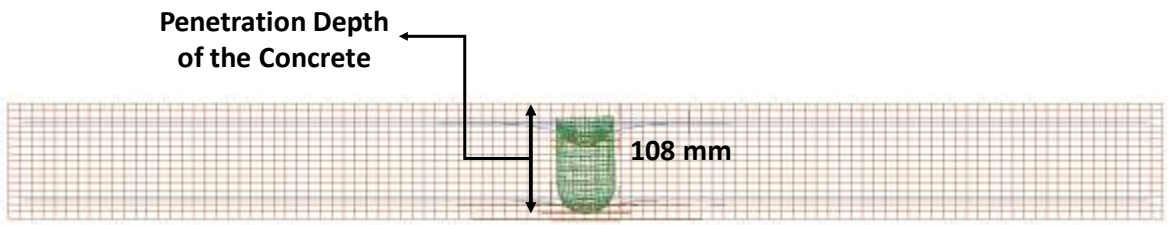

Figure 5.5 FE model of Missile Impacting RC Slab, 164 m/s

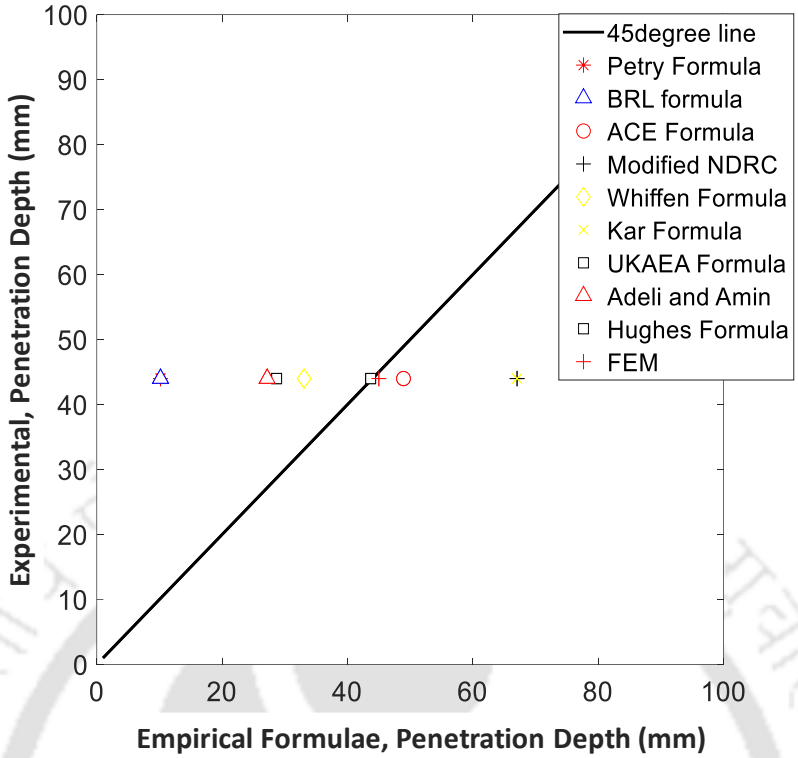

Figure 5.6 Comparison of experimental penetration with empirical formulae, FEM, 95 m/s

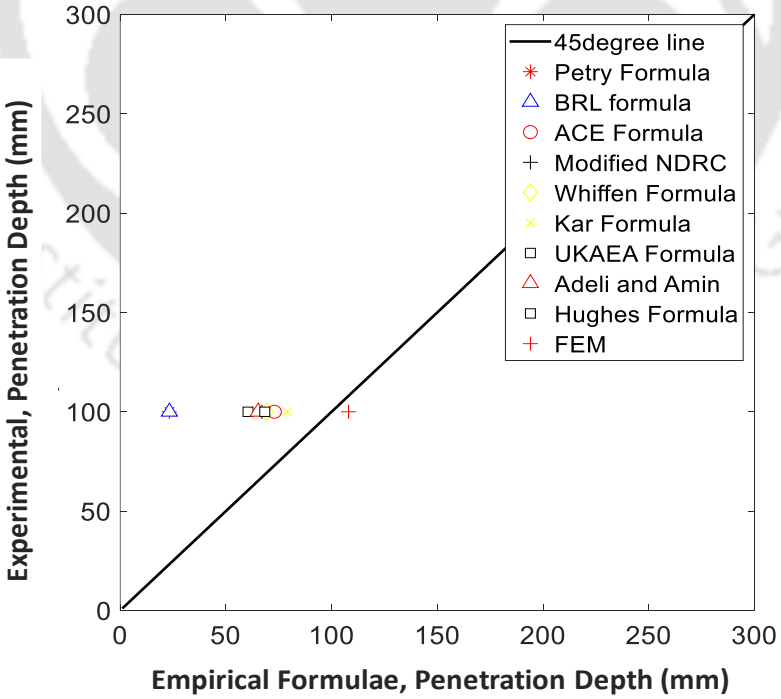

Figure 5.7 Comparison of experimental penetration with empirical formulae, FEM, 164 m/s

Figure 5.6 and Figure 5.7 presents the comparison of the Finite element simulation carried out in the present study with different empirical formulation for the different velocity of the impactor. It also shows that the existing empirical formulations are most of the time unable to capture the complex phenomenon such as penetration. This suggests that a probabilistic framework for predicting the damage phenomenon accurately is required.

5.4.2. Validation – 2

Improving Robustness Assessment Methodologies for Structures Impacted by Missiles (IRIS_2012) has conducted a few experiments subject to hard and soft missile impact. In this study, RC panel subject to bending failure and impacted by 50 kg mass impactor with a failure strain of 50% following detailing is explained in Orbovic et al., 2015 (Figure 5.8). Table 5.3 details the structural configuration as well as results obtained from experimental as well as Finite element study in the present research. It can be seen that the formulation is able to capture the deflection of the structure with admissible accuracy.

Table 5.3 Details of IRIS Bending Test

Reference	Target Dimensions	Impactor velocity, mass, Shape and Type	Deflection, mm	
			Expt	FEM
(Nuclear and Agency, 2014)	2.082 m *2.082 m* 0.15 m	95 m/s, 50 kg, Hemispherical and Soft Missile	28.9	23.9

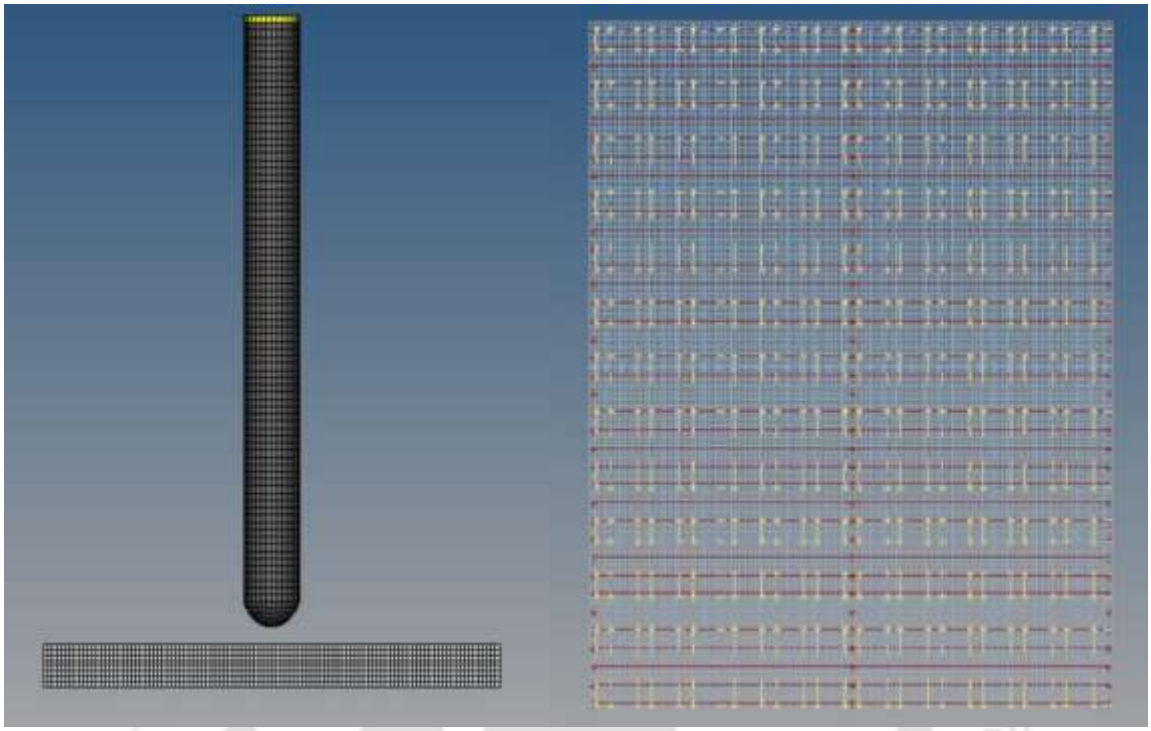

Figure 5.8 Hypermesh Model of IRIS Soft Missile and RC Slab

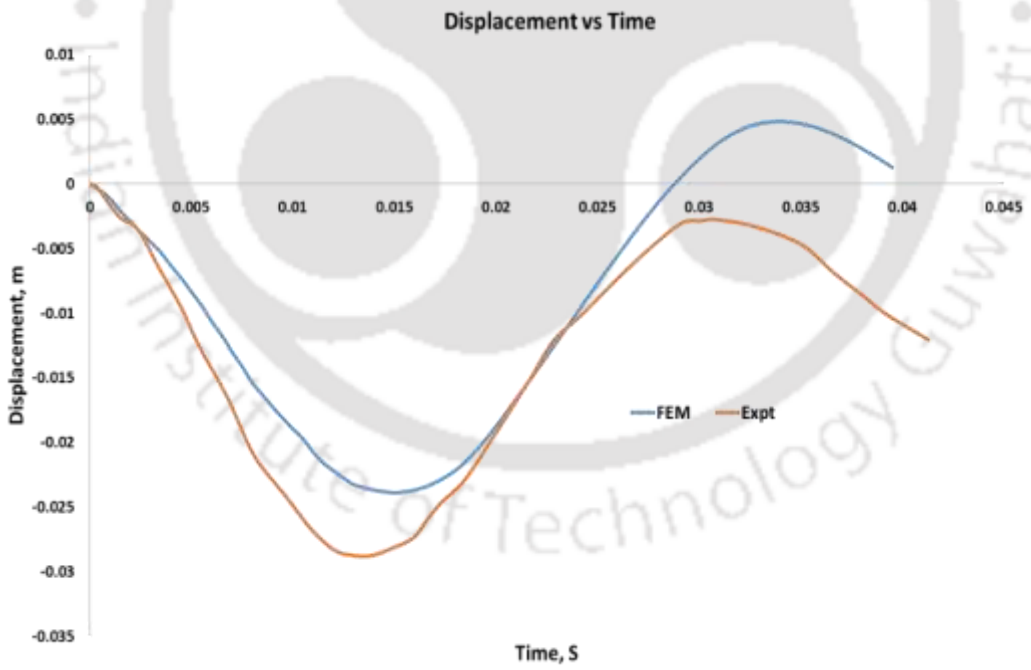

Figure 5.9 IRIS Bending Experiment showing comparison of Displacement profile

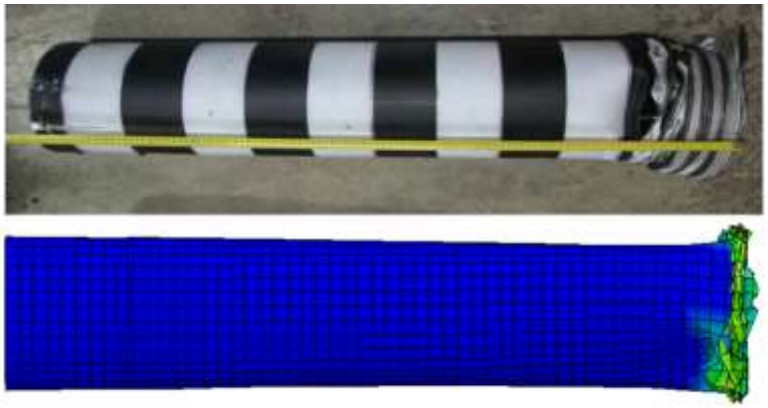

Figure 5.10 Soft Missile after impacting Slab

In Figure 5.9, it can be seen that the FE approach is able to capture the deflection profile of the structure subject to missile impact with great accuracy. In Figure 5.10, the damage profile of the missile is also replicated with accuracy. This chapter thus establishes that FE technique is able to capture the complex phenomenon of missile impact on RC structures. The damage mechanisms, the deflection, penetration and damage to missile can be accurately simulated by the Finite element technique. The next Chapter 6 presents a similar formulation for Prestressed Concrete (PC) structures subject to missile impact. The material model used for concrete, missile, element formulation and other common things follow the same treatment.

Chapter 6. FINITE ELEMENT MODEL FOR PC MEMBERS SUBJECT TO MISSILE IMPACT

In the same lines as the previous Chapter 5, the current chapter presents a detailed analysis of Prestressed Concrete (PC) member subject to missile impact. The material model, structural configuration, element type remains the same as the previous chapter. The details of the prestressing technique is presented here. Two sets of independent validation are carried out to establish the accuracy of Finite element method in order to simulate the complex phenomenon.

6.1. Numerical Approach for PC Members

6.1.1. Prestressing techniques

The literature review discusses a few methods of prestressing techniques numerically such as Spot-weld method, Temperature-induced shrinkage, Initial hogging deformation, Initial stress to concrete and tendons, etc. (Thai and Kim, 2017)(Li *et al.*, 2017)(Rajput *et al.*, 2016)(Do *et al.*, 2018)(Jiang and Chorzepa, 2015)(Thai and Kim, 2017)(Chen *et al.*, (Schwer, 2016). Exquisite realistic detailed procedure and keyword file for post-tensioned prestressing to reinforced concrete beams are delineated (Jiang and Chorzepa, 2015)(Johansson and Fredberg, 2015)(Thai and Kim, 2017). Introducing prestressing to reinforced concrete members excel in the complexity of modelling but significantly uncomplicated than the construction of realistic structures (Johansson and Fredberg, 2015). Realistic post-tensioning is uneconomical and required skilled technicians, but finite element procedures are relatively flexible to model and can be remodeled easily.

6.1.2. FE Post-Tensioning Techniques

In Finite Element software such as LS-DYNA the techniques available are as follows:

1. Dynamic Relaxation
   - Explicit
   - Implicit
2. Transient Explicit with Mass Damping
3. Implicit Analysis
4. Temperature-induced shrinkage technique, which is an explicit method, i.e. a negative temperature, is provided for prestressing of the tendons. Negative temperature produces contraction in tendon eventually transfer force to concrete. This is one of the most used technique until now in the literature (Jiang and Chorzepa, 2015) (Figure 6.2).

Figure 6.1 Numerical FE model of beam after prestressing effect (Johansson and Fredberg, 2015)

6.2. Finite Element Validation

One of the crucial objectives of FE modelling is the realistic validation of attained results with experimentation or concurrence with the physical phenomenon. Different aspects of FE model validation are like, confirmed to the material model used, and to exhibit the physical properties of the original material have achieved, and the realistic boundary conditions have achieved, contact between different parts and materials have met, and the loading type has modelled

realistically. This research presents three cases for validation as detailed in Table 6.1. Table 6.2 details the LS-DYNA material models sued in the present research.

Table 6.1 Dimensions of prestressing members and Impactor detailing used in Validation

References	Dimensions	Impactor	
		Weight	Velocity
(Kumar and Mittal, 2018), Prestress Slab	800 mm * 800 mm* 100 mm	243 kg	3.13 m/s
(Jiang and Chorzepa, 2015), Prestress Beam	130 mm * 200 mm * 3000 mm	221.4 kg	4.7 m/s
(Johansson and Fredberg, 2015), Prestress Beam	220 mm * 220 mm* 2600mm	50 kg	4.43 m/s

Table 6.2 Keywords of LS-DYNA used for PC members

Material	Keyword
Concrete	Winfrith Concrete MAT_084 with the erosion of 10 %
Rebars & Tendons	Plastic Kinematic, MAT_003
Guided Cable	Null, MAT_009
Missile	Plastic Kinematic with infinity failure Strain, MAT_003
Anchorage Plate	Nodal Rigid Body
Contact between Missile and Concrete	Eroding Surface to Surface, Missile – Master & Concrete – Slave
Contact between Missile and Beam elements	Eroding Nodes to Surface, Missile – Master & Beam elements - Slave
Contact between Concrete and Steel Liner	Tied Surface to Surface, Steel Liner – Master & Concrete - Slave
Post Tensioning of Tendons	Dynamic Relaxation technique with THERMAL_VARIABLE

6.2.1. Validation – 1

Four series of experiments on two reinforced concrete panels and two prestressed concrete panels have been considered for validation with freely falling impactor heights of 500 mm and 1000 mm, as shown in Figure 6.2 (Kumar and Mittal, 2018). Square shaped panels of 800mm subject to 243 kg falling impactor due to gravity had considered in this study, as shown in Figure 6.3. The setup had modelled in Hypermesh in Figure 6.4, and rigid anchorage nodes are created in LS-DYNA as in Figure 6.5, and the prestressing effect due to dynamic relaxation on concrete panels at zero time is noticeable in Figure 6.6.

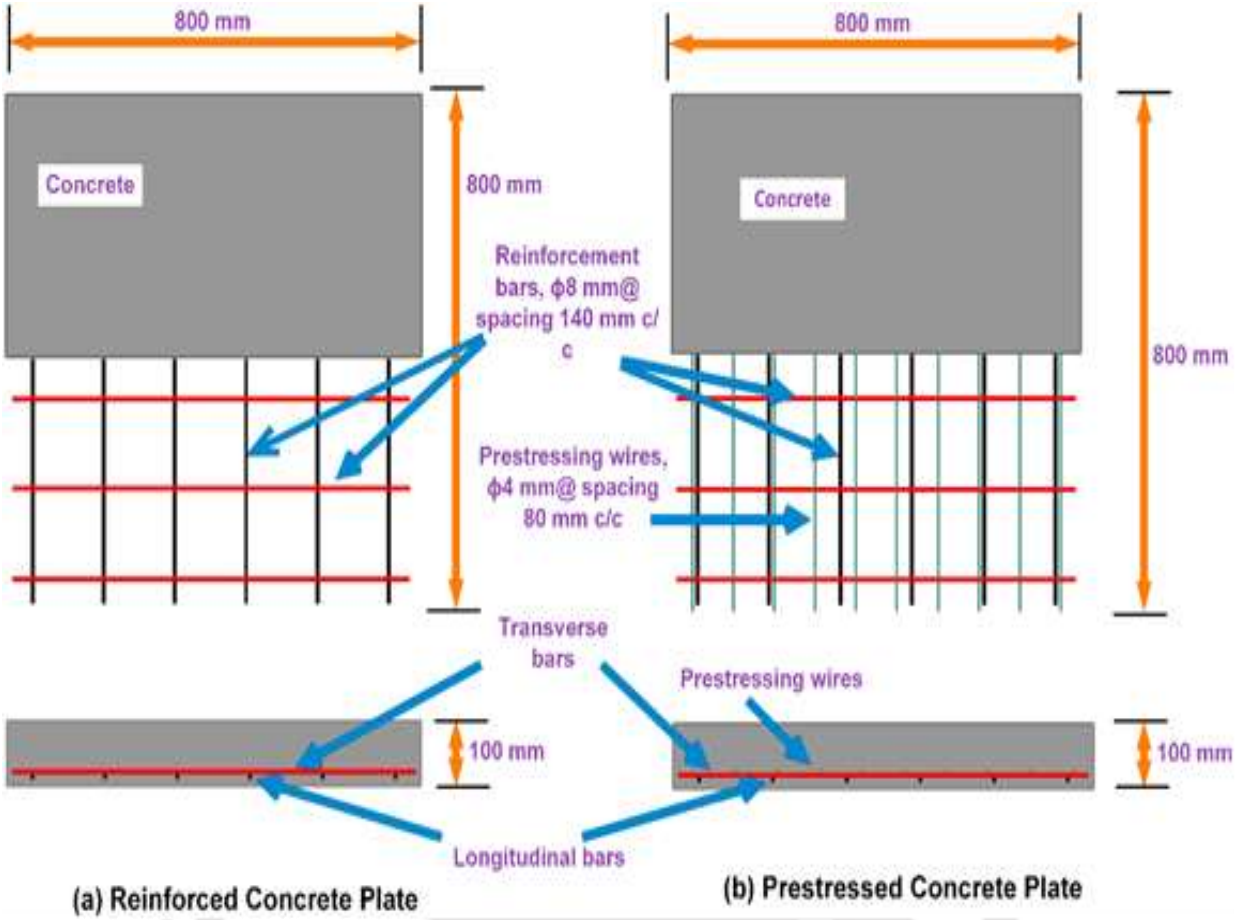

Figure 6.2 Reinforced and Prestress Reinforced Panels Detailing (Kumar and Mittal, 2018)

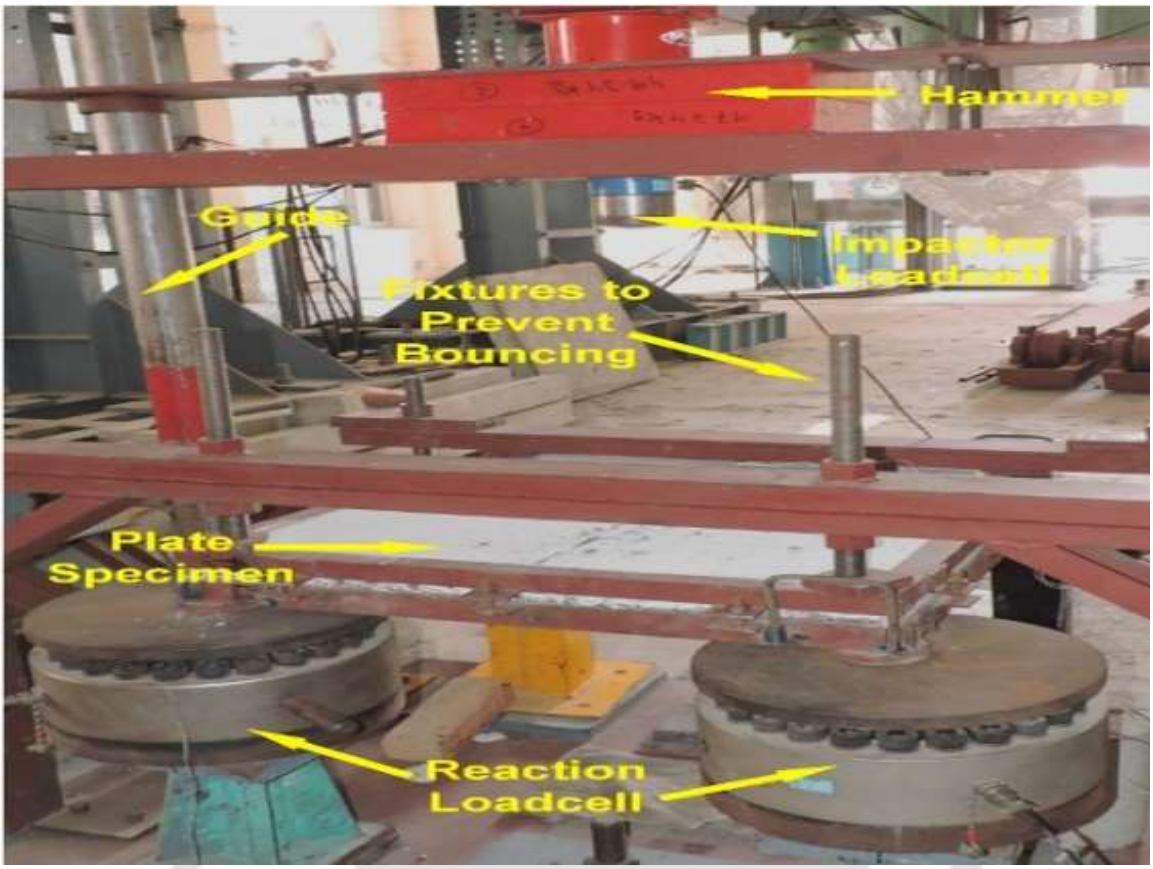

Figure 6.3 Experimental setup for impact test and impactor detailing (Kumar and Mittal, 2018)

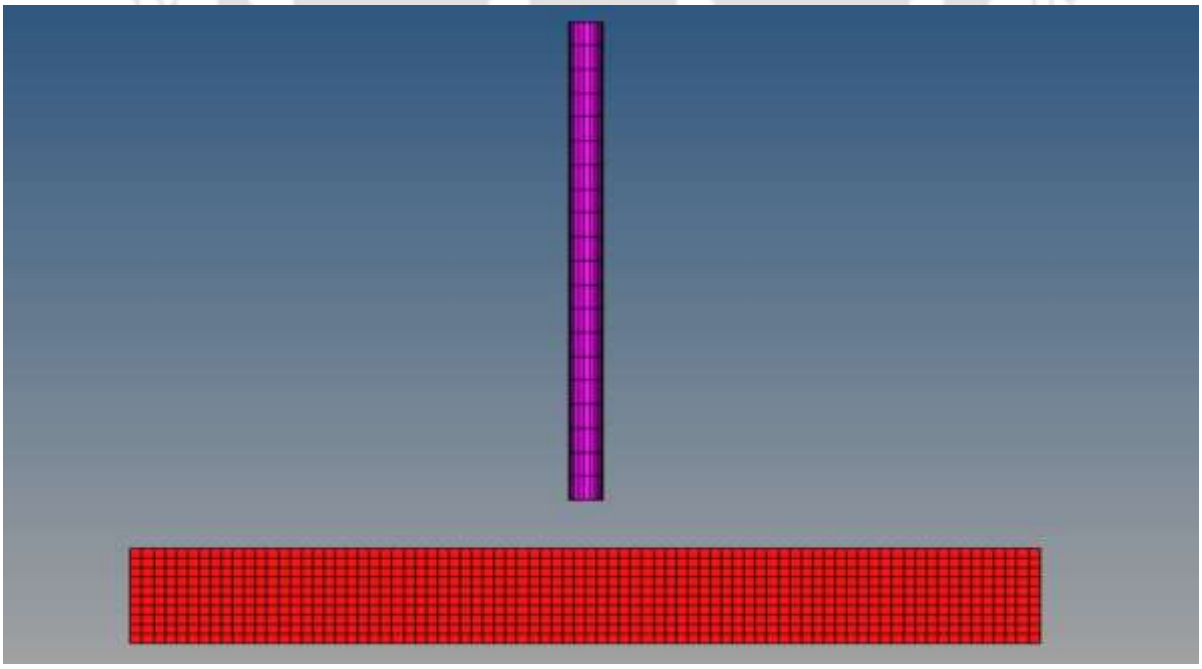

Figure 6.4 (Kumar and Mittal, 2018) Altair Hypermesh Modelling

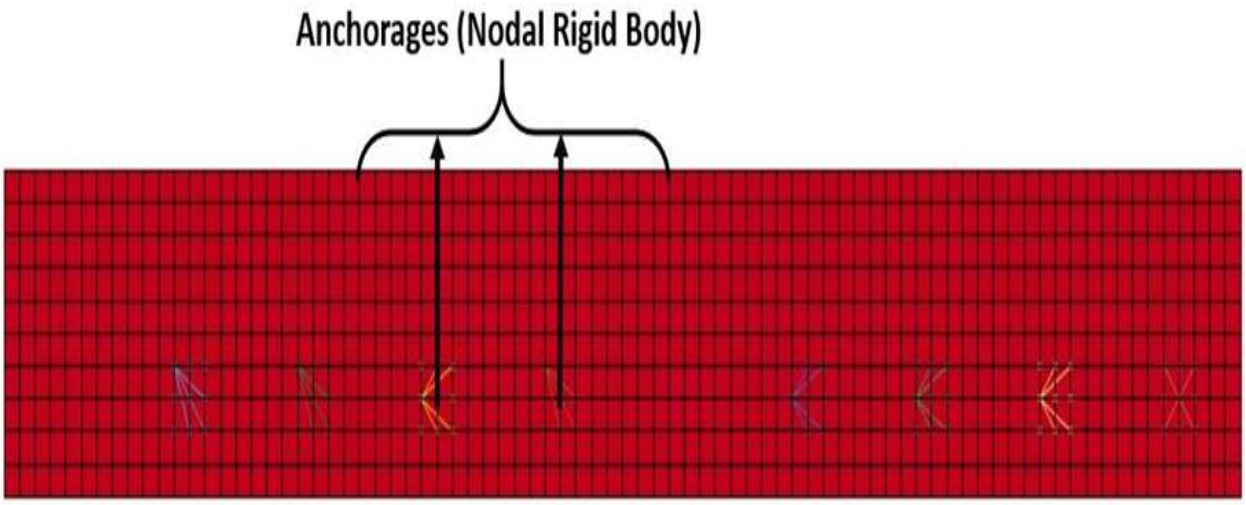

Figure 6.5 Anchorage plates modelled as Nodal Rigid Body, LS-Dyna

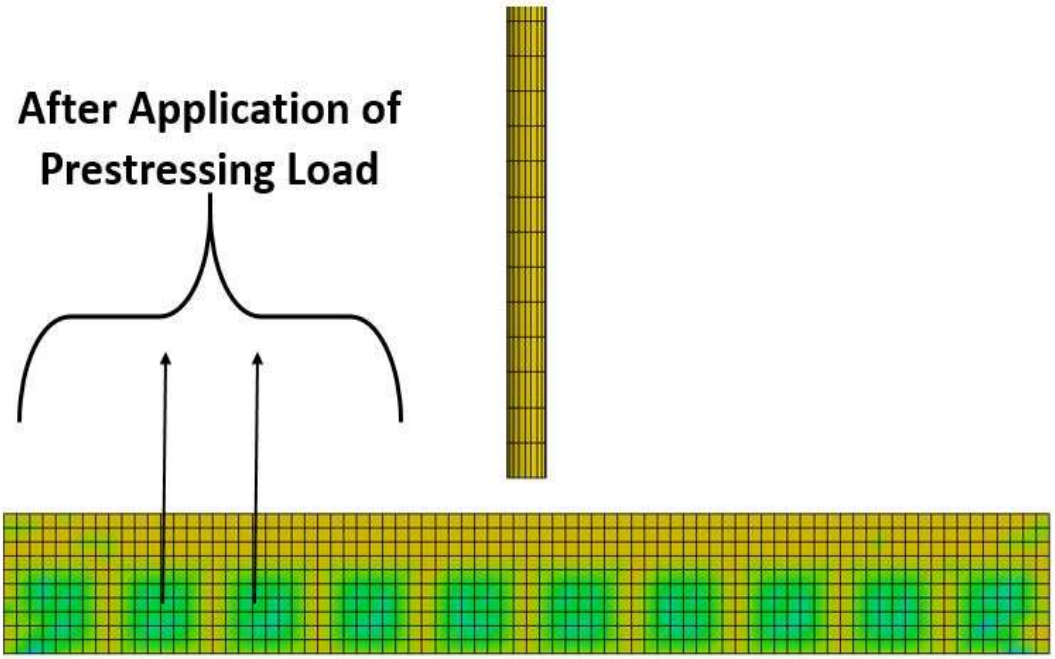

Figure 6.6 Prestressing Effect using Dynamic Relaxation Technique

The first validation is obtained by using the results for solid impactor on prestressed reinforced concrete panel conducted by (Kumar and Mittal, 2018) from a height of 500 mm. Details of the experiment can be obtained from (Kumar and Mittal, 2018). Initial prestress of 10 % is applied with unconfined compressive strength of 48 MPa as can be also inferred from Figure 6.7, i.e. 20 kN. Figure 6.8 shows the accurate simulation of the displacement profile from FE which conforms with the experiment. Figure 6.9 shows the accurate simulation of Impact –time history which agrees well with the experiment. Figure 6.10 shows good agreement between the FE and experimental results for the reaction force. Though peaks of impact force and reaction force of FEM and test are not similar, the profile phenomena identically matched with each other.

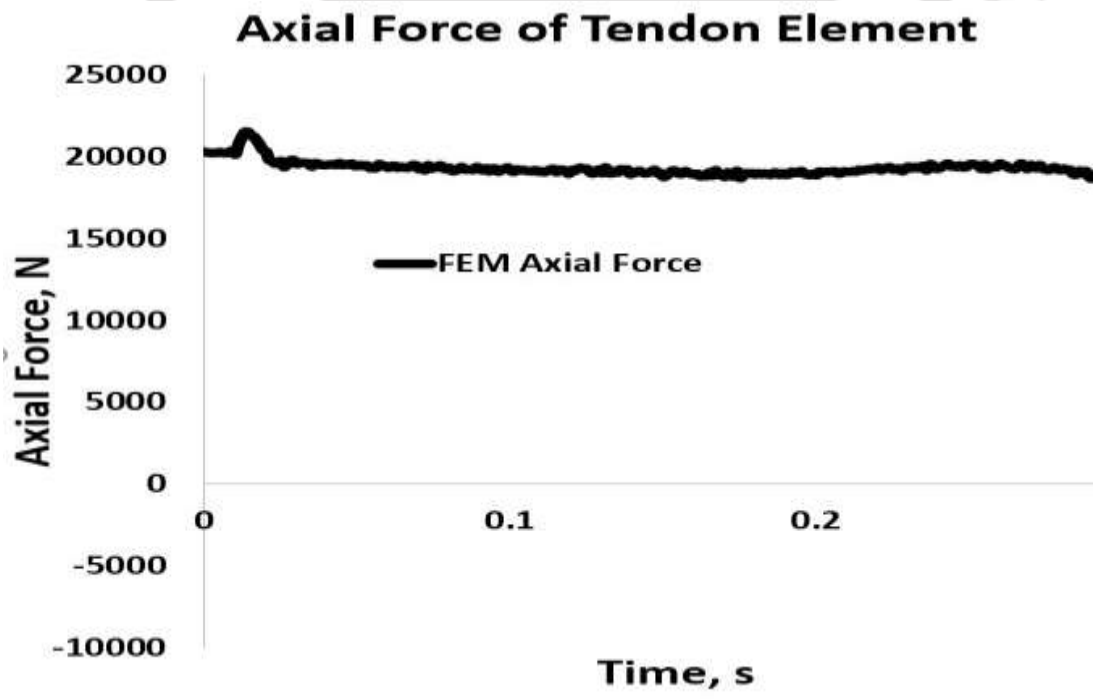

Figure 6.7 Axial Force comparison in Tendon Element for Validation -1

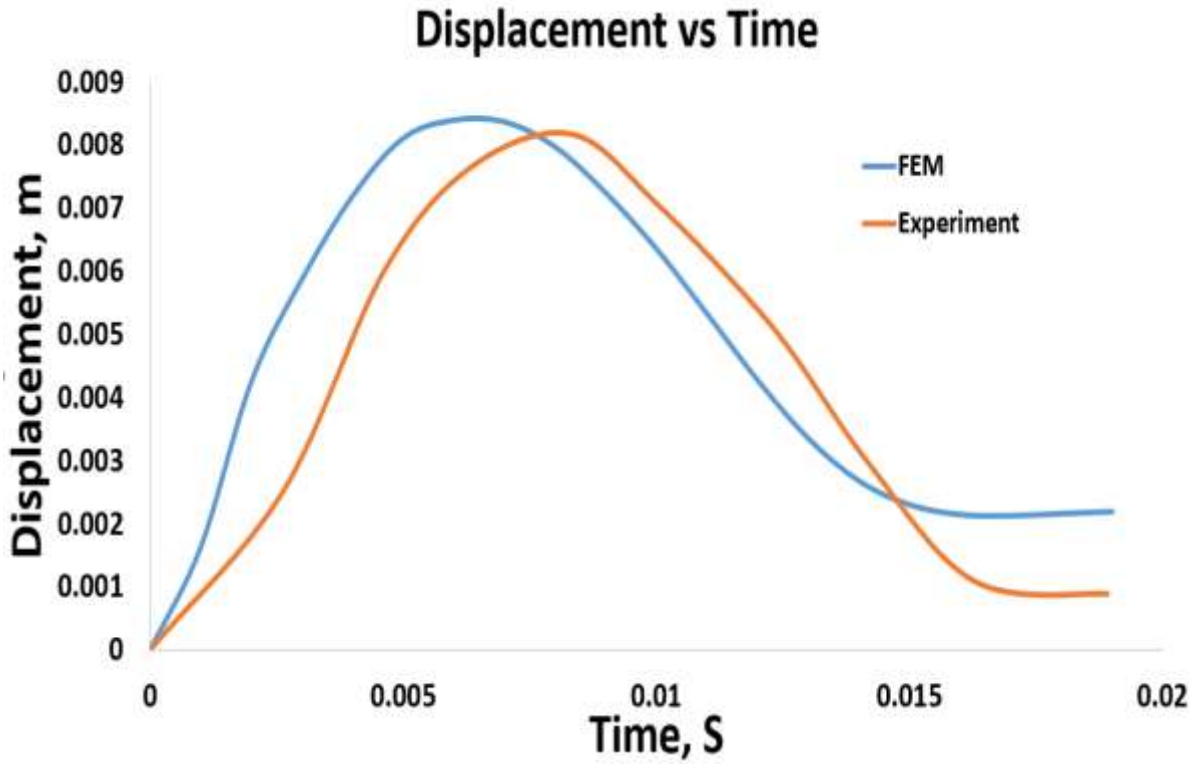

Figure 6.8 Displacement profile comparison for Validation -1

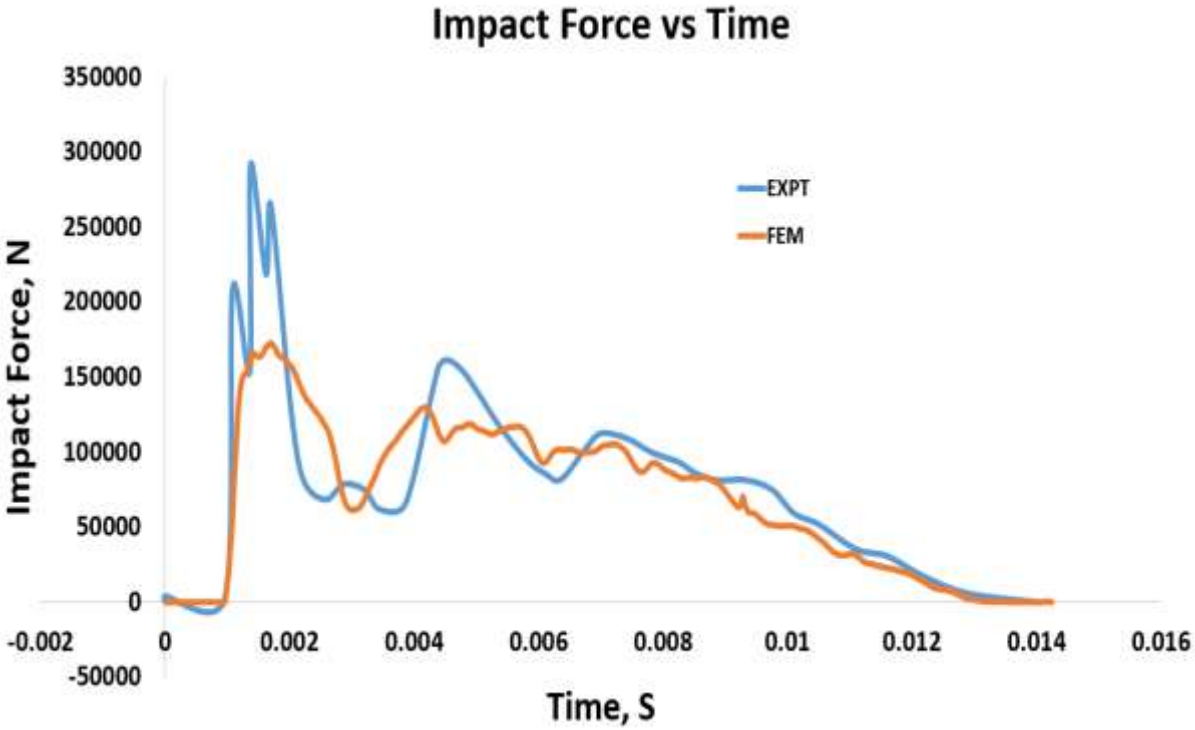

Figure 6.9 Impact Force comparison for Validation -1

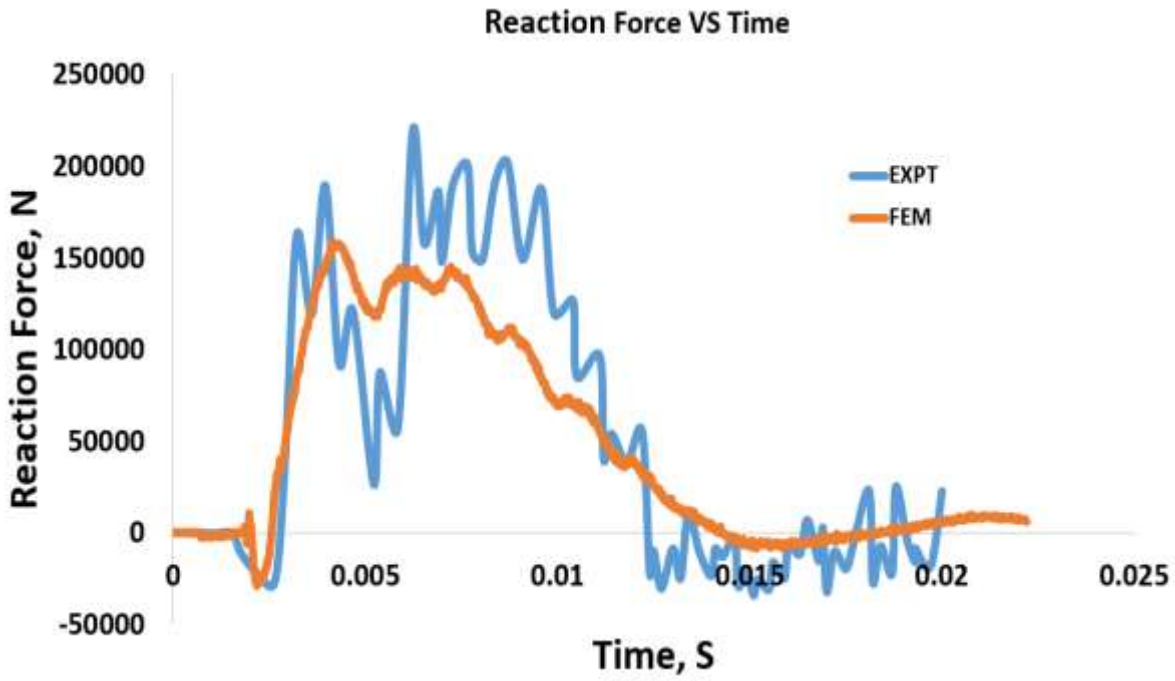

Figure 6.10 Reaction Force comparison for Validation -1

6.2.2. Validation – 2

Out of a few experiments, prestress concrete beam subject to 221.4 kg weight impactor is considered for validation (Jiang and Chorzepa, 2015). Beam length is 3000 mm and cube strength of 40 MPa with prestressing axial load of 195 kN each (Figure 6.11).

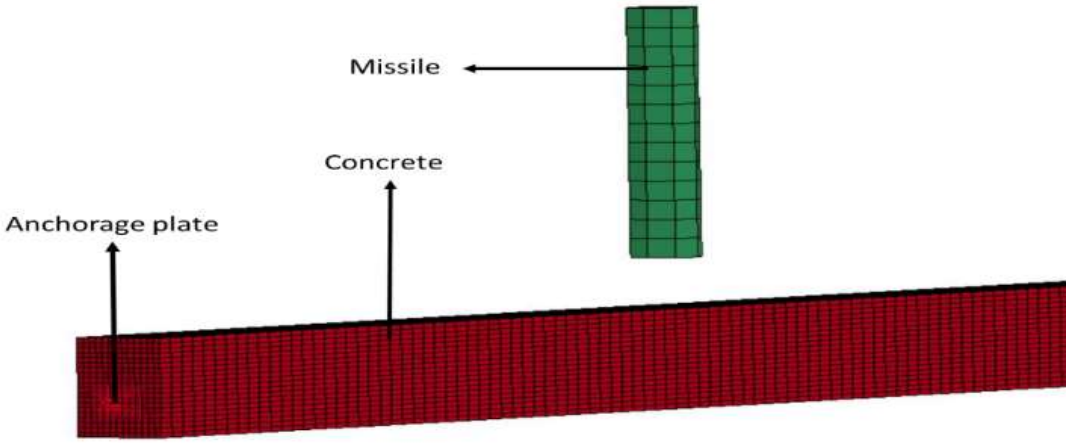

Figure 6.11 Anchorage rigid nodes in LS-DYNA

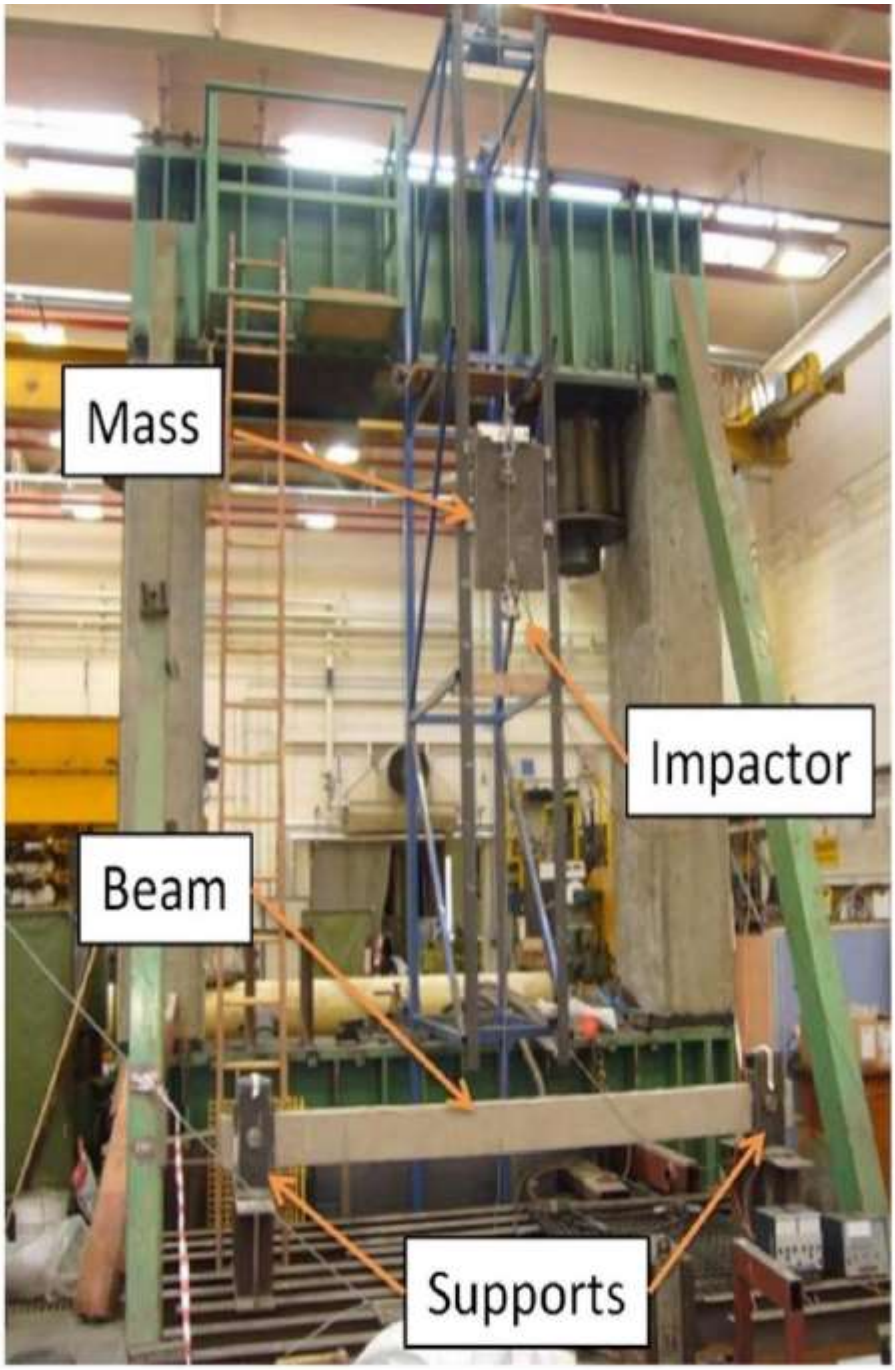

Figure 6.12 Experimental Setup of Jiang and Chorzepa, 2015

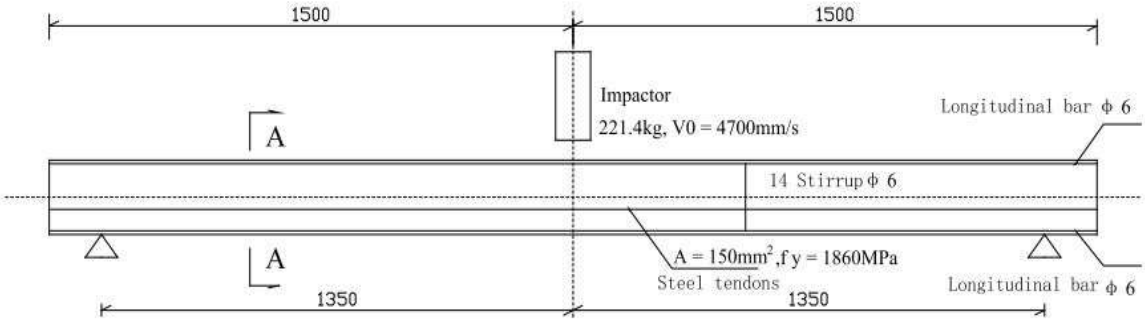

(b) Beam details and test setup.

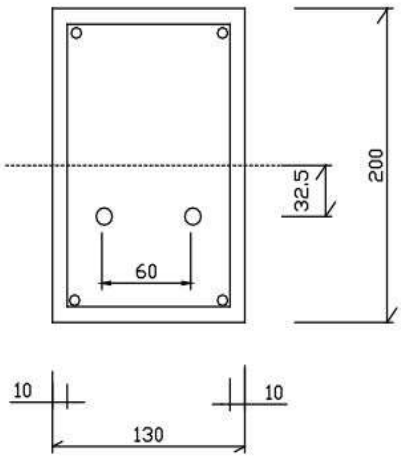

(c) cross section

Figure 6.13 Layout of Prestress Beam with the impactor

Figure 6.12 and Figure 6.13 shows the experimental setup. Parameters considered from experiments are displacement time history at the mid-span of a beam and impact force on concrete by impactor is compared with FE numerical simulation in Figure 6.16 and Figure 6.17. Prestressing axial force, deflection and concrete erosion due to impact is presented in Figure 6.14, Figure 6.15 and Figure 6.18. It is observed that all the physical phenomenon simulated by FE is in good agreement with the quantities obtained from experiments. Mesh size of 25 mm is used for the validation and boundary condition as per experiment i.e. beam is pin-end supported, and thus the two ends are free to rotate over a clear span of 2700 mm as shown in

Figure 6.13. This establishes that the FE simulation is able to simulate the presented experiment accurately.

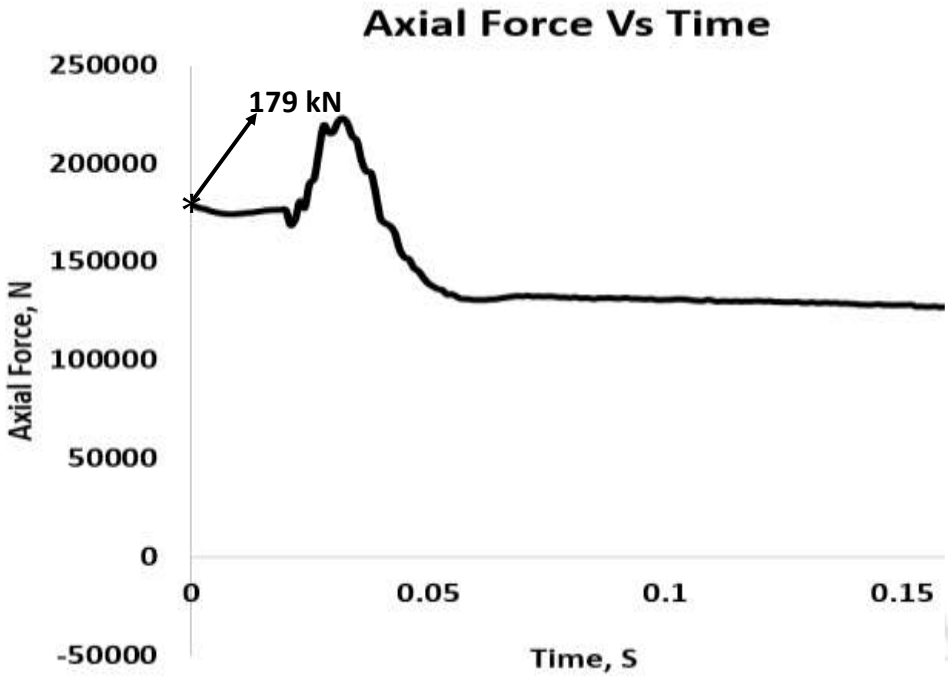

Figure 6.14 Axial Force of Tendon Element

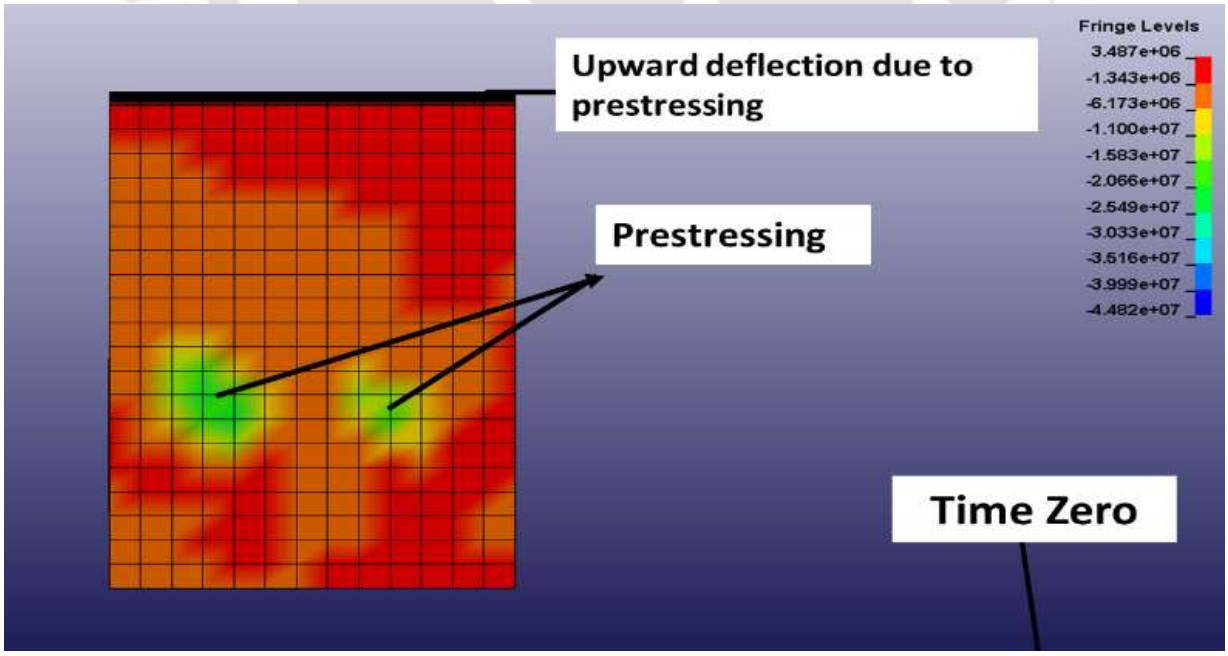

Figure 6.15 Deflection due to prestress at time zero

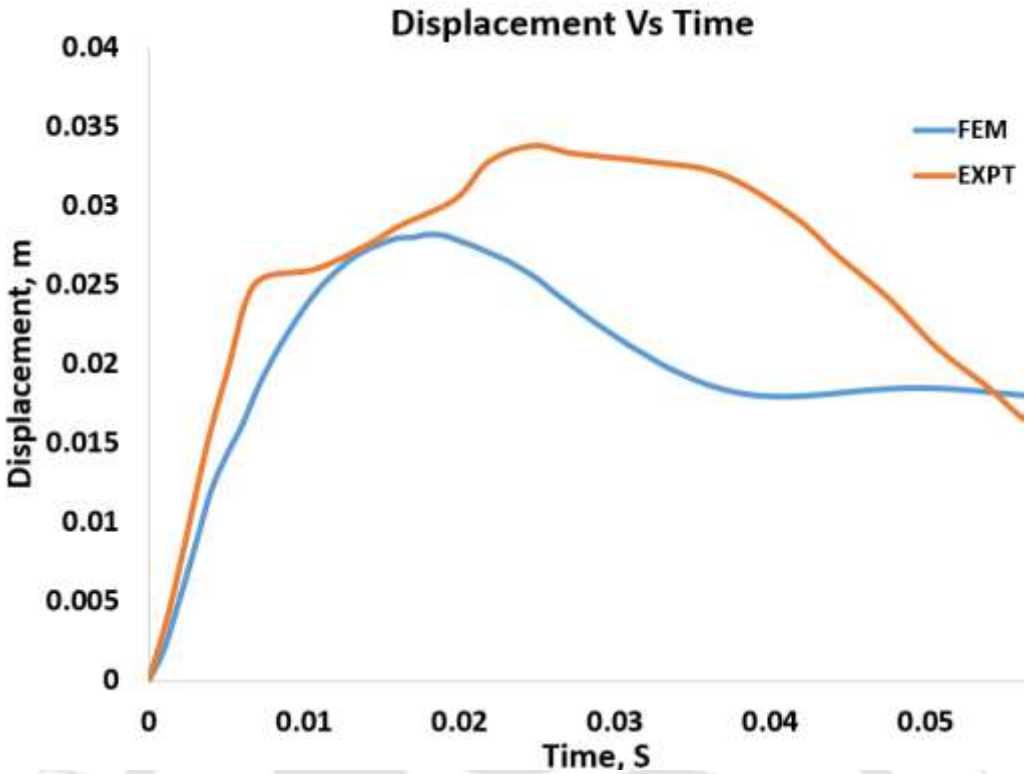

Figure 6.16 Displacement profile comparison for for Validation -2

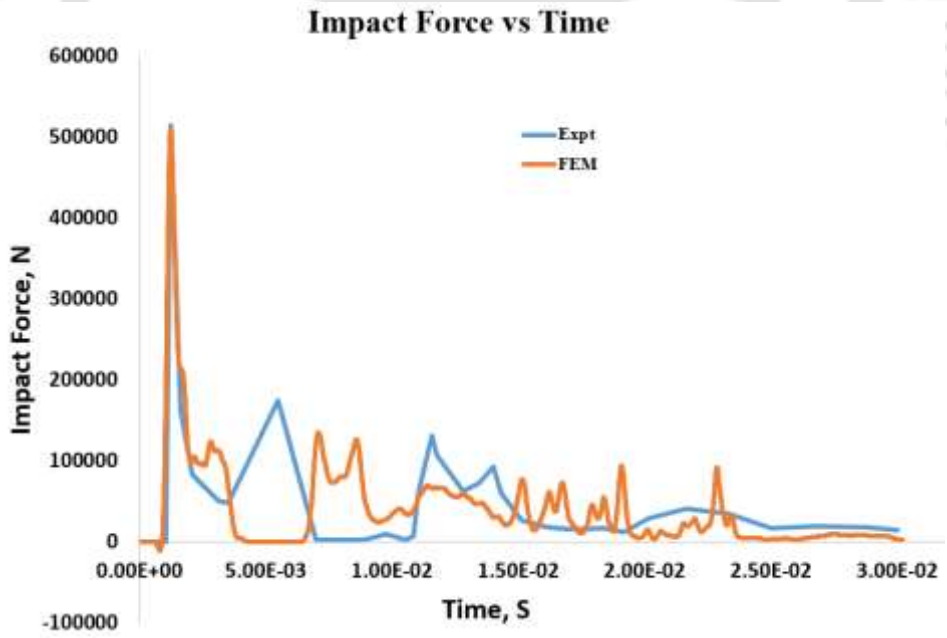

Figure 6.17 Impact force comparison for for Validation -2

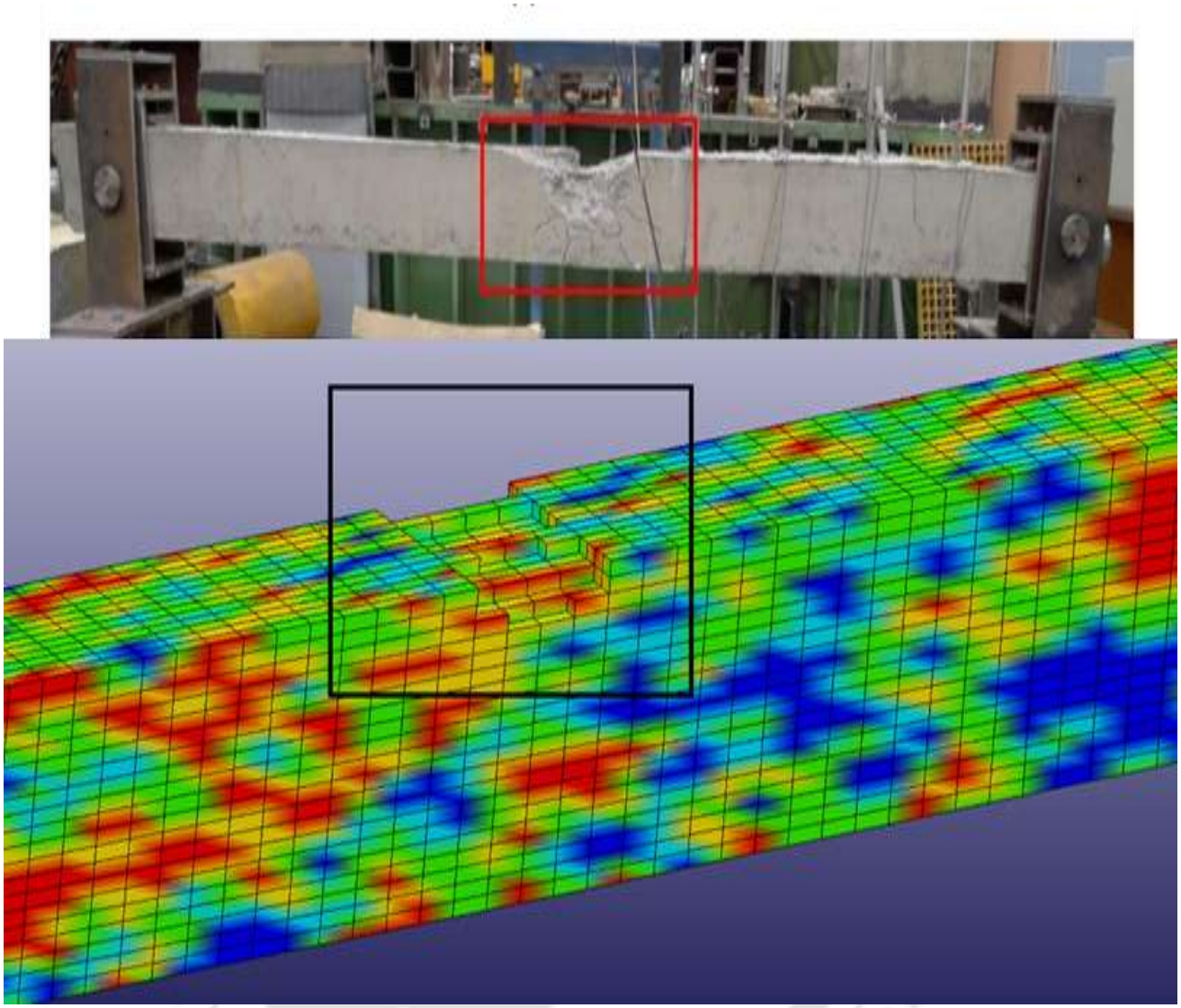

Figure 6.18 Concrete Erosion comparison for for Validation -2

6.2.3. Validation – 3

This validation is considering displacement obtained from analytical equations (Euro code), FE simulation results obtained from (Johansson and Fredberg, 2015) and FE simulation results obtained from this research as shown in Figure 6.19. One prestressed beam model has been considered with impactor mass of 50 kg and velocity of 4.43 m/s. Axial force used analytically is 164 kN and is validated the same as in numerical analysis as shown in Figure 6.20.

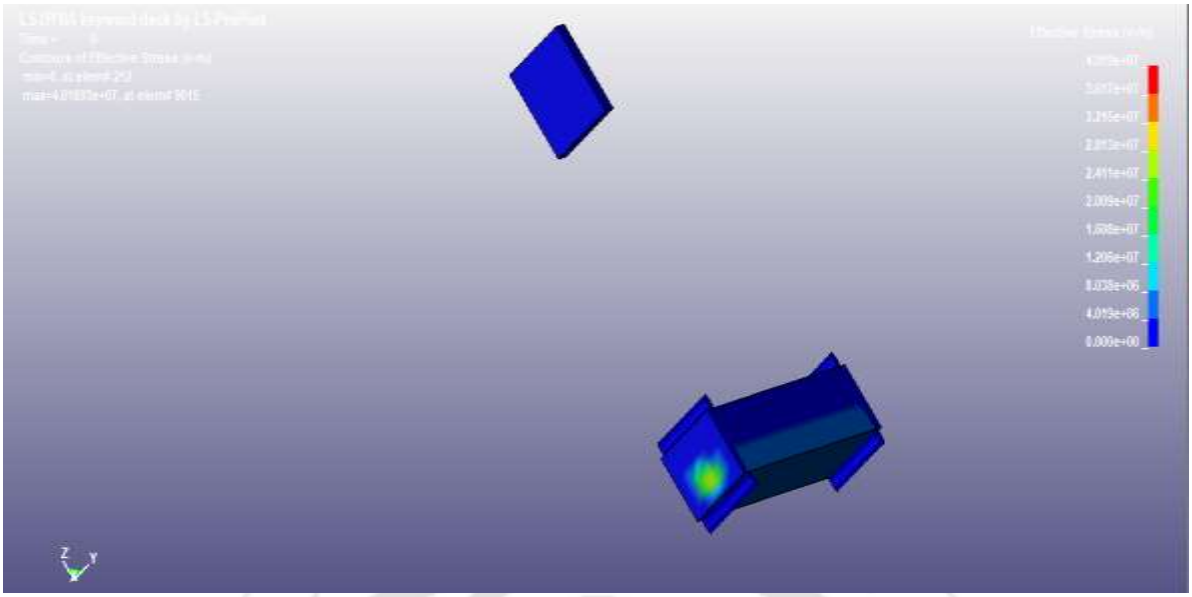

Figure 6.19 Beam with Prestressing Effect at Time Zero

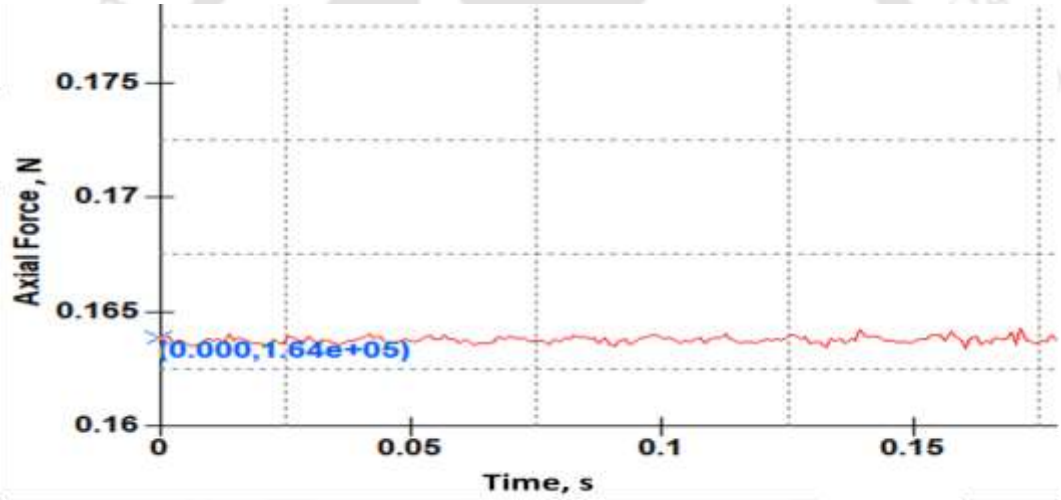

Figure 6.20 Numerical Axial Force in Prestressing Tendon

Figure 6.21 shows the comparison between the displacement profile as obtained from the analytical formulation, FE simulation of (Johansson and Fredberg, 2015) and FE simulation presented in the current study. All the three profiles are in good agreement.

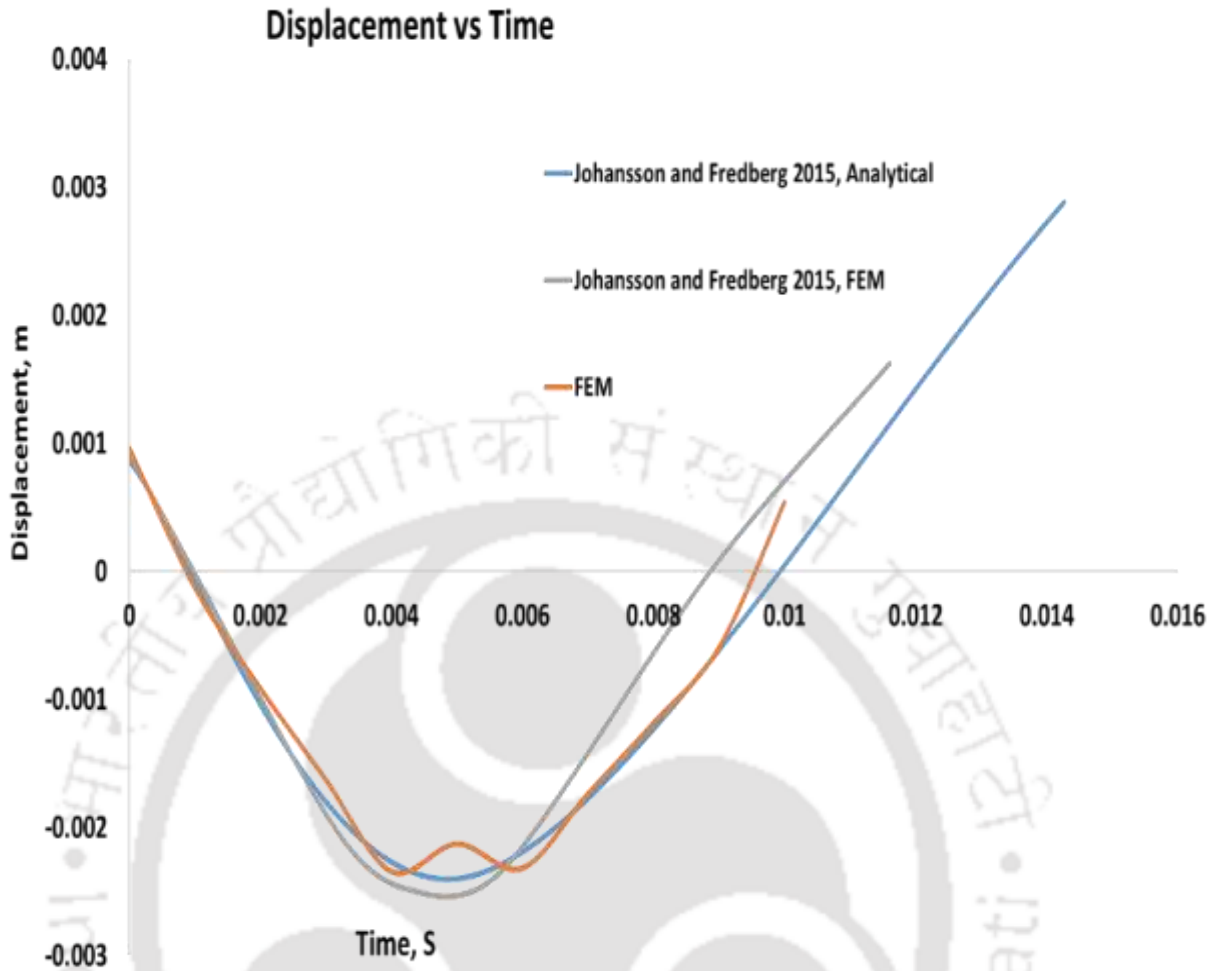

Figure 6.21 Displacement profile comparison for Validation – 3

Table 6.3 and Table 6.4 presents the comparison between the results obtained from the experiments and the FE simulated results presented in this study. A good agreement is achieved between the simulation and the experimental results. This establishes the accuracy of the FE simulation for modelling the phenomenon of missile impact on Prestressed Concrete (PC) members subject to missile impact.

Table 6.3 Comparison of results obtained from FE simulation and Experiment

References	Displacement, mm		Impact Force, kN		Reaction Force, kN	
	Expt/ Analytical	FEM	Expt/ Analytical	FEM	Expt/ Analytical	FEM
(Kumar and Mittal, 2018)	8.29 [E]	8.37	291 [E]	165	222 [E]	161
(Jiang and Chorzepa, 2015)	33.5 [E]	28.1	515[E]	511	-	-
(Johansson and Fredberg, 2015)	2.38 [A]	2.34	-	-	-	-

Table 6.4 Validation of Axial Force with FEM

References	Axial Force, kN	
	Analytical / Expt	FEM
(Kumar and Mittal, 2018)	20 [E]	20
(Jiang and Chorzepa, 2015)	195 [E]	179
(Johansson and Fredberg, 2015)	164 [A]	164

In order to obtain probabilistic models a range of experimental data is to be considered based on realistic data available like compressive strength of concrete, steel reinforcement ratio of rebars & tendons, the thickness of panel along with steel liner, missile mass and velocity, etc. These ranges are presented in following Chapter 7 which clearly explains the need for experimental design.

Chapter 7. FINITE ELEMENT DESIGN

7.1. Introduction

Estimation of key parameters for performance-based design such as missile impact effects, capacity and demand on RC and PC panels due to missile impact through data obtained from experiments involve more effort and cost. In this study, the focus is to develop probabilistic models for estimating the effects of missile impact on RC and PC panels and develop energy-based capacity and demand models which will be used for performance-based analysis and design of RC panels and PC panels forming the building blocks of Nuclear containment panels. The validity of a probabilistic model is only within the range of the data used for the model. Therefore, an accurate probabilistic model requires representative data that cover the entire range of the input variables. Also, there should be a sufficiently large amount of data to minimize the statistical uncertainty (Gardoni et al., 2002). Therefore, a large number of full-scale experiments would be needed to generate the required data. However, the availability of a number of full-scale experiments on RC and PC panels subject to different scenarios of missile impact is currently limited. Furthermore, creating an adequate database would require a large amount of resources and time. So, in this thesis, virtual experiments are conducted using refined FE analyses. The range of variables used for the experimental design is optimally selected so that they are representative of the range of actual RC and PC panels and applied missile loading scenarios. The FE analyses have the additional advantage of providing any response of interest and allow for parametric variations. Using the results of the obtained from the FE simulation, probabilistic models for estimating the local impact effects, capacity and demand on RC and PC are developed in subsequent chapters.

7.2. Selection of Variables and Range

For the FE simulations, instead of considering whole containment structure, a regular panel subject to missile impact load is considered based on the length to depth ratio. In order that the developed models are valid in the realistic scenarios, the entire range of input variables should be considered. In order to minimize the statistical uncertainty, there is a requirement of a huge amount of data. The existing literature is analyzed to obtain the ranges of variables which realistically cover the parameters such as the geometric and material properties for panels, rebars and tendons ratio, missile mass and velocity (Wen & Xian, 2015) (Balomenos and Pandey, 2017; Huang *et al.*, 2017; Jin *et al.*, 2019) (Choi *et al.*, 2017). The range of variables taken in this study covers both the existing as well as the upcoming range of nuclear containment panels. The range of missile weight and velocity in this research are confined to mainly cruise type missiles which are existing globally. The experimental design is considered a total of flat 50 RC panels and 100 curved PC panels subject to various missile velocities and mass combinations at the central part of the structure. Steel liner is placed at the rear side of the containment structure to resist internal hazards like an internal blast.

7.3. D-Optimal Point Selection Scheme

The prosperity of finite element based simulations to amplify or to replace the physical representation of experiments has accelerated the development of simulation based optimization in recent years (Stander et al., 2002). Response surface methodology (RSM) (Box & Wilson, 1951; Myers et al., 1995) is having its roots in statistics of realistic experimentation. Due to the advantage this method is used as primary gradient-free simulation-based approach. The unavailability of general analytical code arises a problem in non-linear finite element formulation. In case of no codal provisions by means of finite differences may result in invalid gradient information. However, these reasons RSM has become a well-used technique

especially in impact related problems where the response is highly nonlinear. LS-OPT is computer based tool which comprises of D-Optimal design of experiments.

The methodology for this technique is to fix the range of the variables i.e. lower bound and higher bound of the design variables which is based on the structural configuration. Number of cases required for probabilistic analysis need to be fixed. In the design of experiments for appraisal of statistical models, optimal designs allow parameters to be evaluated impartially and with minimal variance. A non-optimal design requires a more significant number of experimental runs to estimate the parameters with the same precision as an optimal design. In general terminology, optimal experiments can minimize the expenditure of experimentation.

Based on the considered range the best set of cases are selected using D-optimal point selection scheme (Myers et al., 1995). This D-optimal plan is considered due to its flexibility of permitting any number of designs to be arranged in design space with an irregular boundary. The D-optimal scheme is also the recommended point selection scheme for polynomial response surfaces (Livermore Software Technology Corporation 2006). Overall, 150 cases are simulated to obtain data for the missile impact effects on RC and PC panels in order to develop probabilistic models for performance levels, capacity and demand models. Table 7.1 and 7.2 shows the range of variables considered in this research. FE models of the 50 combinations of RC panels and 100 combinations of concrete nuclear PC containment with the flat hard missile impact loading scenarios are simulated to obtain the database for the development of probabilistic models. In general, panel size ranges from 2 – 7 m in length. The thickness of the concrete panels range is based on realistic data available in the literature. The grade of concrete for Nuclear Containment structures usually uses in between 30 – 55 MPa but in this study up to 80 MPa is considered. Yield strength of rebars and liner is taken based on the availability of commercially available grade of steel. The thickness of steel liner is as per guidelines of Nuclear containment structure obtained from the literature. Boundary conditions for panels are

fixed for all sides of the top and bottom edges. Missile mass and velocity are based on available ranges of existing missiles all over the world.

Table 7.1 Range of Basic Variables for RC panels

Variable	Symbol	Range
Length of Panel (m)	L_s	2 – 6
Thickness of Concrete Panel (m)	t_c	0.2 – 0.5
Longitudinal Reinforcement Ratio (%)	-	1 – 3
Transverse Reinforcement Ratio (%)	-	1 – 3
Compressive strength of concrete (MPa)	f_c	25 - 55
Yield strength of reinforcement (MPa)	f_y	250 – 550
The boundary condition of the slab	-	Four side top and bottom edge fixed
Missile Mass (kg)	M	0 – 2500
Missile Velocity (m/s)	V_0	0 - 1000

Table 7.2 Range of Basic Variables for PC panels

Variable	Symbol	Range
Length of Panel (m)	L_s	2 .8 – 7.5
Thickness of Concrete Panel (m)	t_c	0.7 – 1.5
Longitudinal Reinforcement Ratio (%)	-	1 – 3
Transverse Reinforcement Ratio (%)	-	1 – 3
Longitudinal Tendon Ratio (%)	-	1 – 3
Transverse Tendon Ratio (%)	-	1 – 3
Concrete's Compressive Strength (MPa)	f_c	30 – 80
Yield strength of reinforcement (MPa)	f_y	250 – 550
Steel Liner Yield Strength (MPa)	-	250 – 550
Steel Liner Thickness (m)	t_s	0.06 – 0.1
The Boundary Condition of the Panel	-	Four side top and bottom edge fixed
Missile Mass (kg)	M	0 – 2500
Missile Velocity (m/s)	V_0	0 - 1000

7.4. Illustration of Curved PC Panel

This section illustrates the modelling of a curved PC panel based on the database generated from the experimental design as detailed in the previous section. Hypermesh (Altair Computing, 2006) is used to model the geometry of the panel (Table 7.3 and Table 7.4). The panel consists of a concrete slab with curvature, steel liner at the rear side of the concrete, double steel reinforcement in both directions, tendons placed above and below the centerline subjected to a flat-nosed missile (Figure 7.1). A three-dimensional solid model is utilized for modelling concrete slab, steel liner and missile. All these three parts are modelled by a constant stress solid element. Reinforcement and tendons are modelled as one-dimensional beam element and modelled as Hughes-Liu with cross-section integration; the hourglass is minimized. Anchorage nodes are modelled to ensure post-tensioning prestress to the concrete panel (Figure 7.2 and Figure 7.3). The simulation is done in two stages. In the first phase, prestressing of tendons is done, i.e. stress initialization using dynamic relaxation technique and in second phase transient analysis for impact, analysis is performed. Boundary conditions are restrained in the top and bottom edge nodes. Initial velocity generation keyword is used to initiate missile velocity after dynamic relaxation.

Table 7.3 Detailing of Curved PC panel

Dimensions	Steel Liner		Rebars		Tendons		Temper
Concrete (l*b*h)	Thick - ness	Yield Stress	Dia	Yield Stress	Dia	Yield Stress	- ature
4m*4m*1m	0.8m	535 MPa	40 mm	535 MPa	130 mm	1220 MPa	-31^0 C

Table 7.4 Missile Properties

Yield Stress	Dia	Weight	Velocity	Strain
250 MPa	0.13 m	208.5 kg	440 m/s	1e+28

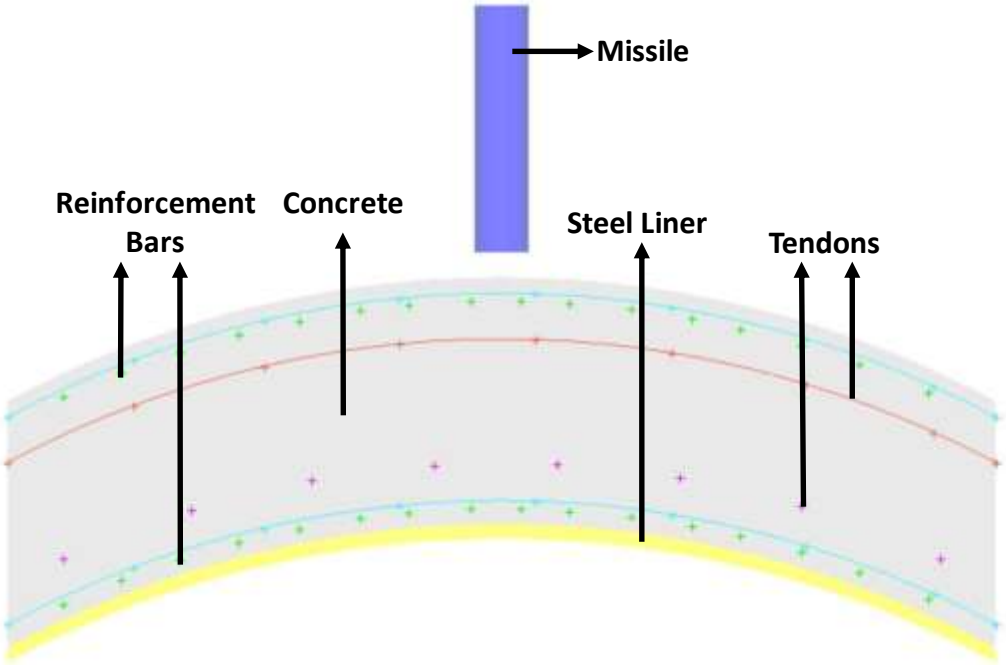

Figure 7.1 Hypermesh modelling of considered geometry

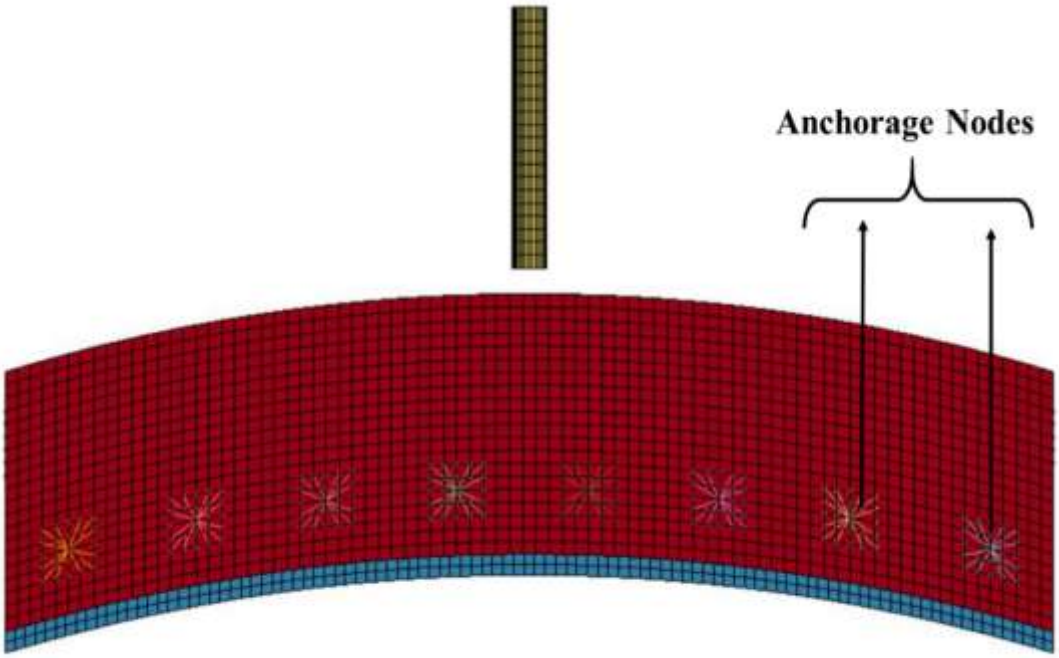

Figure 7.2 Modelling of Anchorage Nodes in LS-Dyna

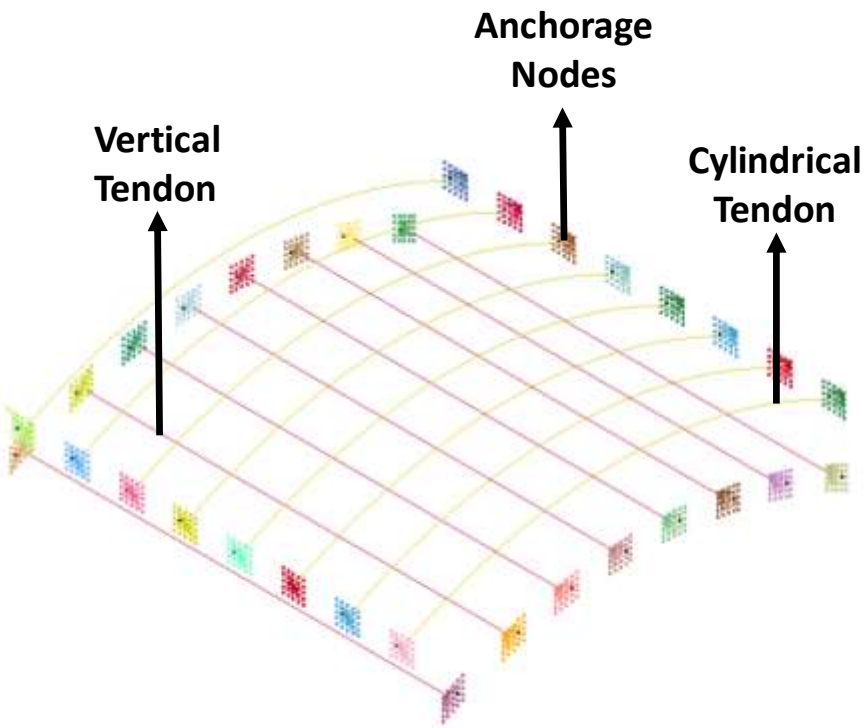

Figure 7.3 Cylindrical and Vertical Tendons with anchorage

7.4.1. Results

Figure 7.4 shows the value of the initial prestresses obtained from the simulation. The general axial force provided to prestress tendon is in between 4000 kN – 10000 kN but in this illustration, it is observed near to 8000 kN prestressing force with a negative temperature of 31^0 C. Figure 7.5 and Figure 7.6 shows the same phenomenon as an illustration applied in the PC panel across different planes. Figure 7.7 shows the penetration of the missile inside the curved PC panel. This illustrative example shows that a curved PC panel will be used to generate the database for the development of probabilistic models which closely resembles the realistic Nuclear containment structures which are vulnerable to missile impact.

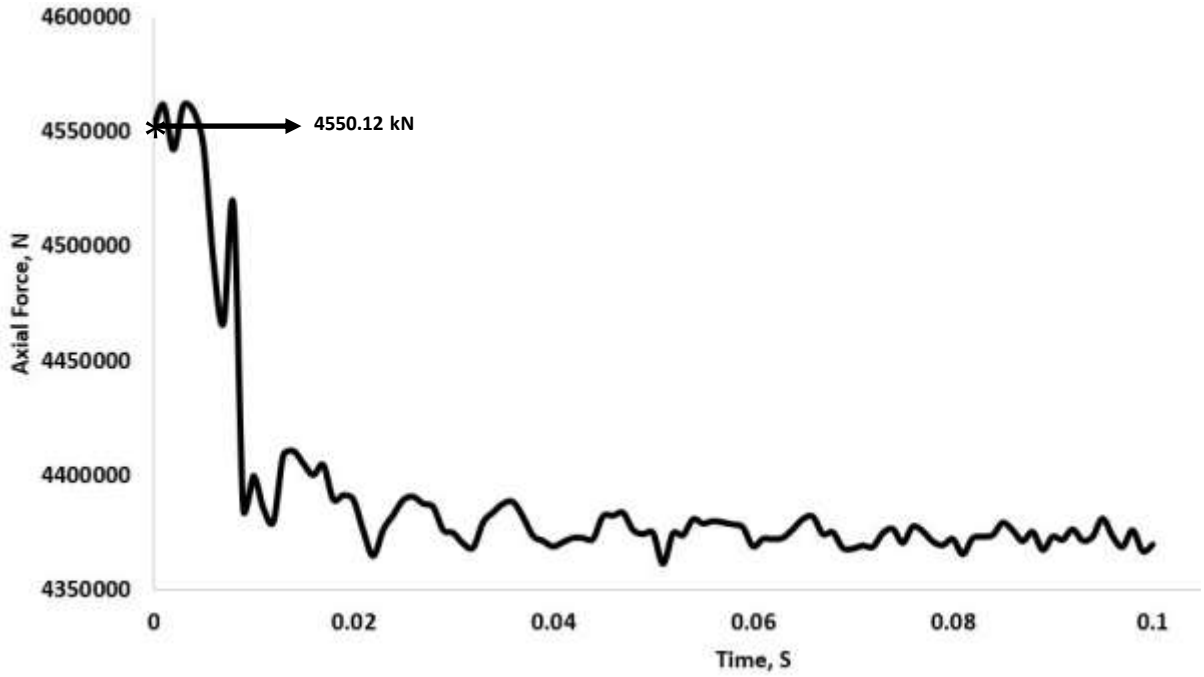

Figure 7.4 Axial Force of Tendon element

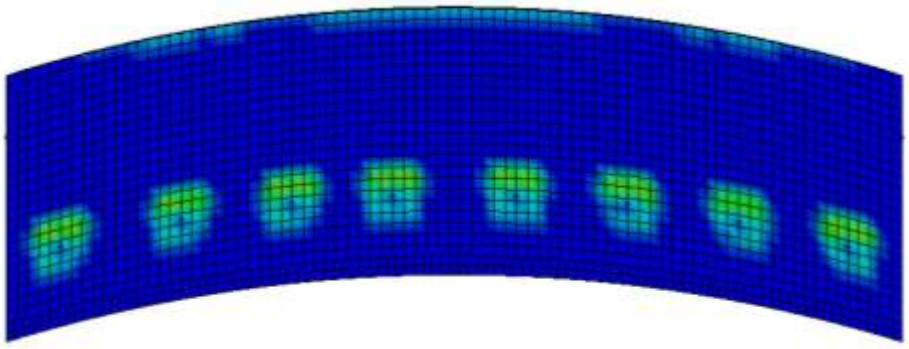

Figure 7.5 Prestressing effect on panel in XZ-Plane

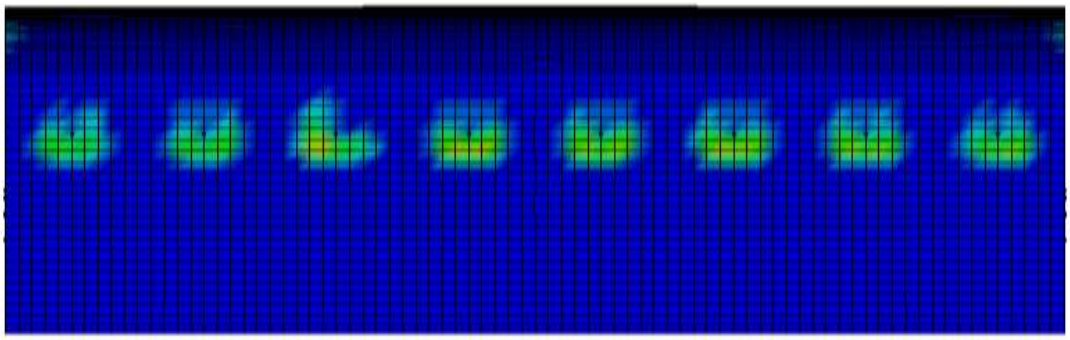

Figure 7.6 Prestressing effect on a panel in YZ-Plane

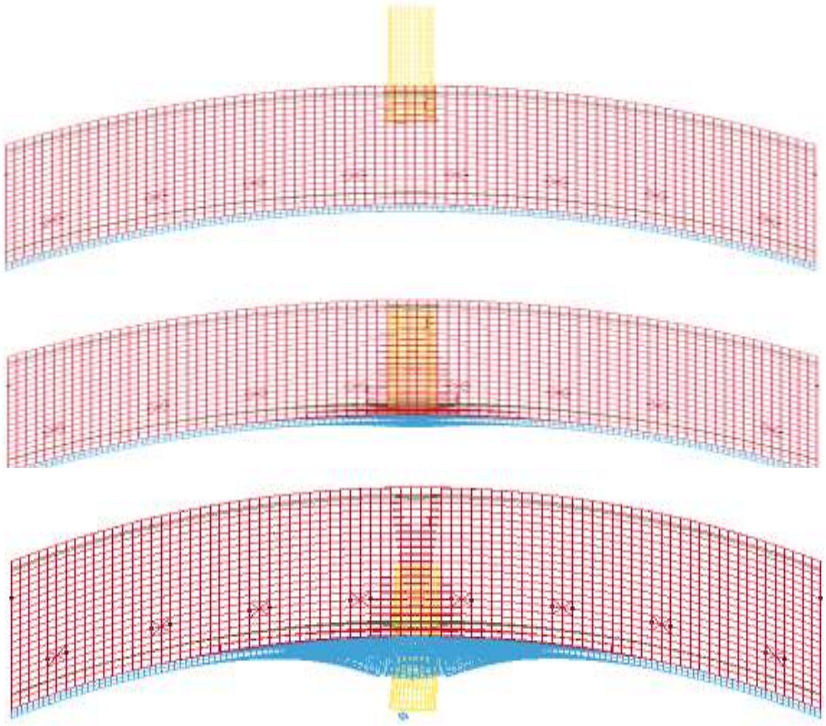

Figure 7.7 Missile Impacting into Target

Likewise, 50 RC and 100 PC panels are simulated and the database is generated from these FE simulations for the development of probabilistic models for estimating the different performance levels, capacity and demand of RC and PC panels subject to missile impact. The development of the models is presented in subsequent chapters.

Chapter 8. PROBABILISTIC PERFORMANCE LEVELS FOR RC AND PC PANELS OF NUCLEAR CONTAINMENT STRUCTURES

In Chapter 4, performance levels of the target structure where the panel are subject to missile impact were identified to define damage states. In Chapter 2, a different empirical formulation which already exists in the literature were presented which represents the physical quantities for defining the different performance levels. But, due to the complex phenomenon, large variation in the material properties, boundary conditions, uncertainty involved, these empirical formulations are not always able to capture the quantities accurately. As such, a probabilistic approach is taken in this research to develop accurate formulations for different performance levels. The formulation of probabilistic models is made from a database obtained from FE design done in the previous chapter (Chapter 7). For RC panels, a total of 50 simulations without steel liner and curvature is considered, and for PC panels, 100 FE simulations with a steel liner and curvature is used for the development of probabilistic models.

In this chapter, probabilistic models are developed for parameters like penetration depth of panel, perforation limit of the target structure and residual velocity of a missile for both PC and RC panels subject to missile impact.

These probabilistic models account for various relevant uncertainties like material modelling, statistical uncertainty, panel curvature, strain rate, boundary condition, and other aleatoric and epistemic uncertainties. It is assumed that the data used in model assessment from FE simulations have no uncertainty in measurements. Since FE simulations (HYPERMESH, LS-DYNA) is used for modelling and analyzing the probabilistic models, the measurements

and model inexactness errors are taken care of automatically. Increasing in data can lead to diminish the error like statistical uncertainties. The probabilistic models developed in this research are unbiased and incorporate a good understanding of the mechanics of the problem. This study is following a general methodology proposed by (Gardoni *et al.*, 2002) to formulate probabilistic models. Set of experimental or FE simulated data is required in order to develop these models. Various constraints for the availability of experimental data, FE simulations are used to produce the data through the Design of Experiments (DOE) as given in Chapter 7. Available data utilised to calibrate the probabilistic models. The equality data, as well as lower bound data, are used to construct the probabilistic models.

Construction of the current formulation of probabilistic models is by adding required correction terms to the mechanical models. As the data assessed in FE simulations are without error or uncertainty, as mentioned above. A general formulation for probabilistic models proposed by (Gardoni *et al.*, 2002) is formulated as

$$\left[P_i\left(x, \Theta_{P_i}\right)\right] = \quad [p_i(x)] + \gamma_{P_i}\left(x, \theta_{P_i}\right) + \sigma_{P_i} e_{P_i} \tag{8.1}$$

Where P_i = Probabilistic performance level of a panel for different parameters such as penetration depth of missile, perforation limit of concrete target and residual velocity of missile and; p_i = Mechanical performance level of a panel for different parameters such as penetration depth of missile, perforation limit of concrete target and residual velocity of a missile; $\gamma_{P_i}\left(x, \theta_{P_i}\right)$ = correction term for the bias inherent in the mechanical model defined as

$$\gamma\left(x, \theta_{P_i}\right) = \sum_{\mathrm{j}=1}^{\mathrm{n}} \theta_{P_i,j} h_{P_i,j}(x) \tag{8.2}$$

Where $h_{P_i,j}(x)$, j = 1,…,n = explanatory function (or regressors) defined as functions of x, $\theta_{P_i,j}$, j=1,…,n are the parameters associated with explanatory functions, $\sigma_{P_i} e_{P_i}$ = model error,

e_{P_i} =Gaussian error and Θ_{P_i} = θ_{P_i} = set of unknowns model parameters in which θ_{P_i}=($\theta_{P_i,1}$,K,$\theta_{P_i,k}$).

In this thesis the procedure for developing probabilistic models for RC and PC panels is given below,

- The required parameters like penetration depth, residual velocity, perforation limit are recorded from FE simulations.
- Validation with existing formulae as shown in Figure 5.6 and Figure 5.7 (Due to significant error in the results, a novel probabilistic formulation is developed)
- With the advantage of existing formulae and intuitions, mathematical terms are designed e.g. energy based terms of missile and panel, slenderness ratio, etc.
- The aim of validating FE recorded data with probabilistic formulation is established using Regression analysis.

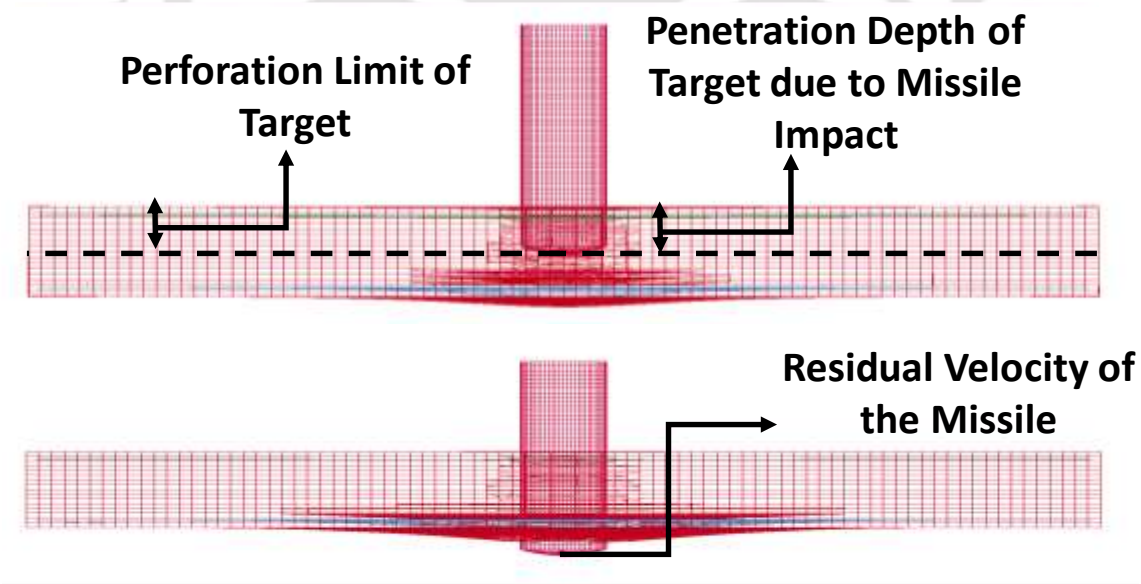

Figure 8.1 Penetration depth of the missile, Perforation limit of the target and Residual Velocity of the Missile in FE model.

8.1. Probabilistic Models of RC Panels

Using the results from FE simulation following the experimental design as detailed in Chapter 7 for 50 RC panels, this section develops probabilistic models for predicting the penetration depth (x), residual velocity (V_r).

8.1.1. Probabilistic Model for Penetration Depth (x)

The penetration depth of missile into target for all FE simulations is noted down as shown in Figure 8.1. The newly proposed equation in this thesis by the author to estimate the probabilistic penetration depth (x) of an RC panel subject to flat nose missile impact loading after the probabilistic analysis is,

$$\frac{x}{d} = -2.0556 + 2.1393 \ln\left(\frac{MV_0^2}{d^3 f_c}\right) \tag{8.3}$$

σ=0.0047, cov=0.0299, d – diameter of the missile (m), M –Mass of the missile (kg), f_c – Compressive strength of concrete (N/m^2), V_0 – Velocity of missile (m/s), x – Penetration depth into the concrete target (m), σ = Standard Deviation, cov = Coefficient of Variation

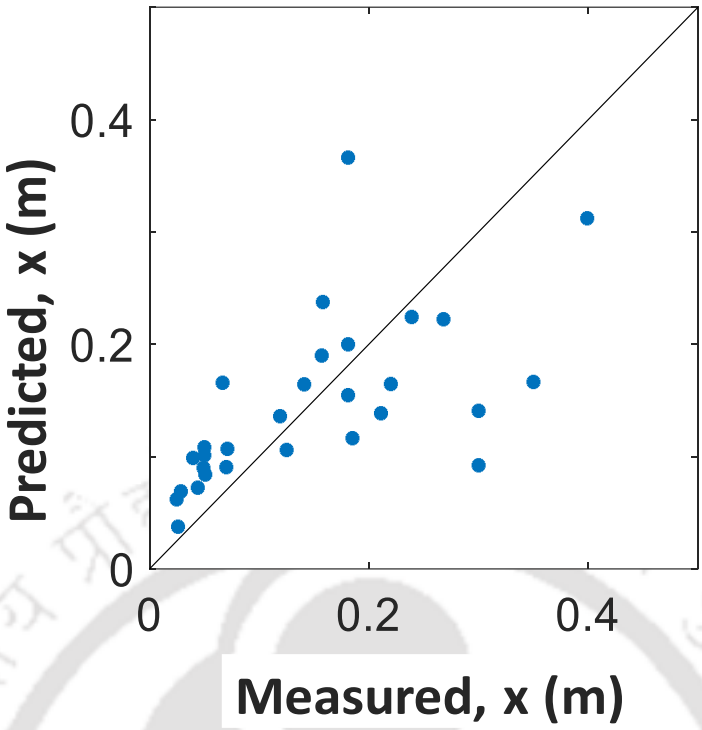

Figure 8.2 Probabilistic Penetration vs Simulation Penetration depth of RC Panels

Figure 8.1 shows the comparison between probabilistic and simulated penetration depth of missile into RC target. The data contains equality data. The predictions of the probabilistic model show that the equality data lays both above and below the 1:1 line. The probabilistic model corrects this inherent bias in the determistic model. The cov is 3% which details the accuracy of the developed probabilistic model for estimating the penetration depth of missile into RC target.

8.1.2. Probabilistic Model for Residual Velocity (V_r)

The residual velocity of the missile for all FE simulations is noted down as shown in Figure 8.1. A plot of residual velocity of a missile is shown in Figure 8.3, and rest of the FE simulations are recorded same by selecting a node of the missile. The newly proposed probabilistic equation in this thesis by the author to estimate the residual velocity (V_r) of missile after impacting a RC panel is:

$$\frac{V_r}{V_0} = 0.7585 - \left(1.0081 * \left(\frac{H.d}{x}\right)^{0.5}\right) \quad (8.4)$$

σ=11.83, cov=0.0951, V_r – Residual Velocity of the Missile, V_0 – Velocity of the Missile, H – Thickness of concrete target (m), d – diameter of the missile, x – Penetration depth of concrete target from Eq (8.3).

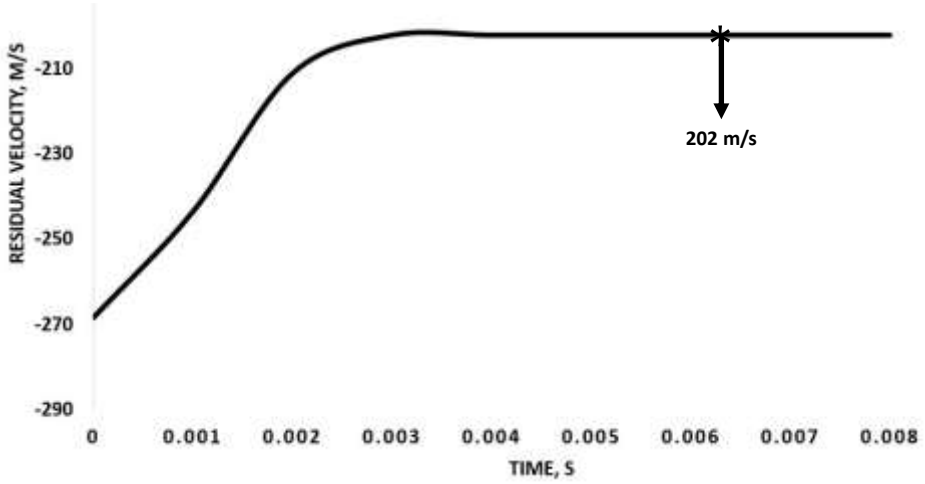

Figure 8.3 An example to Record Residual Velocity of the Missile

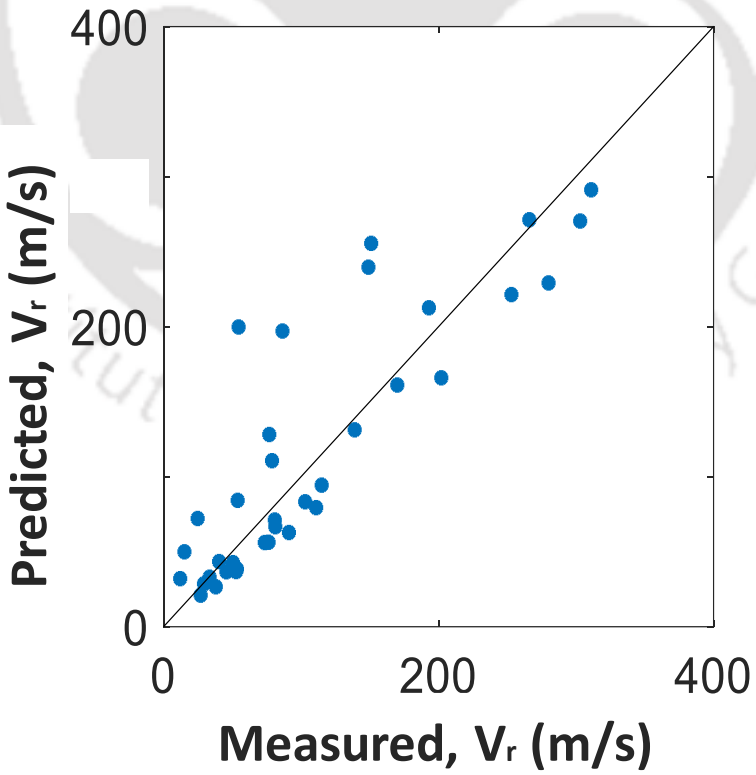

Figure 8.4 Probabilistic Residual Velocity vs Simulated Residual Velocity of RC Panels

Figure 8.2 shows the comparison between the probabilistic and simulated residual velocity of the missile into the RC target. Majority of data points are lying near to 1:1 line. The data contains equality data. The predictions of the probabilistic model show that the equality data lays both above and below the 1:1 line. The probabilistic model corrects this inherent bias in the model. The cov is 9.5% which details the accuracy of the developed probabilistic model for estimating the residual velocity of missile into RC target.

8.2. Probabilistic Models for PC Panels

Using the results from FE simulation following the experimental design as detailed in Chapter 7 for 100 PC panels, this section develops probabilistic models for predicting penetration depth (x_p), perforation limit (h_{p1}) and residual velocity (V_{rp}) of PC panels.

8.2.1. Probabilistic Model For Penetration Depth ($\mathbf{x_p}$)

The same procedure is followed to capture penetration depth of PC target due to missile impact as shown in Figure 8.1. For PC panels, no formulation exists for predicting penetration depth due to the complexity involved because of enormous thickness, curvature, steel liner and post-tensioning effect. The newly proposed equation in this thesis by the author to estimate the probabilistic penetration depth (x_p) of an PC panel subject to flat nose missile impact loading after the probabilistic analysis is,

$$\frac{x_p}{d} = -0.7497 + 1.1646\ln\left(\frac{M.V_0^2}{d^3.f_c}\right) - 0.1150\ln\left(\frac{M.V_0^2}{M_c}\right) \qquad (8.5)$$

σ=0.0234, cov = 0.0384, d – diameter of the missile (m), M – Mass of the missile (kg), V_0 – Velocity of the missile (m/s), f_c – Compressive strength of concrete (N/m^2), M_c – Moment Capacity of panel (N-m), x_p – Penetration depth into target (m), σ – Standard Deviation, cov – Coefficient of Variation.

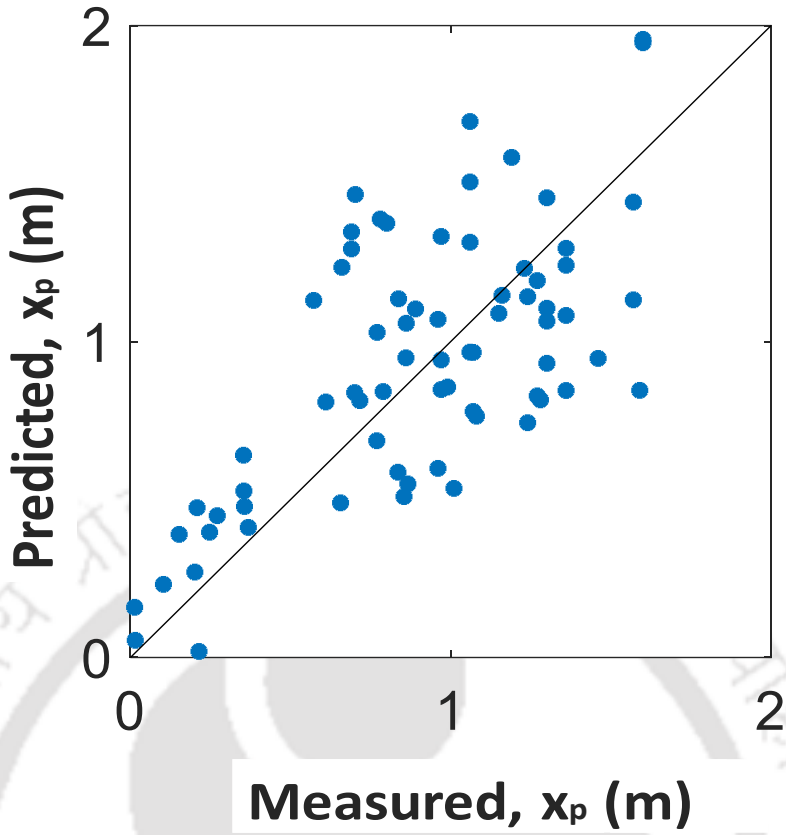

Figure 8.4 Probabilistic Penetration Depth vs Simulated Penetration Depth for PC Panels

Figure 8.3 shows the comparison between probabilistic and simulated Penetration Depth of the missile into PC target. Majority of data points are lying near to 1:1 line. The data contains equality data. The predictions of the probabilistic model show that the equality data lays both above and below the 1:1 line. The probabilistic model corrects this inherent bias in the model. The cov is 4% which details the accuracy of the developed probabilistic model for estimating the Penetration Depth of missile into the PC target.

8.2.2. Probabilistic Model For Perforation Limit (h_{p1})

The same procedure is followed to capture perforation limit of the target and provided factor of safety to the panel, so that the missile can be arrested outside of the panel. For PC panels no formulation exists for predicting perforation limit due to the complexity involved because of immense thickness, curvature, steel liner and post-tensioning. The newly proposed equation in

this thesis by the author to estimate the probabilistic the perforation limit (h_{p1})of an PC panel subject to flat nose missile impact loading after the probabilistic analysis is,

$$\frac{h_{p1}}{d} = 3.0850 + 0.1771 * \left(\frac{x_p}{d}\right)^2 \quad (8.6)$$

σ = 0.1472, cov = 0.0566, where, $\frac{x_p}{d}$ is consider from Eq (8.5), h_{p1} – Perforation Limit of the Target, d – diameter of the missile, x_p – Penetration depth of the missile.

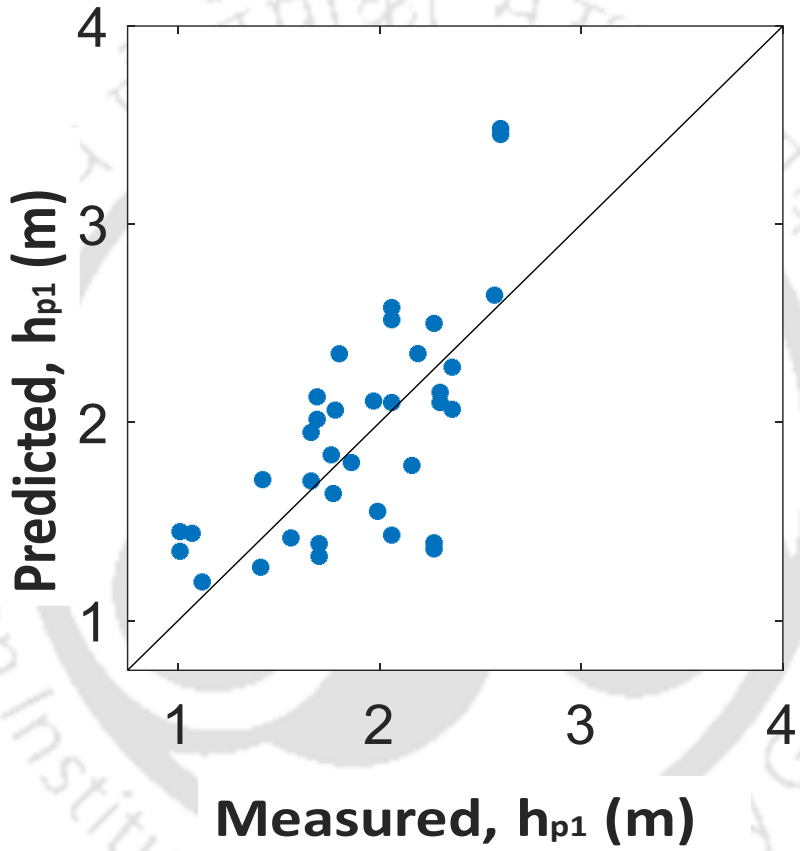

Figure 8.5 Probabilistic Perforation Limit vs Simulated Perforation Limit of PC Panels

Figure 8.4 shows the comparison between probabilistic and simulated Perforation Limit of the missile into the PC target. Majority of data points are lying near to 1:1 line. The data contains equality data. The predictions of the probabilistic model show that the equality data lays both above and below the 1:1 line. The probabilistic model corrects this inherent bias in the model. The cov is 15% which details the accuracy of the developed probabilistic model for

estimating the Perforation Limit of PC panels. The missile can be arrested by providing the perforation limit obtained from the above analysis which serves for better performance and damage is minimal.

8.2.3. Probabilistic Model For Residual Velocity (V_{rp})

The same procedure is followed to capture residual velocity of the missile as shown in Figure 8.1. A plot of residual velocity of a missile is shown in Figure 8.3, and rest of the FE simulations are recorded same by selecting a node of the missile. For PC panels, residual velocity variation as compared to the initial velocity of the missile is huge due to massiveness in the PC structure. The capacity of the PC panel is large than typical RC structures due to curvature, steel liner, large tendons, etc. The newly proposed equation in this thesis by the author to estimate the probabilistic the residual velocity (V_{rp}) of a missile upon PC panel after the probabilistic analysis is,

$$V_{rp} = V_0 - \left(-286.7826 - 0.0001 \left(\frac{MV_0^2}{M_c} \right)^2 + 26.2843 \ln \left(\frac{\Delta^2}{t_c t_s} \right) \right) \quad (8.7)$$

σ=0.0019, cov = 2.0051× 10^{-6}, Δ - Hump in PC target (m), t_c - Thickness of concrete(m), t_s - Thickness of steel liner (m).

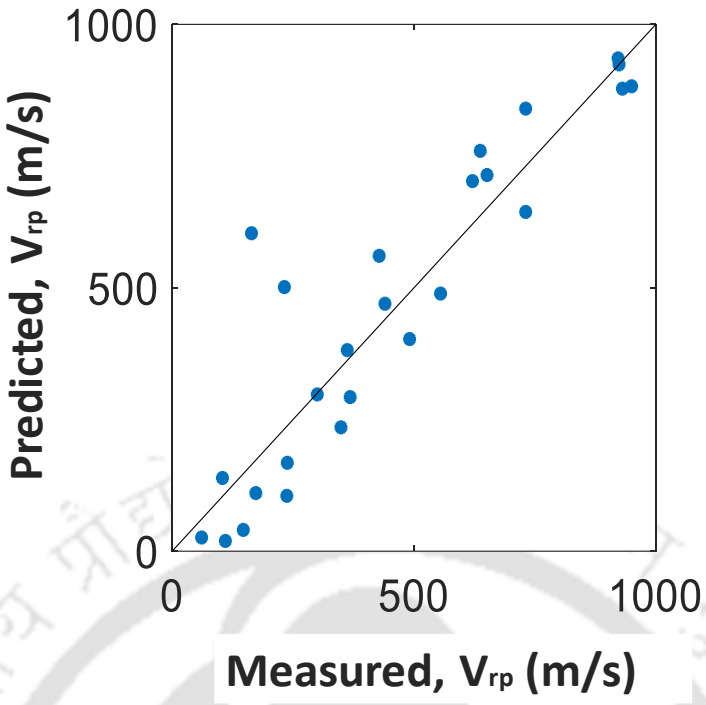

Figure 8.6 Probabilistic Residual Velocity vs Numerical Residual Velocity of missile impacting PC Panel

Figure 8.5 shows the comparison between probabilistic and simulated Residual Velocity of missile impacting PC Panel. Majority of data points are lying near to 1:1 line. The data contains equality data. The predictions of the probabilistic model show that the equality data lays both above and below the 1:1 line. The probabilistic model corrects this inherent bias in the model. The cov is 0.2% which details the accuracy of the developed probabilistic model for estimating the Residual Velocity of missile impacting PC Panel.

8.3. Inference

In this chapter, probabilistic models are developed for parameters like penetration depth of panel, perforation limit of the target structure and residual velocity of a missile for both PC and RC panels subject to missile impact. These probabilistic models account for various relevant uncertainties like material modelling, statistical uncertainty, panel curvature, strain rate, boundary condition, and other aleatoric and epistemic uncertainties. The estimated cov for these models are within 15% and considering the complexity of the phenomenon which is further associated with the uncertainties involved, these developed models estimate the required performance levels with greater accuracy.

The developed performance levels will be used in the subsequent chapters to develop probabilistic capacity and demand models for RC and PC panels subject to missile impact at different performance levels which will be indicated in each scenario by the results estimated from these developed models.

Chapter 9. PERFORMANCE-BASED CAPACITY MODELS FOR RC PANELS

The performance levels are defined in Chapter 4 and the subsequent probabilistic formulation for performance levels are developed in Chapter 8. Based on this categorization of different damage levels, the associated capacity of the RC panel subject to missile impact will be estimated in this Chapter. The probabilistic capacity models will be developed corresponding to the three different performance levels as developed in Chapter 4 earlier. The dynamic capacity is defined as the maximum internal energy resisted by target structure such as the resistance offered by a Nuclear Containment RC panel during a missile impact scenario at each performance level. That is, the dynamic capacity for the performance level of operation with minimal damage (P_1) where P_{p1} is defined as maximum internal resistance energy by the target structure before D2 begins. Similarly, the dynamic capacity for the performance level of operational with some damage (P_2) where P_{p2} is defined as the maximum internal resistance energy by the target structure before D2 begins. Finally, P_{p3} is defined as the maximum internal energy resisted by the target structure before D4 begins to occur. This section develops probabilistic capacity models for performance levels P_1, P_2 and P_3.

From the obtained results of the FE simulations which is based on Chapter 7 of Experimental Design, this Chapter develops probabilistic models for estimating the internal energy (Capacity) of Nuclear containment RC panel subject to missile impact for each of the three performance levels. These models take into consideration of relevant uncertainties which includes statistical uncertainty and model error as explained in (Gardoni *et al.*, 2002). Data utilised for model assessment from FE simulations are assumed to be no error in measurement.

Following the probabilistic model's general formulation by (Gardoni *et al.*, 2002), the dynamic resistance model for performance level Pi, i=1, 2, 3 is formulated as

$$P_{pi}(x, \Theta_{pi}) = \hat{P}_{pi}(x) * \Upsilon_{pi}(x_i, \Theta_{pi}) + \sigma_{P_i} e_{P_i} \tag{9.1}$$

Where, P_{pi}=normalized dynamic capacity for performance level Pi, $\hat{P}_{pi}$ = normalized dynamic capacity from mechanical model, $\Upsilon_{pi}(x_i, \Theta_{pi})$ = correction term for the bias inherent in the mechanical model.

$$\Upsilon_{pi}(x_i, \Theta_{pi}) = \sum_{j=1}^{K_{pi}} \Theta_{Pi,j} h_{Pi,j}(x) \tag{9.2}$$

Where $h_{P_{i,j}}(x)$, j = 1,…,n = explanatory function (or regressors) defined as functions of x, $\theta_{P_i,j}$, j=1,…,n are the parameters associated with explanatory functions, $\sigma_{P_i} e_{P_i}$ = model error, e_{P_i} =Gaussian error and $\Theta_{P_i} = \theta_{P_i}$ = set of unknowns model parameters in which θ_{P_i}=($\theta_{P_i,1}$,K,$\theta_{P_i,k}$).

9.1. Mechanical Model for Performance Level P1:

The estimate of the dynamic capacity for performance level 1 (P1) is based on the resistance energy of target structure. Considered terms for this mechanical model are (Performance level – 1, no damage and spalling of cover only) compressive strength of concrete, area of missile cross-section and penetration depth of missile upto clear cover. The proposed formula is,

$$\hat{P}_{p1} = \left[f_c \left(\frac{\pi}{4} d^2 \right) \right] X_{p1} \tag{9.3}$$

where, f_c=compressive strength of concrete (N/m^2), d=diameter of the missile (m), X_{p1}=penetration of the missile up to clear cover (m).

9.2. Mechanical Model for Performance Level P2:

The estimate of the dynamic capacity for performance level 2 (P2) is based on the resistance energy of the target structure. Considered terms for this mechanical model are (Performance level – 2, missile penetrated into the half slab, moderate damage) compressive strength of concrete, the perimeter of missile & mid-depth of concrete target and penetration depth of missile up to the mid depth of target. The proposed formula is,

$$\hat{P}_{p2} = (0.1 f_c \pi d) {X_{p2}}^2 \tag{9.4}$$

where, f_c=compressive strength of concrete (N/m^2), d=diameter of the missile (m), X_{p2}=penetration of the missile half depth (m).

9.3. Mechanical Model for Performance Level P3

The estimate of the dynamic capacity for performance level 3 (P3) is based on the resistance energy of the target structure. Considered terms for this mechanical model are (Performance level – 3, significant damage, Full penetration by missile) are compressive strength of concrete, the perimeter of missile & mid-depth of concrete target and penetration depth of missile up to mid-depth of the target. The proposed formula is,

$$\hat{P}_{p3} = (0.1 f_c \pi d) {X_{p3}}^2 \tag{9.5}$$

f_c=compressive strength of concrete (N/m^2), d=diameter of the missile (m), X_{p3}=full penetration of the missile (m).

9.4. Model Correction

Appropriate model correction terms are considered to capture exact phenomena which is not accounted in mechanical models. Based on available literature (Gardoni et al., 2002, Sharma et al., 2012) and intuitions of the researcher these explanatory functions are considered. Selected explanatory functions are listed in Table 9.1 below. Considered functions are dimensionless, and table lists the exact quantities which influence model and are captured by the explanatory functions.

Table 9.1 List of Explanatory Functions for Capacity Models

Variable	Expression
$\boldsymbol{h_1(x)}$	1
$\boldsymbol{h_2(x)}$	$\left(\frac{L_s}{t_c}\right)$
$\boldsymbol{h_3(x)}$	$\left(\frac{L_m}{d}\right)$
$\boldsymbol{h_4(x)}$	$\left(\frac{MV_0^2}{d^3 f_c}\right)$
$\boldsymbol{h_5(x)}$	$\left(\frac{MV_0}{TLt_c f_c}\right)$
$\boldsymbol{h_6(x)}$	$\left(\frac{MV_0^2}{M_c}\right)$
$\boldsymbol{h_7(x)}$	$\left(\frac{t_c}{X_{pn}}\right)$

Where L_s = Length of panel, t_c = thickness of concrete target, L_m = Length of missile, d= diameter of missile, M = mass of missile, V_0 = Velocity of missile, f_c = concrete compressive strength, 1/T = frequency, M_c = Moment Capacity of target structure, X_{pn} = penetration at different levels, n = 1,2,3

The first explanatory function $h_1(x)$ is considered to catch a potential constant bias which is present in the mechanical model. The second explanatory function $h_2(x)$ accounts for the contribution slenderness ratio of the panel structure. The slenderness ratio of the missile is captured by third explanatory function $h_3(x)$. The fourth explanatory function $h_4(x)$ contributes to the effect of the energy of the missile imposed on the target. The effect of the natural frequency of the system is accounted by fifth explanatory function $h_5(x)$. The sixth explanatory function $h_6(x)$ contributes the moment capacity resistance of the total system. The various performance levels penetration depth is considered by seventh explanatory function $h_7(x)$. Figure 9.1 shows a representative simulation as per the details presented in Chapter 5 and Chapter 7.

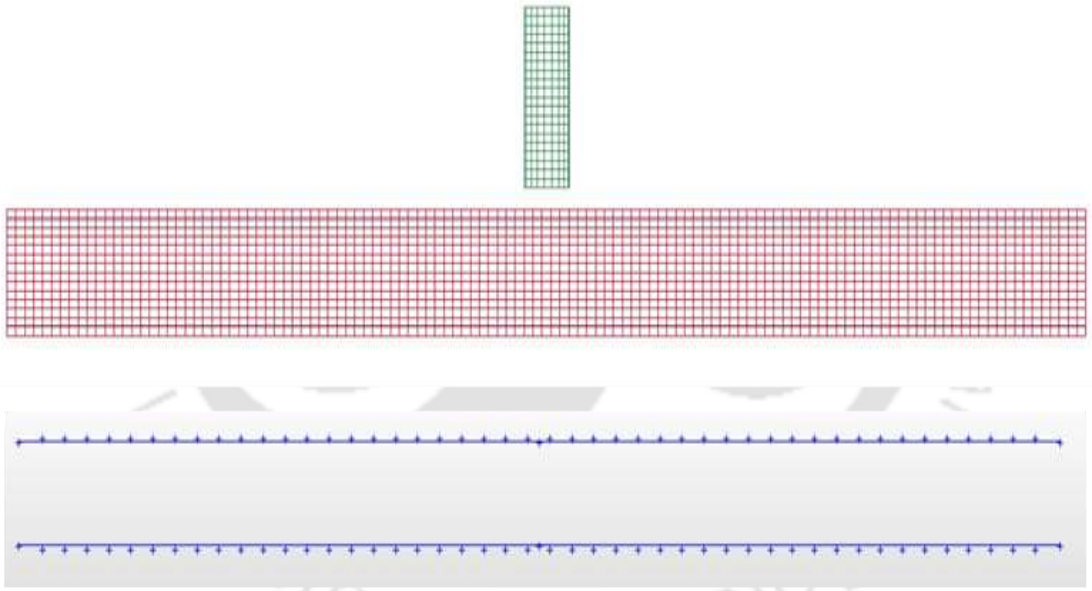

Figure 9.1 FE Simulation of missile impact on RC Slab

9.5. Model Assessment

Bayesian inference is chosen for the estimation of the model parameters Θ. A non-informative prior is selected (Box & Tiao 1992). A stepwise deletion process is used for selecting the parsimonious model. In this method, diagnostic plots are created between the explanatory

function and the residual of the dynamic capacity of the FE model and the mechanical model. Suitable explanatory functions are chosen one at a time which shows the strongest correlation. The mean of the standard deviation is monitored to check the adequacy of the model.

9.6. Parameter Estimation for Performance Level P1

Figure 9.2 shows the data capturing of internal energy of FE capacity models for performance level -1 and same procedure followed for remaining FE models. The most statistically significant explanatory functions for performance level P1 are $h_1(x)$, $h_2(x), h_3(x), h_4(x)$ *and* $h_5(x)$. Considered terms account for correction of constant bias, the contribution concrete panels slenderness ratio, missiles slenderness ratio, energy imposed on target and frequency of the system. The posterior statistics of the model is followed in Table 9.2.

Table 9.2 Posterior Statistics of Parameters in Selected Dynamic Capacity (P1) Model

Parameter	Mean	Standard deviation	Correlation Coefficient				
			Θ_1	Θ_2	Θ_4	Θ_4	Θ_5
Θ_1	1.3345	0.628	1.000				
Θ_2	0.0537	0.0346	-0.776	1.000			
Θ_3	0.2556	0.118	-0.76	0.236	1		
Θ_4	-0.0025	0.0033	0.266	-0.196	-0.322	1	
Θ_5	-0.6516	1.129	-0.525	0.400	0.400	-0.786	1.000

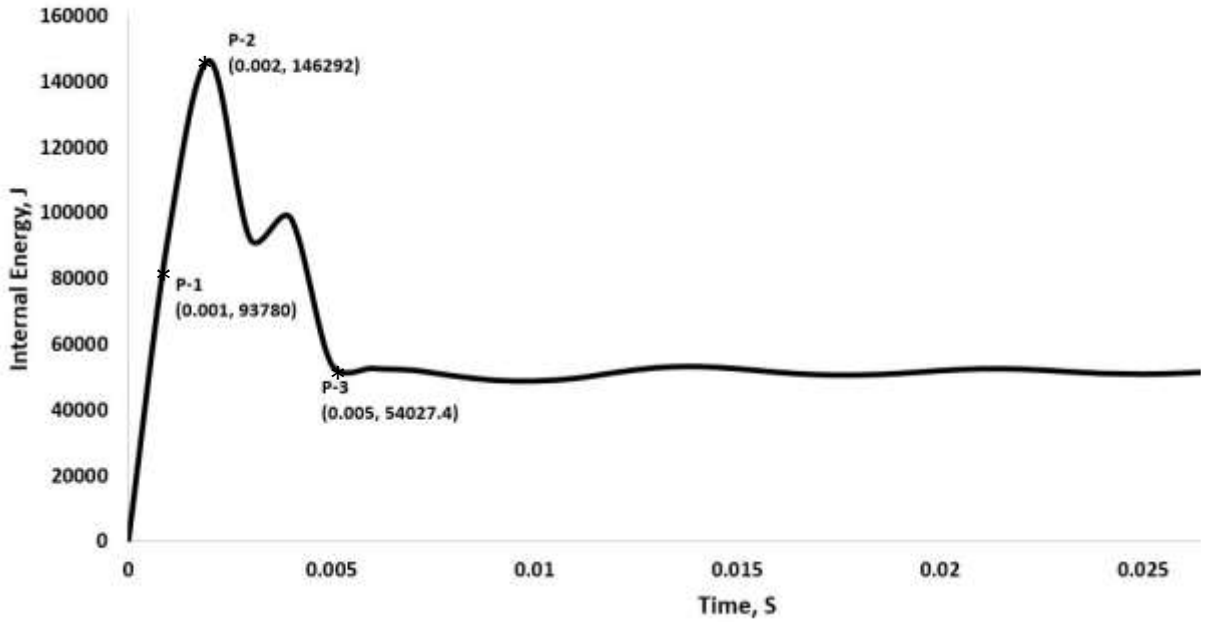

Figure 9.2 Dynamic Capacity of RC Target Structure for Three Performance Levels

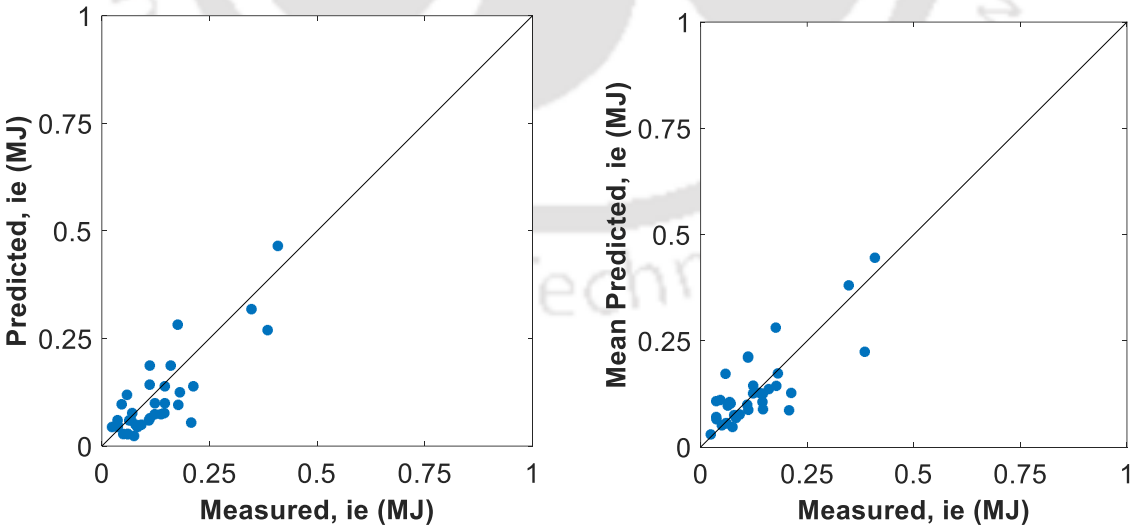

Figure 9.3 Comparison of measured and predicted Dynamic Capacity (P1) of the RC panel based on mechanical (left) and probabilistic (right) model

Figure 9.3 shows the comparison between the estimation of dynamic capacity at performance level P1 in terms of internal energy of Nuclear containment RC panel based on the proposed mechanical model and the mean of the developed probabilistic model where the mean predication for the dynamic capacity P_{P1} is developed as

$$P_{P1} = \hat{P}_{p1}\left(1.3345 + 0.0537\left(\frac{L_s}{t_c}\right) + 0.2556\left(\frac{L_m}{d}\right) - 0.0025\left(\frac{MV_0^2}{d^3 f_c}\right) - 0.6516\left(\frac{MV}{TLt_c f_c}\right)\right) \quad (9.6)$$

Where P_{P1}=Probabilistic dynamic capacity at performance level P1, $\hat{P}_{p1}$ = dynamic capacity at performance level P1given by the mechanical model

The mechanical and probabilistic models are both plotted against the capacity in the term of internal energy of the Nuclear containment RC panel values estimated from the FE simulations. Majority of data points are lying near to 1:1 line. The data contains equality data. The predictions of the probabilistic model show that the equality data lays both above and below the 1:1 line. The probabilistic model corrects this inherent bias in the model. The cov is 6.3% which details the accuracy of the developed probabilistic model for estimating the Capacity of RC panel subject to missile impact at Performance level P1.

9.7. Parameter Estimation for Performance Level P2

Figure 9.4 shows the data capturing of internal energy of FE capacity models for performance level -2 and same procedure followed for remaining FE models. The most statistically significant explanatory functions for performance level P2 are

$h_1(x)$, $h_2(x), h_3(x), h_4(x)$ *and* $h_5(x)$. Considered terms account for correction of constant bias, the contribution concrete panels slenderness ratio, missiles slenderness ratio, energy imposed on target and frequency of the system. The posterior statistics of the model is presented in Table 9.3.

Table 9.3 Posterior Statistics of Parameters in Selected Dynamic Capacity (P2) Model

Parameter	Mean	Standard deviation	Correlation Coefficient				
			Θ_1	Θ_2	Θ_4	Θ_4	Θ_5
Θ_1	-0.7678	0.628	1.000				
Θ_2	0.0879	0.0346	-0.776	1.000			
Θ_3	0.3538	0.118	-0.76	0.236	1		
Θ_4	-0.0062	0.0033	0.266	-0.196	-0.322	1	
Θ_5	-1.7724	1.129	-0.525	0.400	0.400	-0.786	1.000

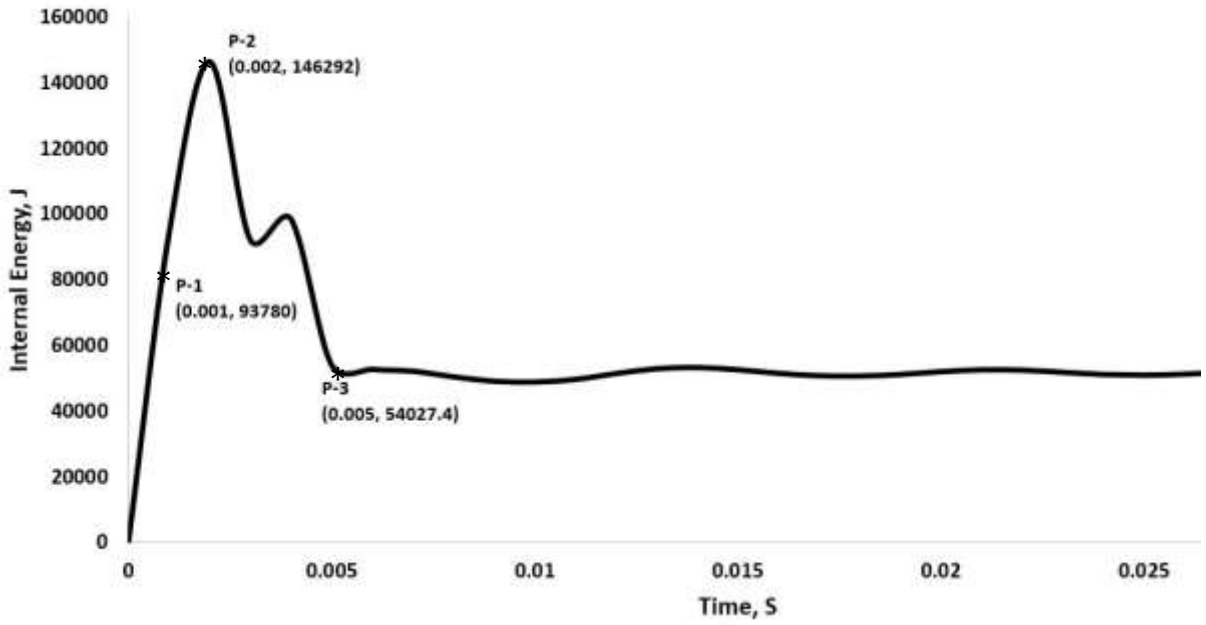

Figure 9.4 Dynamic Capacity of RC Target Structure for Three Performance Levels

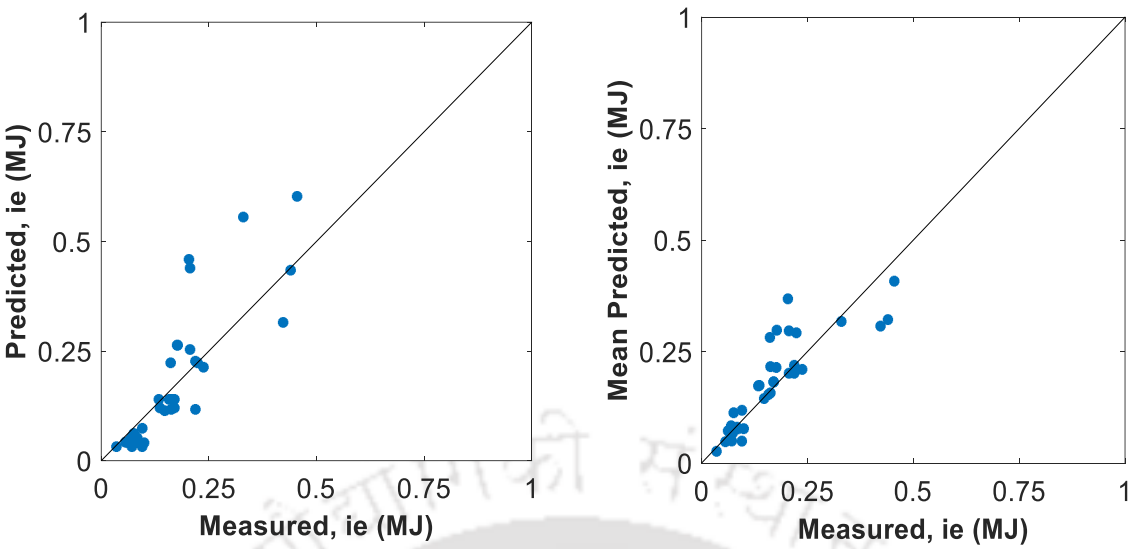

Figure 9.5 Comparison of measured and predicted Dynamic Capacity (P2) of RC panel based on mechanical (left) and probabilistic (right) model

Figure 9.5 shows the comparison between the estimation of dynamic capacity in term of internal energy of Nuclear containment RC panel based on the proposed mechanical model and the mean of the developed probabilistic model where the mean predication for the dynamic capacity P_{P2} is proposed as

$$P_{P2} = \hat{P}_{p2}\left(-0.7678 + 0.0879\left(\frac{L_s}{t_c}\right) + 0.3538\left(\frac{L_m}{d}\right) - 0.0062\left(\frac{MV_0^2}{d^3 f_c}\right) - 1.7724\left(\frac{MV}{TLt_c f_c}\right)\right) \quad (9.7)$$

where P_{P2}= Probabilistic dynamic capacity at performance level P2, $\hat{P}_{p2}$ = dynamic capacity given by the mechanical model.

The mechanical and probabilistic models are both plotted against the capacity in the term of internal energy of the containment panel values estimated from the FE simulations. Majority of data points are lying near to 1:1 line. The data contains equality data. The predictions of the probabilistic model show that the equality data lays both above and below

the 1:1 line. The probabilistic model corrects this inherent bias in the model. The cov is 4.15% which details the accuracy of the developed probabilistic model for estimating the Capacity of RC panel subject to missile impact at Performance level P2.

9.8. Parameter Estimation for Performance Level P3

Figure 9.6 shows the data capturing of internal energy of FE capacity models for performance level -3 and same procedure followed for remaining FE models. The most statistically significant explanatory functions for performance level P3 are $h_1(x)$, $h_2(x), h_3(x), h_4(x)$ *and* $h_5(x)$. Considered terms account for correction of constant bias, the contribution concrete panels slenderness ratio, missiles slenderness ratio, energy imposed on target and frequency of the system. The posterior statistics of the model is shown in Table 9.4.

Table 9.4 Posterior Statistics of Parameters in Selected Dynamic Capacity (P3) Model

Parameter	Mean	Standard deviation	Correlation Coefficient				
			Θ_1	Θ_2	Θ_4	Θ_4	Θ_5
Θ_1	-0.7734	0.628	1.000				
Θ_2	0.0805	0.0346	-0.776	1.000			
Θ_3	0.2785	0.118	-0.76	0.236	1		
Θ_4	-0.0039	0.0033	0.266	-0.196	-0.322	1	
Θ_5	-1.378	1.129	-0.525	0.400	0.400	-0.786	1.000

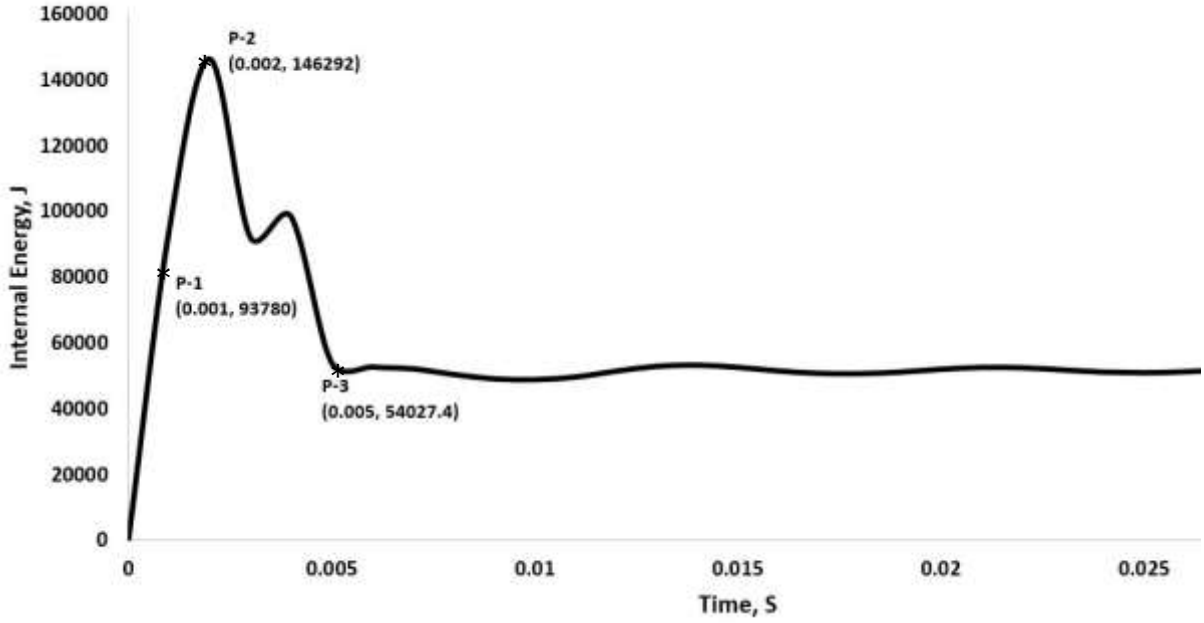

Figure 9.6 Dynamic Capacity of RC Target Structure for Three Performance Levels

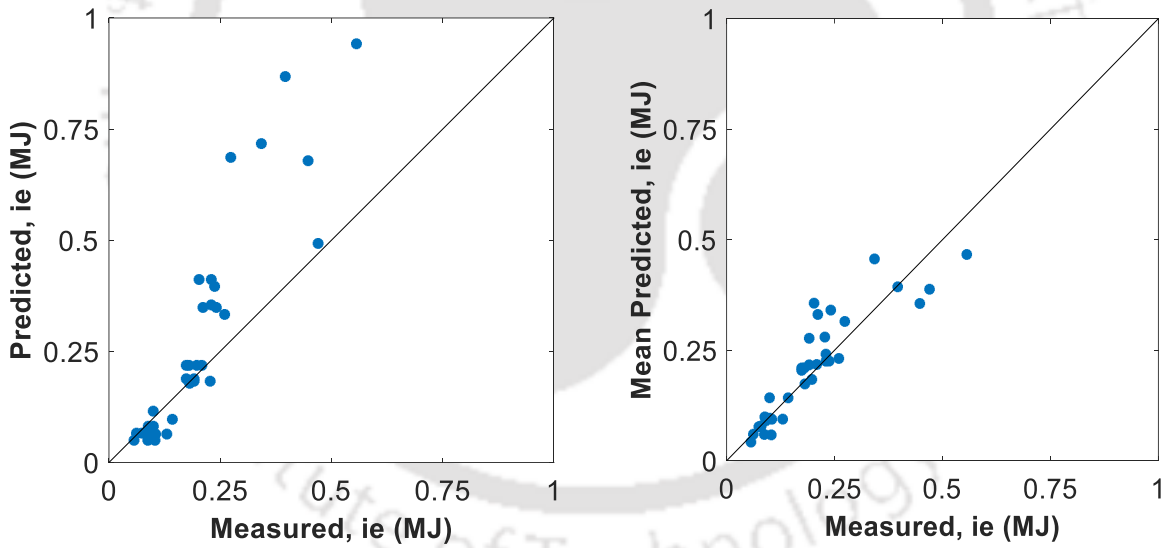

Figure 9.7 Comparison of measured and predicted Dynamic Capacity (P3) of the RC panel based on mechanical (left) and probabilistic (right) model

Figure 9.7 shows the comparison between the estimation of dynamic capacity in term of internal energy of Nuclear containment RC panel based on the proposed mechanical model

and the mean of the developed probabilistic model where the mean predication for the dynamic capacity P_{P3} is developed as

$$P_{P3} = \hat{P}_{p3}\left(-0.7734 + 0.0805\left(\frac{L_s}{t_c}\right) + 0.2785\left(\frac{L_m}{d}\right) - 0.0039\left(\frac{MV_0^2}{d^3 f_c}\right) - 1.378\left(\frac{MV}{TLt_c f_c}\right)\right) \quad (9.8)$$

where P_{P3}= Probabilistic dynamic capacity at performance level P3, $\hat{P}_{p3}$ = dynamic capacity given by the mechanical model.

The mechanical and probabilistic models are both plotted against the capacity in the term of internal energy of the Nuclear containment RC panel values estimated from the FE simulations. Majority of data points are lying near to 1:1 line. The data contains equality data. The predictions of the probabilistic model show that the equality data lays both above and below the 1:1 line. The probabilistic model corrects this inherent bias in the model. The cov is 7.4% which details the accuracy of the developed probabilistic model for estimating the Capacity of RC panel subject to missile impact at Performance level P3.

9.9. Inference

Probabilistic capacity models for RC panels have been developed in this Chapter which corresponds to each performance levels as developed in Chapter 4. The developed probabilistic capacity models accurately estimate the capacity of RC panel at the given performance level as evident from the value of cov which is under 10% for all the cases. The developed capacity models are based on Energy-based formulation.

The following Chapter develops the probabilistic model to estimate the demand on the RC panel subject to missile impact.

Chapter 10. PERFORMANCE-BASED DEMAND MODELS FOR RC PANELS

Based on the results attained from Chapter 5 and Chapter 7, this chapter develops probabilistic demand models for estimating demand in terms of kinetic energy imparted by the missile impact on the target RC structure. These models take into consideration of relevant uncertainties which includes statistical uncertainty and model error as explained in (Gardoni *et al.*, 2002). Data utilised for model assessment from FE simulations are assumed to be no error in measurement. Following the probabilistic model's general formulation by (Gardoni *et al.*, 2002), the dynamic demand for performance level Pi, i=1, 2, 3 is formulated as

$$P_D(x, \Theta_D) = \hat{P}_D(x) * \Upsilon_D(x, \Theta_D) + \sigma_D e_D \tag{10.1}$$

P_D = Probabilistic dynamic demand as the kinetic energy of the missile on RC panel, $\hat{P}_D$ = dynamic demand from the mechanical model, $\Upsilon_D(x, \Theta_D)$ = correction term for the bias inherent in the mechanical model

$$\Upsilon_D(x, \Theta_D) = \sum_{j=1}^{k_D} \Theta_{D,j} h_{D,j}(x) \tag{10.2}$$

$h_{D,j}(x)$ = explanatory functions, where j=1……k, $\Theta_{D,j}$ = parameter associated with explanatory functions, $\sigma_D e_D$= model error, e_D=Gaussian error.

10.1. Mechanical Model

The estimate of the dynamic demand $\hat{P}_D$ is based on the kinetic energy of the missile imposed on RC panel. Considered terms for this mechanical model are the mass of the missile and velocity of the missile. The proposed formula is

$$\hat{P}_D = \frac{1}{2} M {V_0}^2 \tag{10.3}$$

$\hat{P}_D$ = dynamic demand from missile imposed on RC slab, M = Mass of the missile, V_0 = Velocity of the missile

10.2. Model Correction

Model correction terms are considered to capture exact phenomena which are not accounted in mechanical models. Based on available literature (Gardoni et al., 2002, Sharma et al., 2012) and intuitions of the researcher these explanatory functions are considered. Selected explanatory functions are listed in Table 10.1 below. Considered functions are dimensionless, and table lists the exact quantities which influence model and are captured by the explanatory functions.

Table 10.1 List of Explanatory Functions for Demand Models for RC panels.

Variable	Expression
$\boldsymbol{h_1(x)}$	1
$\boldsymbol{h_2(x)}$	$\left(\frac{L_s}{t_c}\right)$
$\boldsymbol{h_3(x)}$	$\left(\frac{L_m}{d}\right)$
$\boldsymbol{h_4(x)}$	$\left(\frac{MV_0^2}{d^3 f_c}\right)$
$\boldsymbol{h_5(x)}$	$\left(\frac{MV_0}{TLt_c f_c}\right)$
$\boldsymbol{h_6(x)}$	$\left(\frac{MV_0^2}{M_c}\right)$
$\boldsymbol{h_7(x)}$	$\left(\frac{t_c}{X_{pen}}\right)$

Where L_s = Length of panel, t_c = thickness of concrete target, L_m = Length of missile, d= diameter of missile, M = mass of missile, V_0 = Velocity of missile, f_c = concrete compressive strength, 1/T = frequency of the system, M_c = Moment Capacity of target structure, X_{pn} = penetration at different levels, n = 1,2,3

The first explanatory function $h_1(x)$ is considered to catch a potential constant bias which is present in the mechanical model. The second explanatory function $h_2(x)$ accounts for the contribution slenderness ratio of the panel structure. The slenderness ratio of the missile is captured by third explanatory function $h_3(x)$. The fourth explanatory function $h_4(x)$ contributes to the effect of the energy of the missile imposed on the target. The effect of the natural frequency of the system is accounted by fifth explanatory function $h_5(x)$. The sixth explanatory function $h_6(x)$ contributes the moment capacity resistance of the total system. The various performance levels penetration depth is considered by seventh explanatory function $h_7(x)$.

10.3. Model Assessment

Bayesian inference is chosen for the estimation of the model parameters Θ. A noninformative prior is selected (Box & Tiao 1992). A stepwise deletion process is used for selecting the parsimonious model. In this method, diagnostic plots are created between the explanatory function and the residual of the dynamic demand of the FE model and the mechanical model. Suitable explanatory functions are chosen one at a time which shows the strongest correlation. The mean of the standard deviation is monitored to check the adequacy of the model.

10.4. Parameter Estimation

Figure 10.1 shows the data capturing of kinetic energy of FE demand model and same procedure followed for remaining FE demand models. The most statistically significant explanatory functions for the demand model is $h_2(x)$. These terms take into correct for the contribution of the length and depth of the concrete panel, respectively. The posterior statistics of the model is presented in Table 10.2.

Table 10.2 Posterior Statistics of Parameters in Selected Dynamic Demand Model

Parameter	Mean	Standard deviation	Correlation Coefficient	
			Θ_1	Θ_2
Θ_1	1.1542	0.154	1.00	
Θ_2	-0.1442	0.122	0.9995	1.00

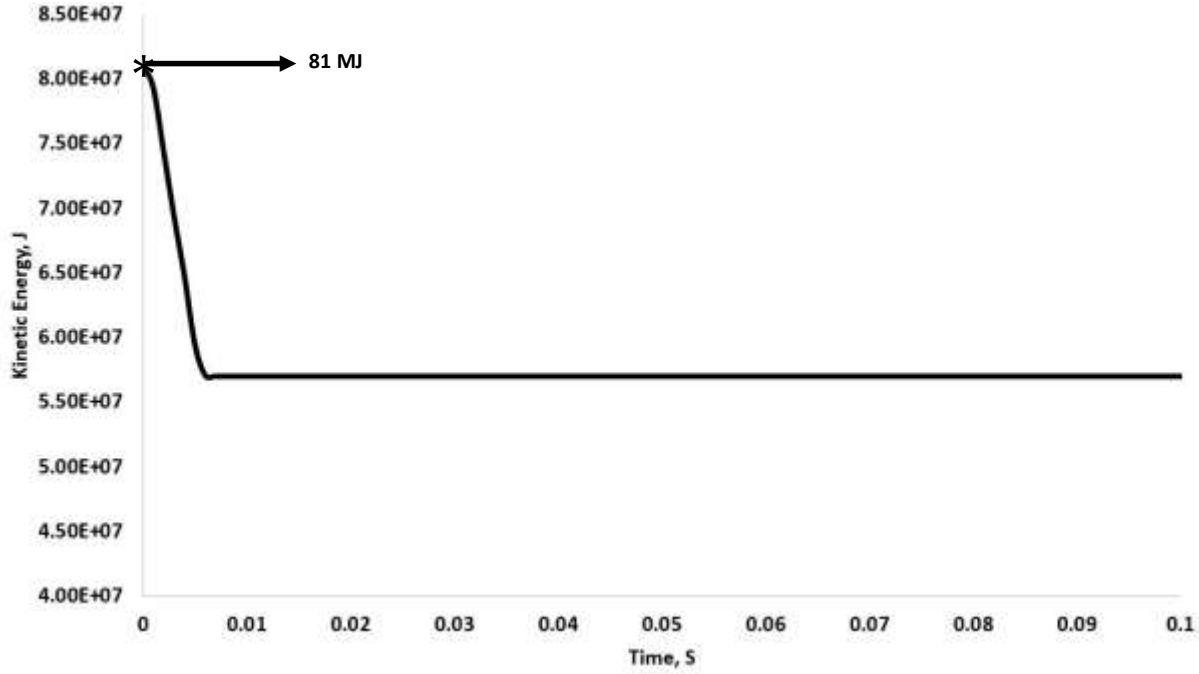

Figure 10.1 Kinetic Energy of Missile for RC Slab

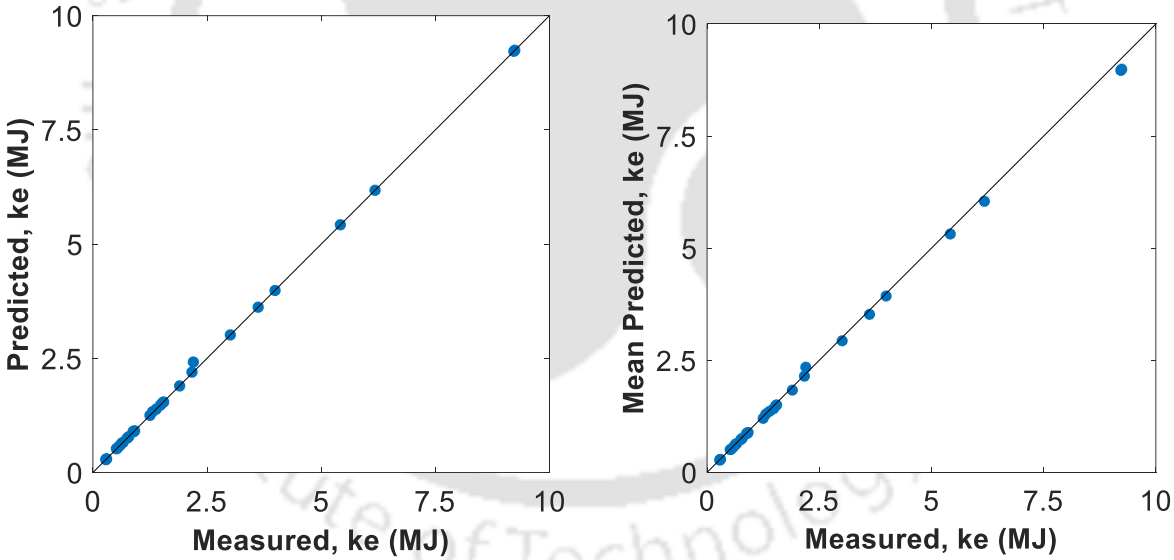

Figure 10.2 Comparison between measured and predicted Dynamic Demand based on mechanical (left) and probabilistic (right) model for missile impact on RC panel

Figure 10.2 shows the comparison between the estimation of dynamic demand in term of the kinetic energy of missile impacting Nuclear containment RC panel based on the proposed

mechanical model and the mean of the developed probabilistic model where the mean predication for the dynamic demand P_D is developed as

$$P_D = \hat{P}_D \left(1.1542 - 0.1442 \left(\frac{L_s}{t_c}\right)^{0.1}\right) \tag{10.4}$$

P_D = Probabilistic dynamic demand imposed on RC panel by missile impact, $\hat{P}_D$ = dynamic demand imposed on RC panel by missile impact from the mechanical model.

The mechanical and probabilistic models are both plotted against the demand in the term of the kinetic energy of the missile impacting the Nuclear containment RC panel in terms of values estimated from the FE simulations. Majority of data points are lying near to 1:1 line. The data contains equality data. The predictions of the probabilistic model show that the equality data lays both above and below the 1:1 line. The probabilistic model corrects this inherent bias in the model. The cov is 0.5% which details the accuracy of the developed probabilistic model for estimating the Demand on RC panel subject to missile impact.

10.5. Fragility Estimates

In this thesis, Fragility is defined as the conditional probability of exceeding a specified performance of a target structure for given initial velocity V_0 and mass M of a impacting missile. Probabilistic demand models are used to establish the fragility of the structural component by providing treatment to aleatory and epistemic uncertainties. Aleatory uncertainties are random in nature and also known as inherent variable and randomness. This uncertainty cannot be observed by the spectator or pattern of observation and is available in the set of quantifiable variables like material property constants, structural member dimensions, and imposed boundary conditions and partly in error terms (Gardoni et al., 2002). The Epistemic uncertainties arose due to our lack of knowledge, from measurement errors, from limited observation samples. This kind of uncertainty are available in capacity, demand models

and partially in error terms. Fragility plots are generated for each performance objectives defined in the research. Each performance level could generate particular fragility curve to show the vulnerability of the specimen.

Based on the variation of the demand imposed on Nuclear containment RC panel, the fragility analysis gives an estimate of the vulnerability of the Nuclear containment RC panel. The fragility of the Nuclear containment RC panel subjected to missile impact is formulated as

$$F(x,\Theta) = P[g(x,\Theta) \leq 0 | V_0, M] \tag{10.5}$$

where, $g_{p_i}(x,\Theta)$ is the limit state function defined as,

$$g_{p_i}(x,\Theta) = P_{p_i}(x,\Theta) - P_D \tag{10.6}$$

and $p_i = 1,2,3$ respectively, for all three performance levels P1, P2, and P3. The performance-based probabilistic models for the performance levels P1, P2, and P3 are developed in Chapter 9. Here, the fragility of a Nuclear containment RC panel is estimated based on varying the initial missile velocity $V_0$and the mass of the missile M while considering the properties and configuration of one FE model from simulations which is subject to impact by a missile as given in Table 10.3. Figure 10.3 shows the fragility estimates in terms of the contour plot of the Nuclear containment RC panel for performance level 1.

Table 10.3 Configuration and Dimensions of RC panel for Fragility analysis

Name of Configuration	Symbol	Dimensions
Length of Panel (square)	L_s	4.22 m
Thickness of Concrete Panel	t_c	0.35 m
Diameter of Missile	d	0.178 m
Length of Missile	H	0.5 m
Mass of Missile	M	217. 4 kg
Velocity of Missile	V_0	90.8 m/s
Compressive Strength	f_c	26 MPa
Yield Stress of Rebars	f_y	280 MPa
Diameter of Rebar	-	0.01 m
Area of Rebars	-	0.007536 m^2

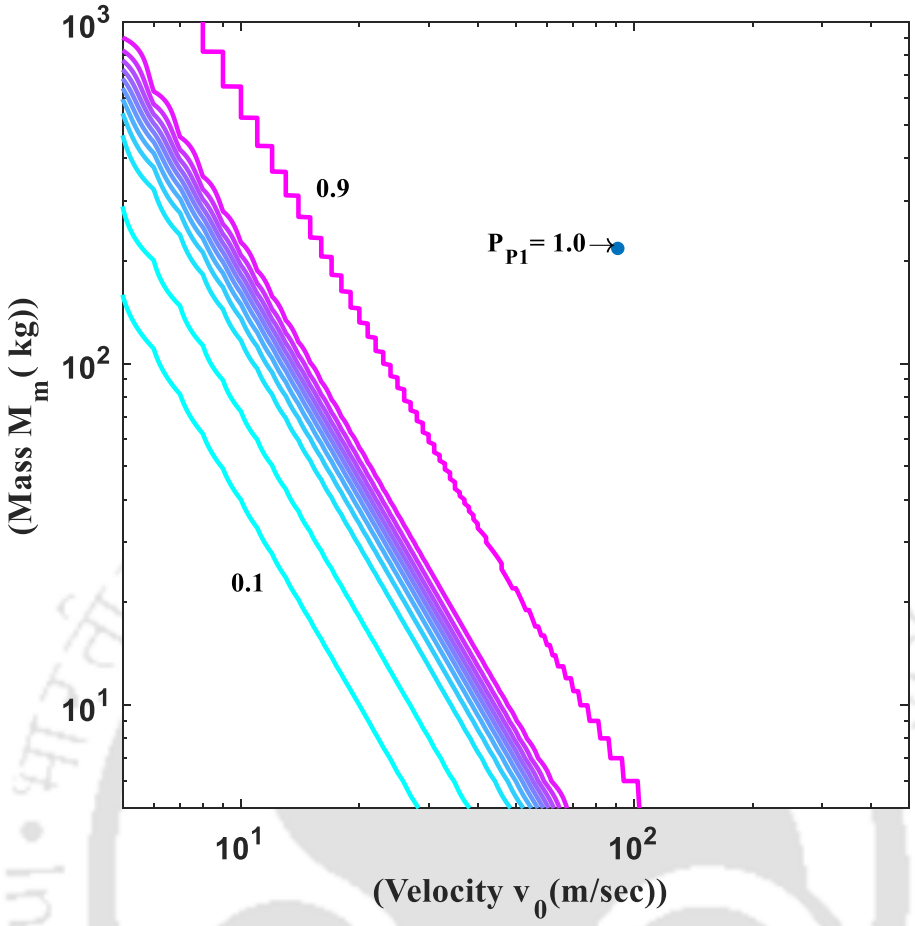

Figure 10.3 Contour plot showing the Fragility estimate for the Nuclear containment RC panel for Performance level P1

The plot is in log scale which comprised of missile initial velocity (m/s) range on the x-axis and missile mass (1000 kg) upon y-axis. The contour plot shows the fragility variation upon the domain of the mass and velocity. Contours of exceedance for performance level – 1 (P1) shows the well-spread nature, as shown the distribution of the lines of fragility from 0.1 to 0.9 (Figure 10.3). The exceedance of performance level – 1 is achieved with a lower value of demand imposed. The FE simulation is shown in Figure 10.3. Confirming to the result of the contour plot of Fragility which attains a value of 1, in the FE simulation as well, the exceedance pf performance level P1, i.e. penetration of cover is achieved.

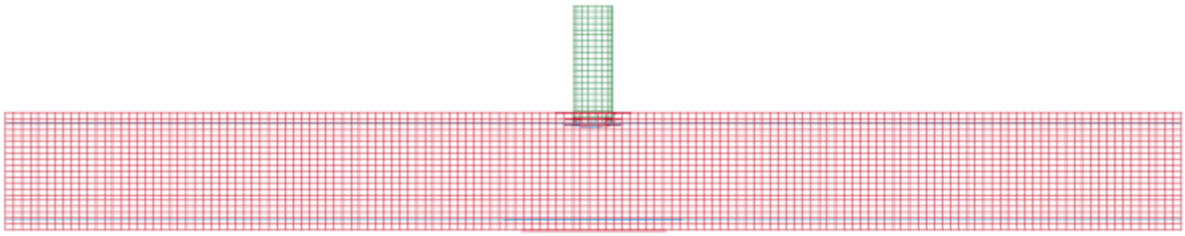

Figure 10.4 Missile impacting RC panel up to clear cover, performance level-1 (P1)

Figure 10.5 shows the contour plot for estimating the Fragility of the Nuclear containment RC panel for Performance level P2. The plot is in log scale which comprised of missile initial velocity (m/s) range on the x-axis and missile mass (1000 kg) upon y-axis. The contour plot shows the fragility variation upon the domain of the mass and velocity. Contours of exceedance for performance level – 2 (P2) shows the well-spread nature, as shown the distribution of the lines of fragility from 0.1 to 0.9 (Figure 10.5). The exceedance of performance level – 2 (P2) is achieved with a higher value of demand imposed as compared to performance level -1 (P1). The FE simulation is shown in Figure 10.6. Confirming to the result of the contour plot of Fragility which attains a value of 1, in the FE simulation as well, the exceedance pf performance level P2, i.e. half penetration of RC slab is achieved.

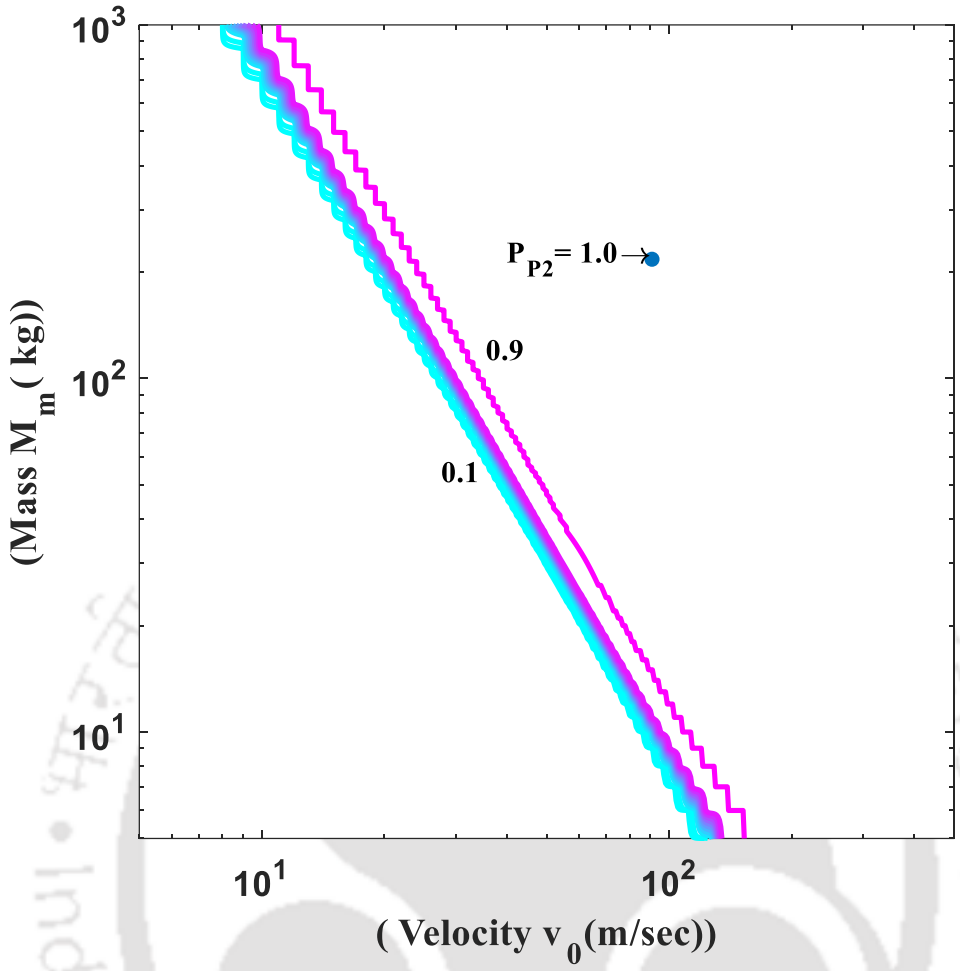

Figure 10.5 Contour plot showing the Fragility estimate for the Nuclear containment RC panel for Performance level P2

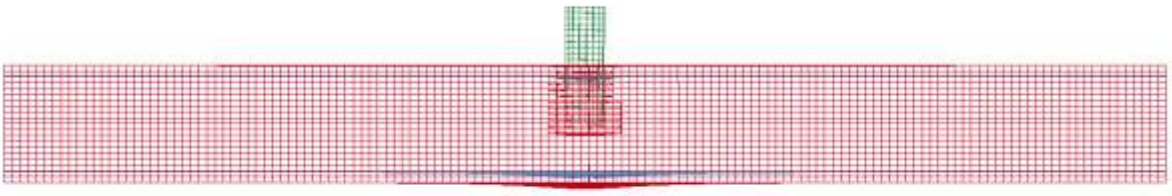

Figure 10.6 Missile impacting RC panel up to mid depth, performance level-2 (P2)

Figure 10.7 shows the contour plot for estimating the Fragility of the Nuclear containment RC panel for Performance level P3. The plot is in log scale which comprised of missile initial velocity (m/s) range on the x-axis and missile mass (1000 kg) upon y-axis. The contour plot shows the fragility variation upon the domain of the mass and velocity. Contours of exceedance for performance level – 3 (P3) shows the well-spread nature, as shown the distribution of the lines of fragility from 0.1 to 0.9 (Figure 10.7). The exceedance of performance level – 3 (P3) is achieved with the highest value of demand imposed as compared to performance level -1 (P1) and performance level -2 (P3). The FE simulation is shown in Figure 10.8. Confirming to the result of the contour plot of Fragility which attains a value of 1, in the FE simulation as well, the exceedance pf performance level P3, i.e. full penetration of RC slab is achieved.

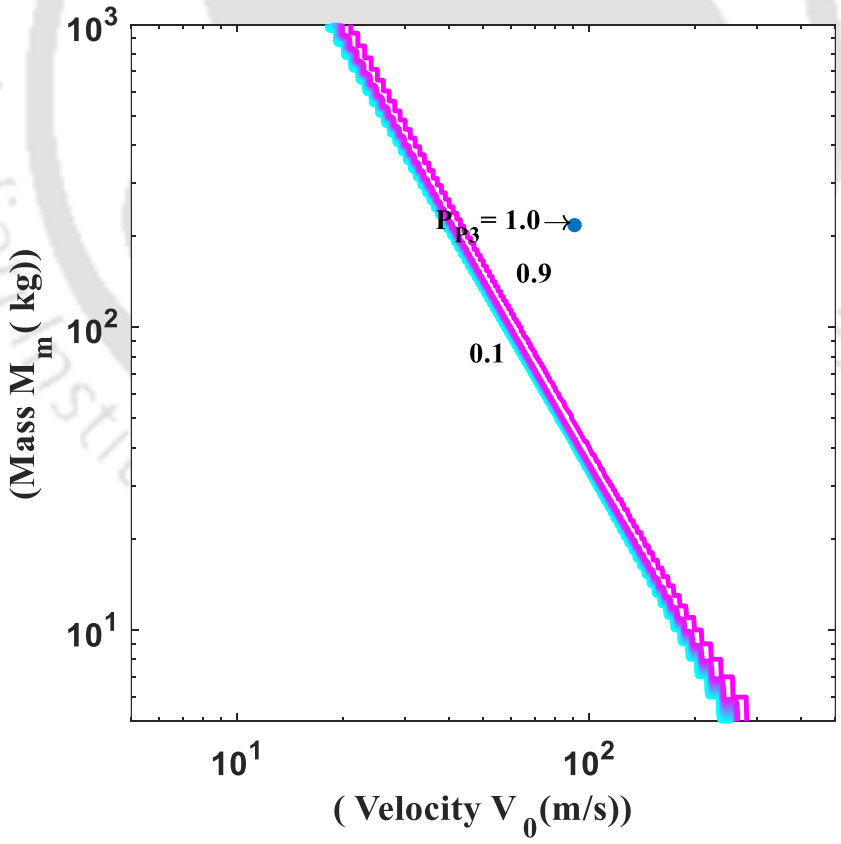

Figure 10.7 Contour plot showing the Fragility estimate for the Nuclear containment RC panel for Performance level P3

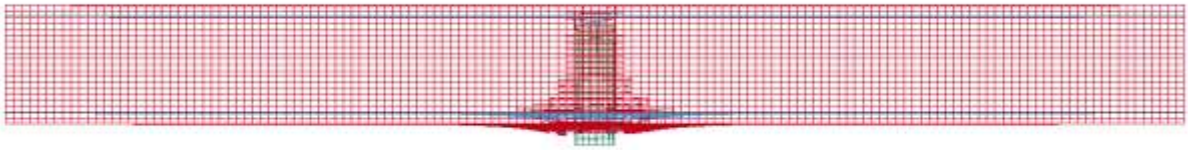

Figure 10.8 Missile impacting RC panel up to full depth, performance level-3 (P3)

10.6. Inference

In this Chapter, the development of the demand model based on kinetic energy formulation for RC panel subject to missile impact is achieved. Probabilistic demand model accounts for the dynamic interaction between the containment panel during missile impact and considers associated uncertainties. This Chapter further shows the framework to evaluate the fragility of Nuclear containment RC panel subjected to missile impact based on developed performance-based capacity models. An accurate estimate of fragility is provided in this framework. Performance and evaluation of the survival of structure for a given scenario can be determined using this performance-based fragility estimation. This research considers realistic loading and structural configurations scenarios to evaluate the response and develop the capacity and demand models. The developed models can be used to design a Nuclear containment RC panel under various impact scenarios.

Performance-based probabilistic capacity models for PC structures are developed in the next Chapter.

Chapter 11. PERFORMANCE-BASED CAPACITY MODELS FOR PC PANELS

The development of the performance-based capacity model for PC panel will follow the same structure as adopted in Chapter 9 for RC panels. The performance levels are defined in Chapter 4 and the subsequent probabilistic formulation for performance levels are developed in Chapter 8. Based on this categorization of different damage levels, the associated capacity of the PC panel subject to missile impact will be estimated in this Chapter. The probabilistic capacity models will be developed corresponding to the three different performance levels as developed in Chapter 4 earlier based on internal energy which is defined as the resistance offered by a Nuclear Containment PC panel during a missile impact scenario at each performance level. That is, the dynamic capacity for the performance level of operation with minimal damage (P_1) where P_{p1} is defined as maximum internal resistance energy by the target structure before D2 begins. Similarly, the dynamic capacity for the performance level of operational with some damage (P_2) where P_{p2} is defined as the maximum internal resistance energy by the target structure before D2 begins. Finally, P_{p3} is defined as the maximum internal energy resisted by the target structure before D4 begins to occur. This section develops probabilistic capacity models for performance levels P_1, P_2 and P_3.

From the obtained results of the FE simulations which is based on Chapter 7 of Experimental Design, this Chapter develops probabilistic models for estimating the internal energy (Capacity) of Nuclear containment PC panel subject to missile impact for each of the three performance levels. These models take into consideration of relevant uncertainties which includes statistical uncertainty and model error as explained in (Gardoni *et al.*, 2002). Data utilised for model assessment from FE simulations are assumed to be no error in measurement.

Following the probabilistic model's general formulation by (Gardoni *et al.*, 2002), the dynamic resistance model for performance level Pi, i=1, 2, 3 is formulated as

$$P_{pi}(x, \Theta_{pi}) = \hat{P}_{pi}(x) * Y_{pi}(x_i, \Theta_{pi}) + \sigma_{P_i} e_{P_i} \tag{11.1}$$

where, P_{pi}=normalized dynamic capacity for performance level Pi, $\hat{P}_{pi}$ = normalized dynamic capacity from mechanical model, $Y_{pi}(x_i, \Theta_{pi})$ = correction term for the bias inherent in the mechanical model.

$$Y_{pi}(x_i, \Theta_{pi}) = \sum_{j=1}^{K_{pi}} \Theta_{Pi,j} h_{Pi,j}(x) \tag{11.2}$$

where $h_{P_{i,j}}(x)$, j = 1,…,n = explanatory function (or regressors) defined as functions of x, $\theta_{P_i,j}$, j=1,…,n are the parameters associated with explanatory functions, $\sigma_{P_i} e_{P_i}$ = model error, e_{P_i} =Gaussian error and $\Theta_{P_i} = \theta_{P_i}$ = set of unknowns model parameters in which θ_{P_i}=($\theta_{P_i,1}$,K,$\theta_{P_i,k}$).

11.1. Mechanical Model for Performance Level P1

The estimate of the dynamic capacity for performance level 1 (P1) is based on the resistance energy of the target structure. Considered terms for this mechanical model are (Performance level – 1, no damage and spalling of cover only) compressive strength of concrete, area of missile cross-section and penetration depth of missile up to clear cover. The proposed formula is,

$$\hat{P}_{p1} = \left[f_c \left(\frac{\pi}{4} d^2 \right) \right] X_{p1} \tag{11.3}$$

Where, f_c=compressive strength of concrete (N/m^2), d=diameter of the missile (m), X_{p1}=penetration of the missile up to clear cover (m).

11.2. Mechanical Model for Performance Level P2

The estimate of the dynamic capacity for performance level 2 (P2) is based on the resistance energy of the target structure. Considered terms for this mechanical model are (Performance level – 2, missile penetrated into the half slab, moderate damage) compressive strength of concrete, the perimeter of missile & mid-depth of concrete target and penetration depth of missile up to mid-depth of the target. And the proposed formula is,

$$\hat{P}_{p2} = (0.1 f_c \pi d) {X_{p2}}^2 \qquad (11.4)$$

f_c=compressive strength of concrete (N/m^2), d=diameter of the missile (m), X_{p2}=penetration of the missile up to mid-depth (m).

11.3. Mechanical Model for Performance Level P3

The estimate of the dynamic capacity for performance level 3 (P3) is based on the resistance energy of the target structure. Considered terms for this mechanical model are (Performance level – 3, significant damage, Full penetration by missile) compressive strength of concrete, the perimeter of missile & mid-depth of concrete target and penetration depth of missile up to the mid depth of target. The proposed formula is,

$$\hat{P}_{p3} = (0.1 f_c \pi d) {X_{p3}}^2 \qquad (11.5)$$

f_c=compressive strength of concrete (N/m^2), d=diameter of the missile (m), X_{p3}= full penetration of the missile (m).

11.4. Model Correction

Appropriate model correction terms are considered to capture exact phenomena which are not accounted in mechanical models. Based on available literature (Gardoni et al., 2002, Sharma et al., 2012) and intuitions of the researcher these explanatory functions are considered. Selected explanatory functions are listed in Table 11.1 below. Considered functions are dimensionless, and table lists the exact quantities which influence model and are captured by the explanatory functions.

Table 11.1 List of Explanatory Functions for Capacity Models

Variable	Expression
$\boldsymbol{h_1(x)}$	1
$\boldsymbol{h_2(x)}$	$\left(\frac{L_s}{t_c}\right)$
$\boldsymbol{h_3(x)}$	$\left(\frac{\Delta^1}{t_c}\right)$
$\boldsymbol{h_4(x)}$	$\left(\frac{L_m}{d}\right)$
$\boldsymbol{h_5(x)}$	$\left(\frac{MV_0^2}{d^3 f_c}\right)$
$\boldsymbol{h_6(x)}$	$\left(\frac{MV_0}{TLt_c f_c}\right)$
$\boldsymbol{h_7(x)}$	$\left(\frac{MV_0^2}{M_c}\right)$
$\boldsymbol{h_8(x)}$	$\left(\frac{t_c}{X_{pen}}\right)$

Where L_s = Length of panel, t_c = thickness of concrete target, Δ = Hump of target from center, L_m = Length of missile, d= diameter of missile, M = mass of missile, V_0 = Velocity of missile, f_c = concrete compressive strength, 1/T = frequency, M_c = Moment Capacity of target structure, X_{pen} = penetration at different levels, n = 1,2,3.

The first explanatory function $h_1(x)$ is considered to catch a potential constant bias which is present in the mechanical model. The second explanatory function $h_2(x)$ accounts for the contribution slenderness ratio of the panel structure. $h_3(x)$ is capturing the interest of the curvature effect of the whole system. The slenderness ratio of the missile is captured by fourth explanatory function $h_4(x)$. The fifth explanatory function $h_5(x)$ contributes to the effect of the energy of the missile imposed on the target. The effect of the natural frequency of the system is accounted for by sixth explanatory function $h_6(x)$. The seventh explanatory function $h_7(x)$ contributes the moment capacity resistance of the total system. The various performance levels penetration depth is considered by eighth explanatory function $h_8(x)$. Figure 11.1 shows a representative simulation as per the details presented in Chapter 6 and Chapter 7.

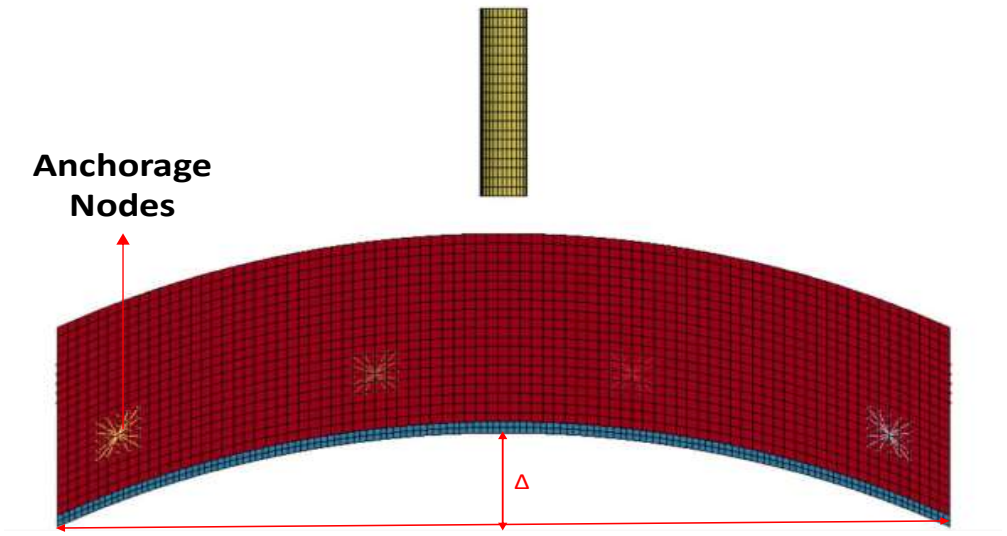

Figure 11.1 FE Simulation of missile impact on PC Slab

11.5. Model Assessment

Bayesian inference is chosen for the estimation of the model parameters Θ. A noninformative prior is selected (Box & Tiao 1992). A stepwise deletion process is used for selecting the parsimonious model. In this method, diagnostic plots are created between the explanatory function and the residual of the dynamic capacity of the FE model and the mechanical model. Suitable explanatory functions are chosen one at a time which shows the strongest correlation. The mean of the standard deviation is monitored to check the adequacy of the model.

11.6. Parameter Estimation for Performance Level P1

Figure 11.2 shows the data capturing of internal energy of FE capacity models for performance level -1 and same procedure followed for remaining FE models. The most statistically significant explanatory functions for P1 are $h_1(x)$, $h_2(x)$ and $h_3(x)$. These terms take into the consideration for constant bias, the slenderness ratio of target structure and curvature effect on the panel which distributes stresses in three directions. The posterior statistics of the model is shown in Table 11.2.

Table 11.2 Posterior Statistics of Parameters in Selected Dynamic Capacity (P1) Model

Parameter	Mean	Standard deviation	Correlation Coefficient		
			Θ_1	Θ_2	Θ_3
Θ_1	-11.2806	6.439	1.00		
Θ_2	3.775	1.525	-0.981	1.00	
Θ_3	-1.8772	2.779	-0.508	0.3514	1.00

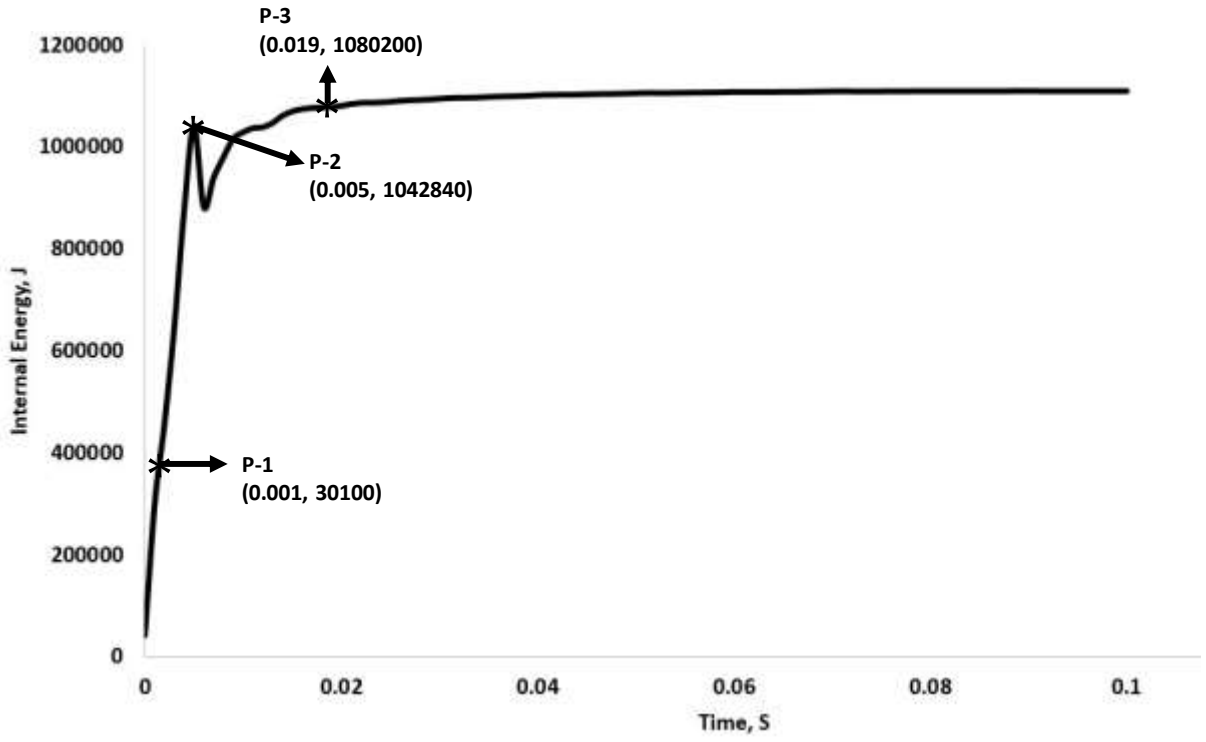

Figure 11.2 Dynamic Capacity of PC Target Structure for Performance Level – 1

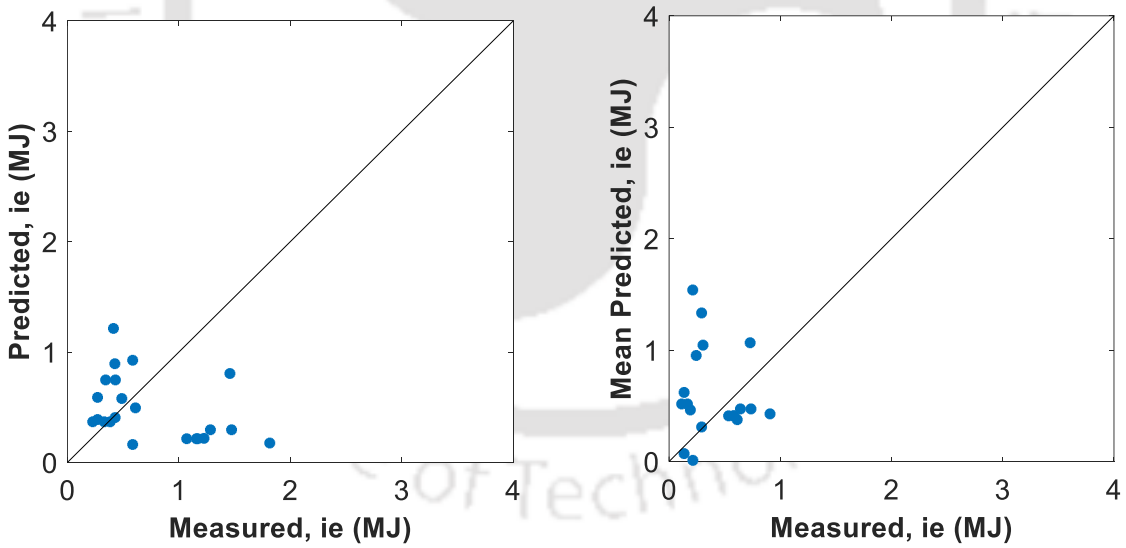

Figure 11.3 Comparison of measured and predicted Dynamic Capacity (P1) of PC panel based on mechanical (left) and probabilistic (right) model

Figure 11.3 shows the comparison between the estimation of dynamic capacity at performance level P1 in terms of internal energy of Nuclear containment PC panel based on the proposed

mechanical model and the mean of the developed probabilistic model where the mean predication for the dynamic capacity P_{P1} is developed by

$$P_{P1} = \hat{P}_{p1}\left(-11.2806 + 3.775\left(\frac{L_s}{t_c}\right) - 1.8772\left(\frac{\Delta}{t_c}\right)\right) \tag{11.6}$$

where P_{P1}=Probabilistic dynamic capacity at performance level P1, $\hat{P}_{p1}$ = dynamic capacity at performance level P1given by the mechanical model.

The mechanical and probabilistic models are both plotted against the capacity in the term of internal energy of the Nuclear containment PC panel values estimated from the FE simulations. Majority of data points are lying near to 1:1 line. The data contains equality data. The predictions of the probabilistic model show that the equality data lays both above and below the 1:1 line. The probabilistic model corrects this inherent bias in the model. The cov is 10% which details the accuracy of the developed probabilistic model for estimating the Capacity of PC panel subject to missile impact at Performance level P1.

11.7. Parameter Estimation for Performance Level P2

Figure 11.4 shows the data capturing of internal energy of FE capacity models for performance level -2 and same procedure followed for remaining FE models. The most statistically significant explanatory functions for performance level P2 are $h_1(x)$, $h_2(x)$ and $h_3(x)$. These terms take into consideration for constant bias, the slenderness ratio of target structure and curvature effect on the panel which distributes stresses in three directions. The posterior statistics of the model is presented in Table 11.3

Table 11.3 Posterior Statistics of Parameters in Selected Dynamic Capacity (P2) Model

Parameter	Mean	Standard deviation	Correlation Coefficient		
			Θ_1	Θ_2	Θ_3
Θ_1	-1.3069	6.439	1.00		
Θ_2	0.5374	1.525	-0.981	1.00	
Θ_3	0.9245	2.779	-0.508	0.3514	1.00

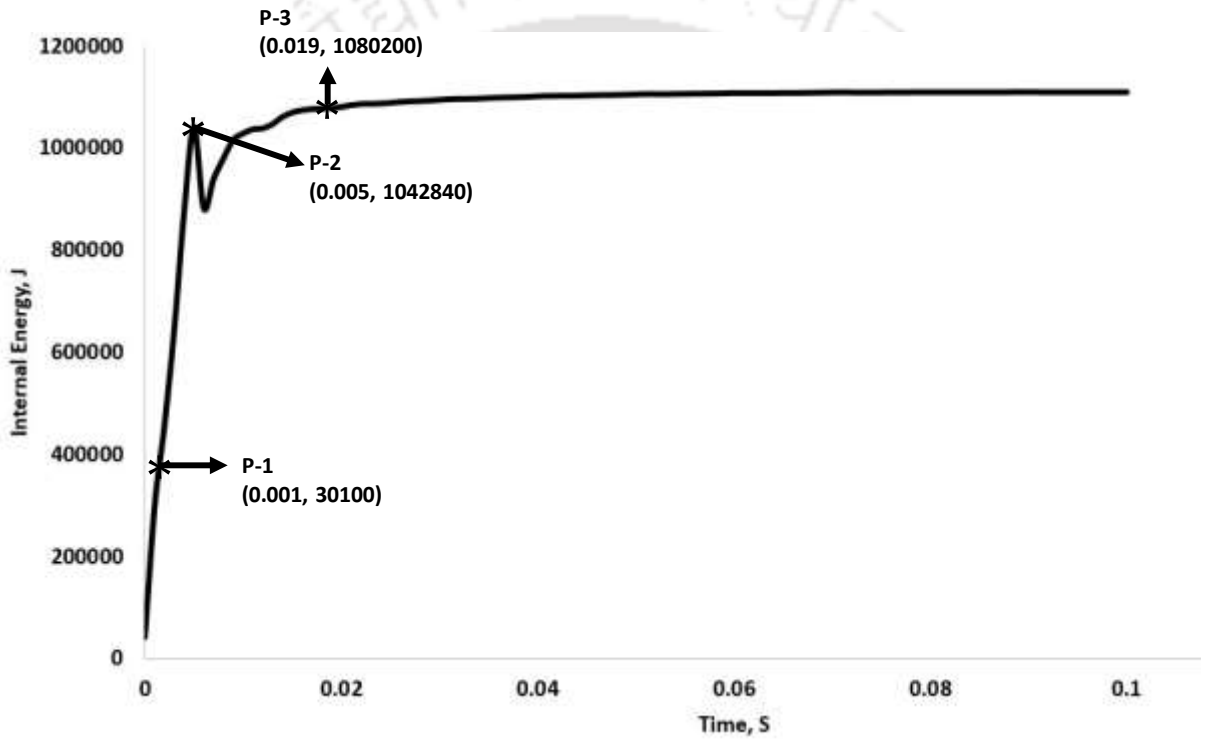

Figure 11.4 Dynamic Capacity of PC Target Structure for Performance Level – 2

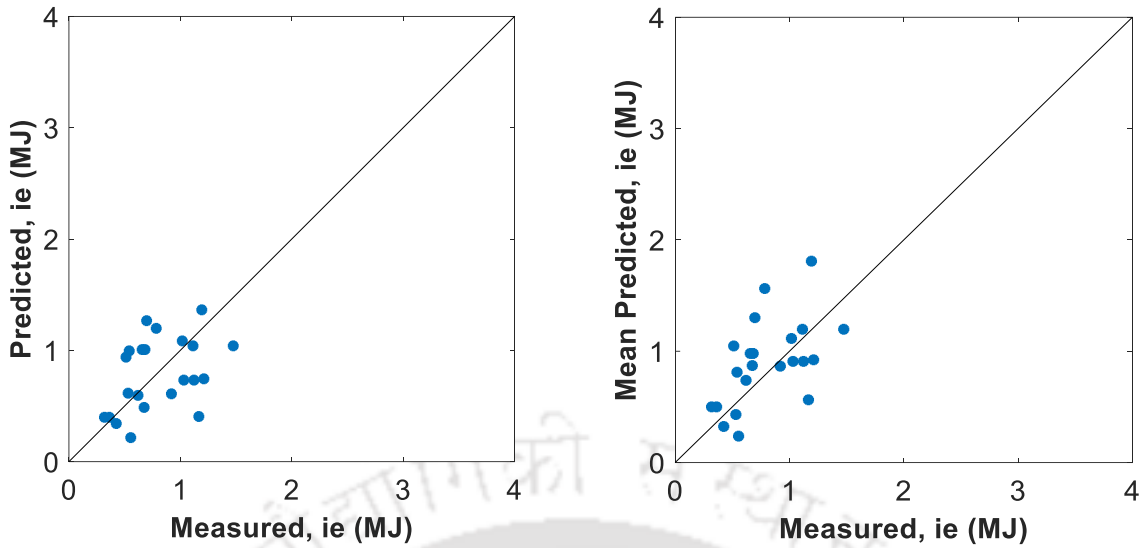

Figure 11.5 Comparison of measured and predicted Dynamic Capacity (P2) of PC panel based on mechanical (left) and probabilistic (right) model

Figure 11.5 shows the comparison between the estimation of dynamic capacity in term of internal energy of Nuclear containment PC panel based on the proposed mechanical model and the mean of the developed probabilistic model where the mean predication for the dynamic capacity P_{P2} is proposed as

$$P_{P2} = \hat{P}_{p2}\left(-1.3069 + 0.5374\left(\frac{L_s}{t_c}\right) + 0.9245\left(\frac{\Delta}{t_c}\right)\right) \tag{11.7}$$

where P_{P2}= Probabilistic dynamic capacity at performance level P2, $\hat{P}_{p2}$ = dynamic capacity given by the mechanical model.

The mechanical and probabilistic models are both plotted against the capacity in the term of internal energy of the containment panel values estimated from the FE simulations. Majority of data points are lying near to 1:1 line. The data contains equality data. The predictions of the probabilistic model show that the equality data lays both above and below the 1:1 line. The probabilistic model corrects this inherent bias in the model. The cov is 1.2%

which details the accuracy of the developed probabilistic model for estimating the Capacity of PC panel subject to missile impact at Performance level P2.

11.8. Parameter Estimation for Performance Level P3

Figure 11.6 shows the data capturing of internal energy of FE capacity models for performance level -3 and same procedure followed for remaining FE models. The most statistically significant explanatory functions for P3 are $h_1(x)$, $h_2(x)$ and $h_3(x)$. These terms take into consideration for constant bias, the slenderness ratio of target structure and curvature effect on the panel which distributes stresses in three directions. The posterior statistics of the model is shown in Table 11.4.

Table 11.4 Posterior Statistics of Parameters in Selected Dynamic Capacity (P3) Model

Parameter	Mean	Standard deviation	Correlation Coefficient		
			Θ_1	Θ_2	Θ_3
Θ_1	-0.7713	6.439	1.00		
Θ_2	0.3593	1.525	-0.981	1.00	
Θ_3	0.6783	2.779	-0.508	0.3514	1.00

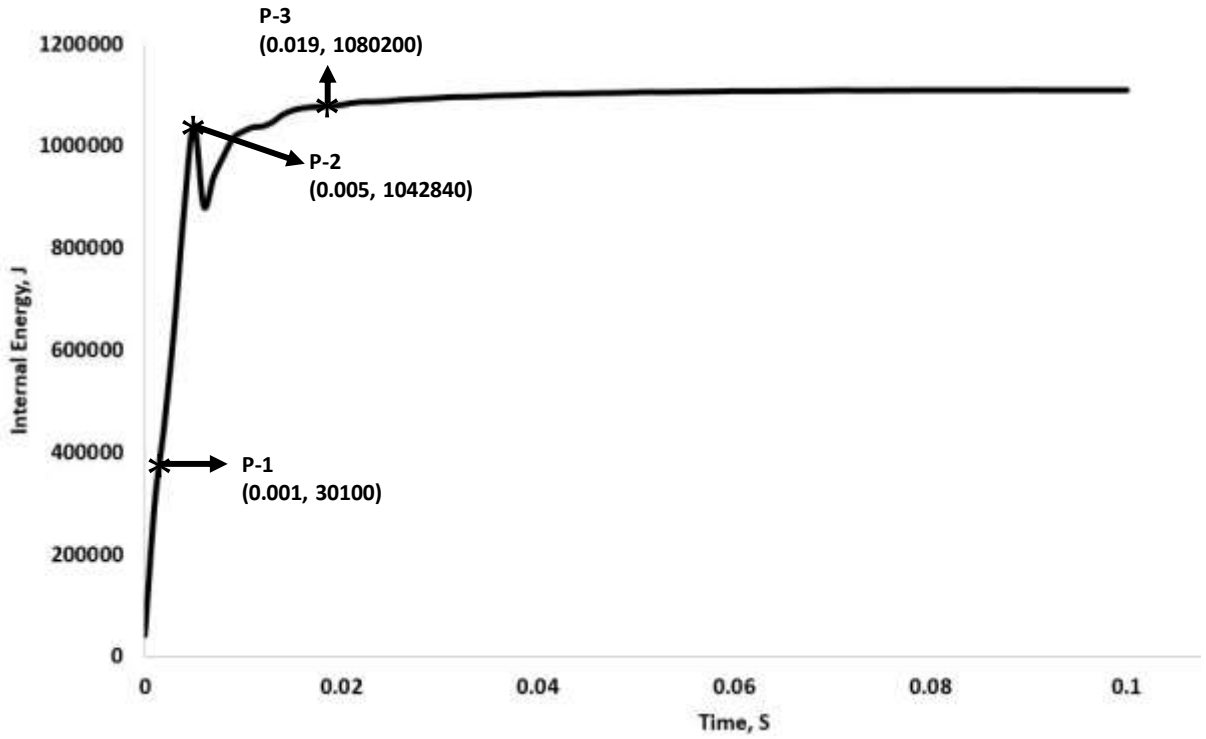

Figure 11.6 Dynamic Capacity of PC Target Structure for Performance Level –3

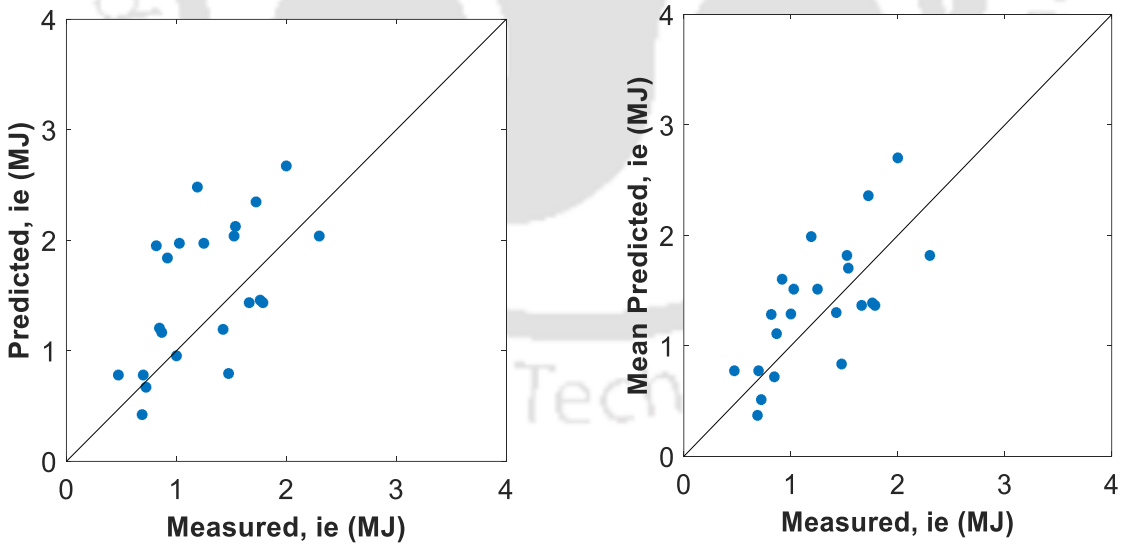

Figure 11.7 Comparison of measured and predicted Dynamic Capacity (P3) of the PC panel based on mechanical (left) and probabilistic (right) model

Figure 11.7 shows the comparison between the estimation of dynamic capacity in term of internal energy of Nuclear containment PC panel based on the proposed mechanical model and the mean of the developed probabilistic model where the mean predication for the dynamic capacity P_{P3} is developed as

$$P_{P3} = \hat{P}_{p3}\left(-0.7713 + 0.3593\left(\frac{L_s}{t_c}\right) + 0.6783\left(\frac{\Delta}{t_c}\right)\right) \tag{11.8}$$

where P_{P3}= Probabilistic dynamic capacity at performance level P3, $\hat{P}_{p3}$ = dynamic capacity given by the mechanical model.

The mechanical and probabilistic models are both plotted against the capacity in the term of internal energy of the Nuclear containment PC panel values estimated from the FE simulations. Majority of data points are lying near to 1:1 line. The data contains equality data. The predictions of the probabilistic model show that the equality data lays both above and below the 1:1 line. The probabilistic model corrects this inherent bias in the model. The cov is 1.88% which details the accuracy of the developed probabilistic model for estimating the Capacity of PC panel subject to missile impact at Performance level P3.

11.9. Inference

Probabilistic capacity models for PC panels have been developed in this Chapter which corresponds to each performance levels as developed in Chapter 4. The developed probabilistic capacity models accurately estimate the capacity of PC panel at the given performance level as evident from the value of cov which is under 10% for all the cases. The developed capacity models are based on Energy-based formulation.

The following Chapter develops the probabilistic model to estimate the demand on the PC panel subject to missile impact.

Chapter 12. PERFORMANCE-BASED DEMAND MODELS OF PC PANELS

Based on the results attained from Chapter 6 and Chapter 7, this chapter develops probabilistic demand models for estimating demand in terms of kinetic energy imparted by the missile impact on the target PC structure. These models take into consideration of relevant uncertainties which includes statistical uncertainty and model error as explained in (Gardoni *et al.*, 2002). Data utilised for model assessment from FE simulations are assumed to be no error in measurement. Following the probabilistic model's general formulation by (Gardoni *et al.*, 2002), the dynamic demand for performance level Pi, i=1, 2, 3 is formulated as

$$P_D(x, \Theta_D) = \hat{P}_D(x) * Y_D(x, \Theta_D) + \sigma_D e_D \tag{12.1}$$

P_D = Probabilistic dynamic demand as the kinetic energy of the missile on PC panel, $\hat{P}_D$ = dynamic demand from the mechanical model, $Y_D(x, \Theta_D)$ = correction term for the bias inherit in the mechanical model

$$Y_{pi}(x_i, \Theta_{pi}) = \sum_{j=1}^{K_{pi}} \Theta_{Pi,j} h_{Pi,j}(x) \tag{12.2}$$

$h_{D,j}(x)$ = explanatory functions, where j=1……k, $\Theta_{D,j}$ = parameter associated with explanatory functions, , $\sigma_D e_D$= model error, e_D=Gaussian error.

12.1. Mechanical Model

The estimate of the dynamic demand $\hat{P}_D$ is based on the kinetic energy of the missile imposed on PC panel. Considered terms for this mechanical model is mass of the missile and velocity of the missile. Units of the mechanical model is energy units joules, and the proposed formula is

$$\hat{P}_D = \frac{1}{2} M {V_0}^2 \tag{12.3}$$

$\hat{P}_D$ = dynamic demand from missile imposed on PC slab, M = Mass of the missile, V_0 = Velocity of the missile

12.2. Model Correction

Model correction terms are considered to capture exact phenomena which are not accounted in mechanical models. Based on available literature (Gardoni et al., 2002, Sharma et al., 2012) and intuitions of the researcher these explanatory functions are considered. Selected explanatory functions are listed in Table 12.1 below. Considered functions are dimensionless, and table lists the exact quantities which influence model and are captured by the explanatory functions.

Table 12.1 List of Explanatory Functions for Demand Models for PC panels.

Variable	Expression
$\boldsymbol{h_1(x)}$	1
$\boldsymbol{h_2(x)}$	$\left(\frac{L_s}{t_c}\right)$
$\boldsymbol{h_3(x)}$	$\left(\frac{\Delta^1}{t_c}\right)$
$\boldsymbol{h_4(x)}$	$\left(\frac{L_m}{d}\right)$
$\boldsymbol{h_5(x)}$	$\left(\frac{MV_0^2}{d^3 f_c}\right)$
$\boldsymbol{h_6(x)}$	$\left(\frac{MV_0}{TLt_c f_c}\right)$
$\boldsymbol{h_7(x)}$	$\left(\frac{MV_0^2}{M_c}\right)$
$\boldsymbol{h_8(x)}$	$\left(\frac{t_c}{X_{pen}}\right)$

Where L_s = Length of panel, t_c = thickness of concrete target, Δ = Hump of target from center, L_m = Length of missile, d= diameter of missile, M = mass of missile, V_0 = Velocity of missile, f_c = concrete compressive strength, 1/T = frequency, M_c = Moment Capacity of target structure, X_{pen} = penetration at different levels, n = 1,2,3.

The first explanatory function $h_1(x)$ is considered to catch a potential constant bias which is present in the mechanical model. The second explanatory function $h_2(x)$ accounts for the contribution slenderness ratio of the panel structure. $h_3(x)$ is capturing the interest of the curvature effect of the whole system. The slenderness ratio of the missile is captured by fourth explanatory function $h_4(x)$. The fifth explanatory function $h_5(x)$ contributes to the effect of the

energy of the missile imposed on the target. The effect of the natural frequency of the system is accounted for by sixth explanatory function $h_6(x)$. The seventh explanatory function $h_7(x)$ contributes the moment capacity resistance of the total system. The various performance levels penetration depth is considered by eighth explanatory function $h_8(x)$.

12.3. Model Assessment

Bayesian inference is chosen for the estimation of the model parameters Θ. A noninformative prior is selected (Box & Tiao 1992). A stepwise deletion process is used for selecting the parsimonious model. In this method, diagnostic plots are created between the explanatory function and the residual of the dynamic demand of the FE model and the mechanical model. Suitable explanatory functions are chosen one at a time which shows the strongest correlation. The mean of the standard deviation is monitored to check the adequacy of the model.

12.4. Parameter Estimation

Figure 12.1 shows the data capturing of kinetic energy of FE demand model and same procedure followed for remaining FE demand models. The most statistically significant explanatory functions for the demand model is $h_2(x)$. These terms take into correct for the contribution of the length and depth of the concrete panel, respectively. The posterior statistics of the model is presented in Table 12.2.

Table 12.2 Posterior Statistics of Parameters in Selected Dynamic Demand Model

Parameter	Mean	Standard deviation	Correlation Coefficient	
			Θ_1	Θ_2
Θ_1	1.0407	0.0225	1.00	
Θ_2	0.0353	0.019	0.9993	1.00

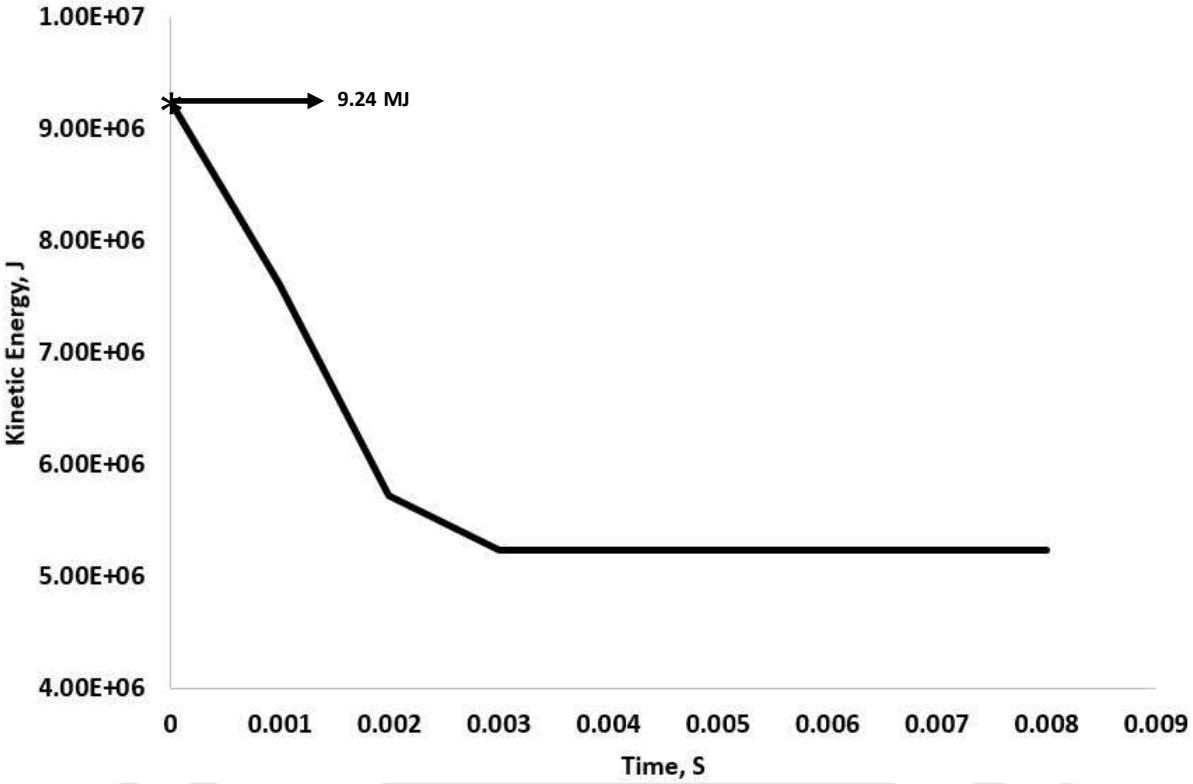

Figure 12.1 Kinetic Energy of Missile for PC Slab

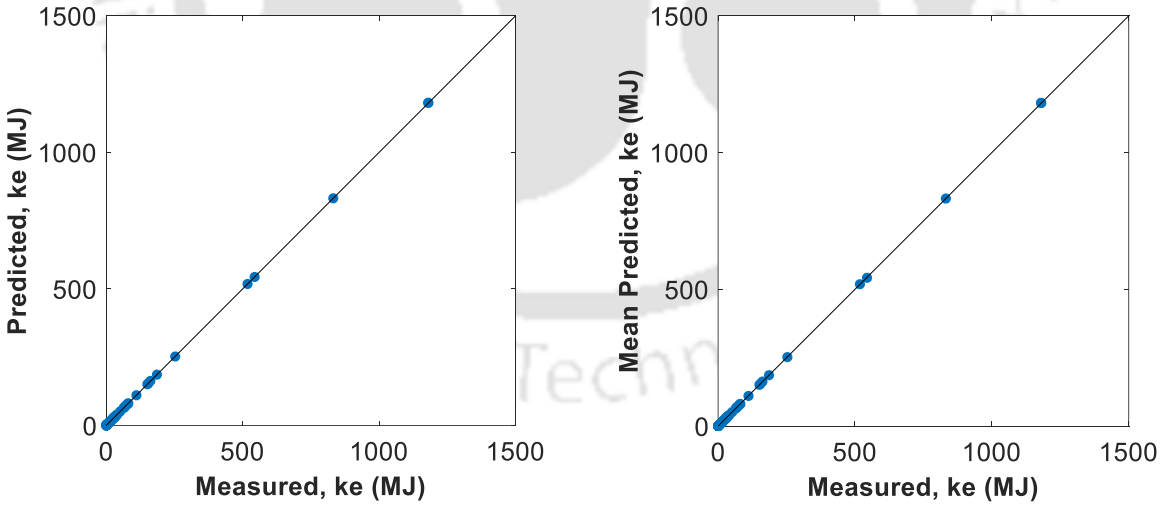

Figure 12.2 Comparison between measured and predicted Dynamic Demand based on mechanical (left) and probabilistic (right) model for missile impact on PC panel

Figure 12.2 shows the comparison between the estimation of dynamic demand in term of the kinetic energy of missile impacting Nuclear containment PC panel based on the proposed mechanical model and the mean of the developed probabilistic model where the mean predication for the dynamic demand P_D is developed as

$$P_D = \hat{P}_D \left\{ 1.0407 - 0.0353 \left(\frac{L_s}{t_c} \right)^{0.1} \right\} \tag{12.4}$$

P_D = Probabilistic dynamic demand imposed on PC panel by missile impact, $\hat{P}_D$ = dynamic demand imposed on RC panel by missile impact from the mechanical model.

The mechanical and probabilistic models are both plotted against the demand in the term of the kinetic energy of the missile impacting the Nuclear containment RC panel in terms of values estimated from the FE simulations. Majority of data points are lying near to 1:1 line. The data contains equality data. The predictions of the probabilistic model show that the equality data lays both above and below the 1:1 line. The probabilistic model corrects this inherent bias in the model. The cov is 0.0001% which details the accuracy of the developed probabilistic model for estimating the Demand on PC panel subject to missile impact.

12.5. Fragility Estimates

In this thesis, Fragility is defined as the conditional probability of exceeding a specified performance of a target structure for given initial velocity V_0 and mass M of an impacting missile. Probabilistic demand models are used to establish the fragility of the structural component by providing treatment to aleatory and epistemic uncertainties. Aleatory uncertainties are random in nature and also known as inherent variable and randomness. This uncertainty cannot be observed by the spectator or pattern of observation and is available in the set of quantifiable variables like material property constants, structural member dimensions, and imposed boundary conditions and partly in error terms (Gardoni et al., 2002). The

Epistemic uncertainties arose due to our lack of knowledge, from measurement errors, from limited observation samples. This kind of uncertainty are available in capacity, demand models and partially in error terms. Fragility plots are generated for each performance objectives defined in the research. Each performance level could generate particular fragility curve to show the vulnerability of the specimen.

Based on the variation of the demand imposed on Nuclear containment PC panel, the fragility analysis gives an estimate of the vulnerability of the Nuclear containment RC panel. The fragility of the Nuclear containment RC panel subjected to missile impact is formulated as

$$F(x,\Theta) = P[g(x,\Theta) \leq 0 | V_0, M]$$

where, $g_{p_i}(x,\Theta)$ is the limit state function defined as,

$$g_{p_i}(x,\Theta) = P_{p_i}(x,\Theta) - P_D$$

$p_i = 1,2,3$ for the all three performance levels P1, P2, and P3. Construction of performance-based probabilistic models for the performance levels P1, P2, and P3 are developed in Chapter 10. Here, the fragility of a Nuclear containment PC panel is estimated based on varying the initial missile initial velocity V_0 and mass of the missile M. Considering the properties and configuration one FE model from simulations subject to impact by a missile as given in Table 12.3. Figure 12.3 shows the fragility estimates contour plot of the Nuclear containment PC panel for performance level 1.

Table 12.3 Configuration and Dimensions of PC panel, Missile for Fragility analysis

Name of Configuration	Symbol	Dimensions
Length of Panel (square)	L_s	4 m
Thickness of Concrete Panel	t_c	1 m
Thickness of Steel Liner	t_s	0.06 m
Hump of Curved Panel (from centre)	Δ	0.5 m
Diameter of Missile	d	0.212 m
Length of Missile	H	1 m
Mass of Missile	M	2083.68 kg
Velocity of Missile	V_0	279 m/s
Compressive Strength	f_c	59 MPa
Yield Stress of Rebars	f_y	266 MPa
Diameter of Rebar	-	0.08 m
Yield Stress of Tendons	f_t	1830 MPa
Diameter of Tendon	-	0.13 m
Area of Rebars	-	0.080384 m^2
Area of Tendons	-	0.106 m^2

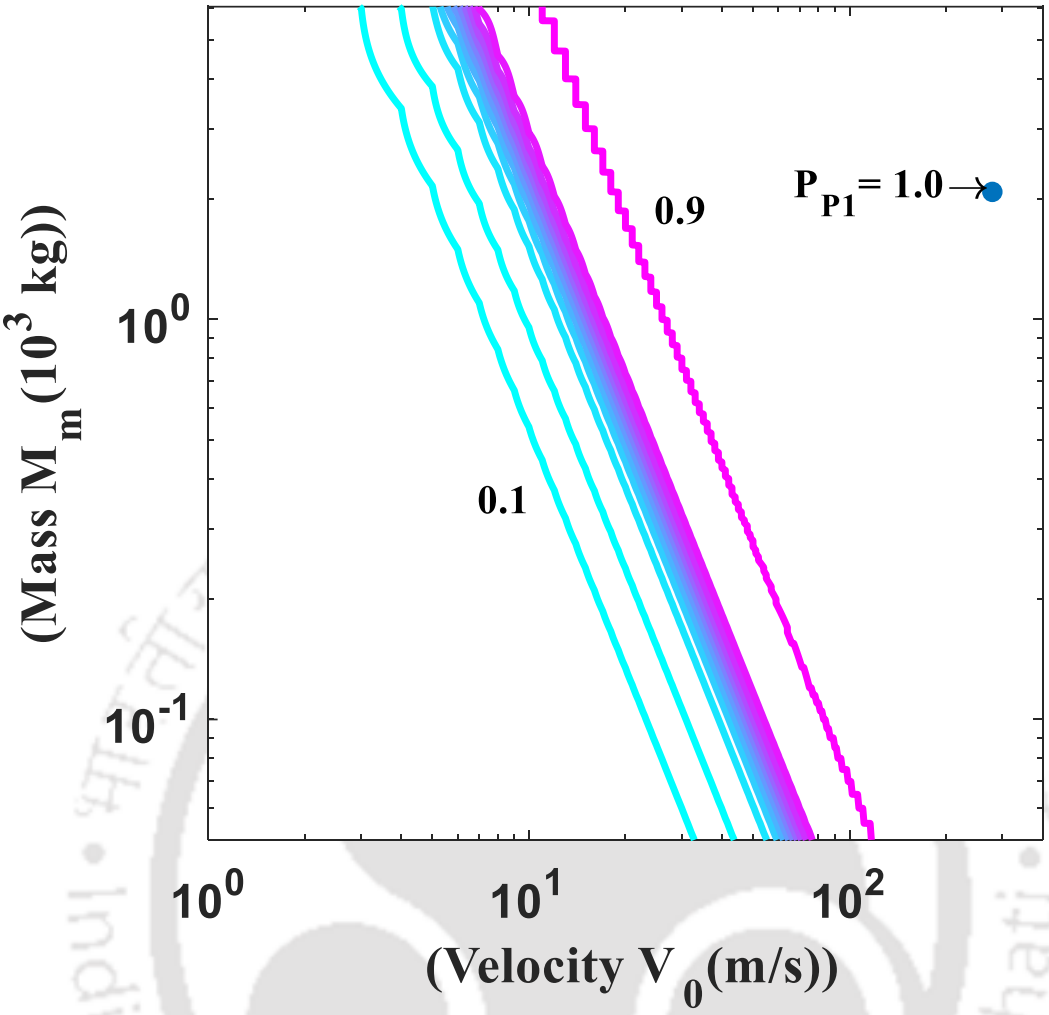

Figure 12.3 Contour plot showing the Fragility estimate for the Nuclear containment PC panel for Performance level P1

The plot is in log scale which comprised of missile initial velocity (m/s) range on the x-axis and missile mass (1000 kg) upon y-axis. The contour plot shows the fragility variation upon the domain of the mass and velocity. Contours of exceedance for performance level – 1 (P1) shows the well-spread nature, as shown the distribution of the lines of fragility from 0.1 to 0.9 (Figure 10.3). The exceedance of performance level – 1 is achieved with a lower value of demand imposed. The FE simulation is shown in Figure 12.4. Confirming to the result of the contour plot of Fragility which attains a value of 1, in the FE simulation as well, the exceedance pf performance level P1, i.e. penetration of cover is achieved.

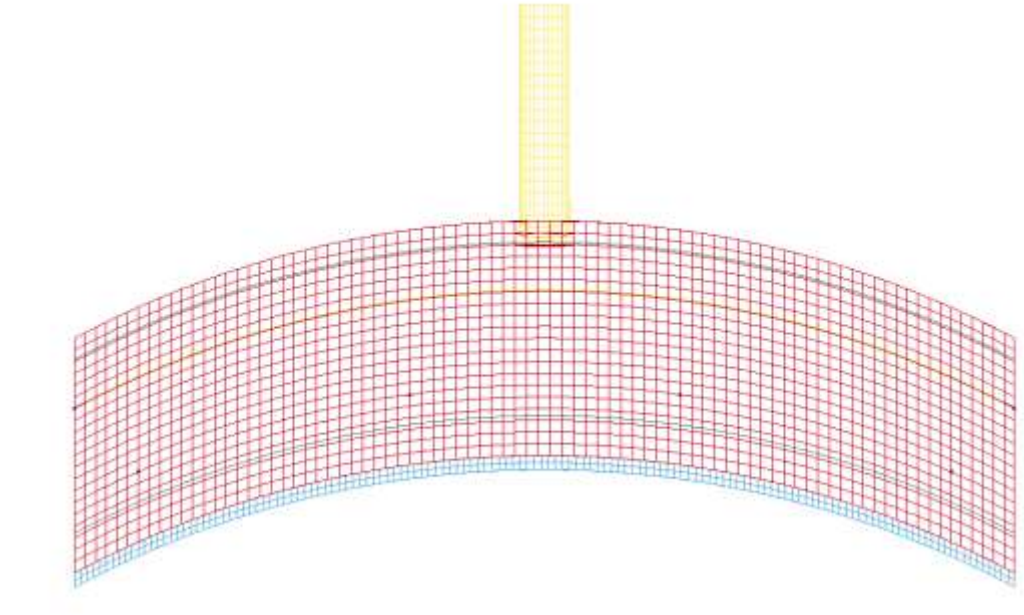

Figure 12.4 Missile impacting PC panel up to clear cover, performance level-1 (P1)

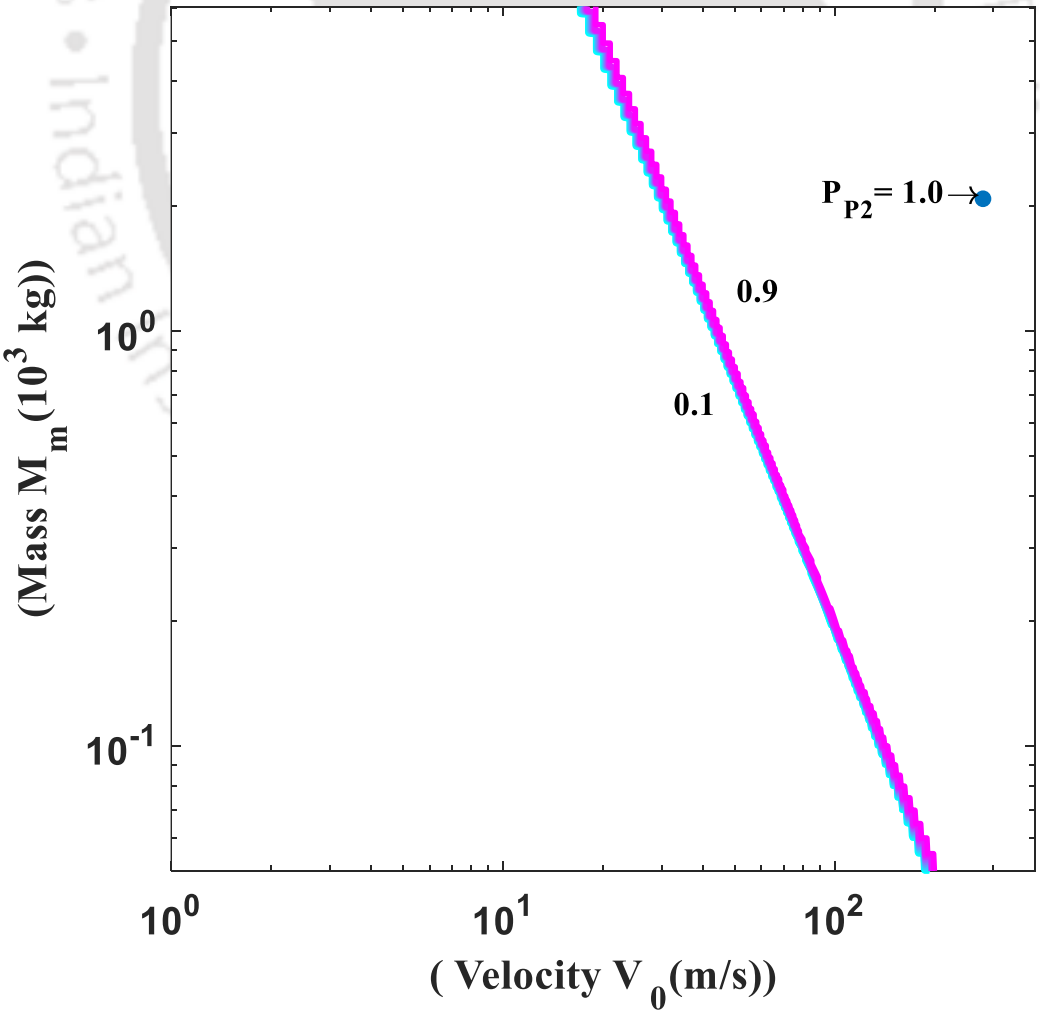

Figure 12.5 Contour plot showing the Fragility estimate for the Nuclear containment PC panel for Performance level P2

Figure 12.4 shows the contour plot for estimating the Fragility of the Nuclear containment PC panel for Performance level P2. The plot is in log scale which comprised of initial missile velocity (m/s) range on the x-axis and missile mass (1000 kg) upon y-axis. The contour plot shows the fragility variation upon the domain of the mass and velocity. Contours of exceedance for performance level – 2 (P2) shows the well-spread nature, as shown the distribution of the lines of fragility from 0.1 to 0.9 (Figure 12.5). The exceedance of performance level – 2 (P2) is achieved with a higher value of demand imposed as compared to performance level -1 (P1). The FE simulation is shown in Figure 12.6. Confirming to the result of the contour plot of Fragility which attains a value of 1, in the FE simulation as well, the exceedance pf performance level P2, i.e. half penetration of PC slab is achieved.

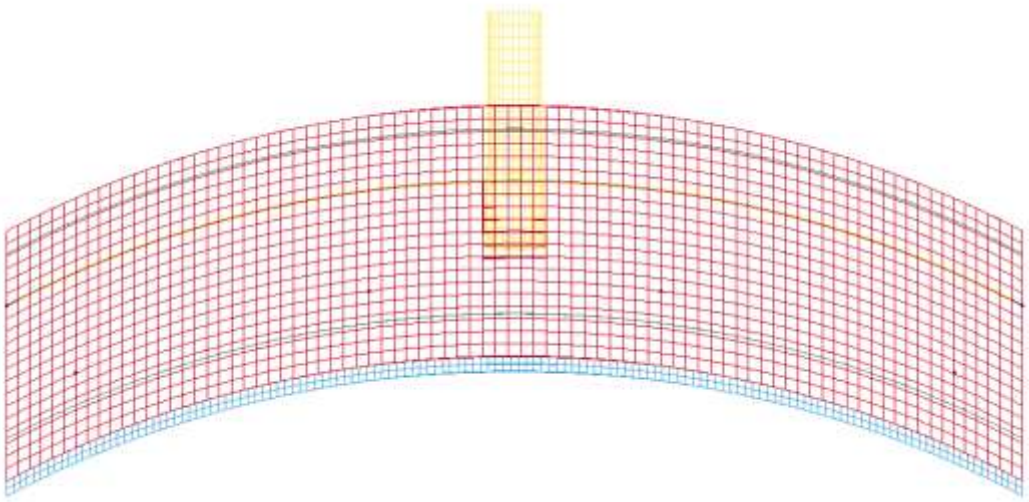

Figure 12.6 Missile impacting PC panel up to mid depth, performance level-2 (P2)

Figure 12.7 shows the contour plot for estimating the Fragility of the Nuclear containment PC panel for Performance level P3. The plot is in log scale which comprised of initial missile velocity (m/s) range on the x-axis and missile mass (1000 kg) upon y-axis. The

contour plot shows the fragility variation upon the domain of the mass and velocity. Contours of exceedance for performance level – 3 (P3) shows the well-spread nature, as shown the distribution of the lines of fragility from 0.1 to 0.9 (Figure 12.7). The exceedance of performance level – 3 (P3) is achieved with the highest value of demand imposed as compared to performance level -1 (P1) and performance level -2 (P3). The FE simulation is shown in Figure 12.8. Confirming to the result of the contour plot of Fragility which attains a value of 1, in the FE simulation as well, the exceedance pf performance level P3, i.e. full penetration of PC slab is achieved.

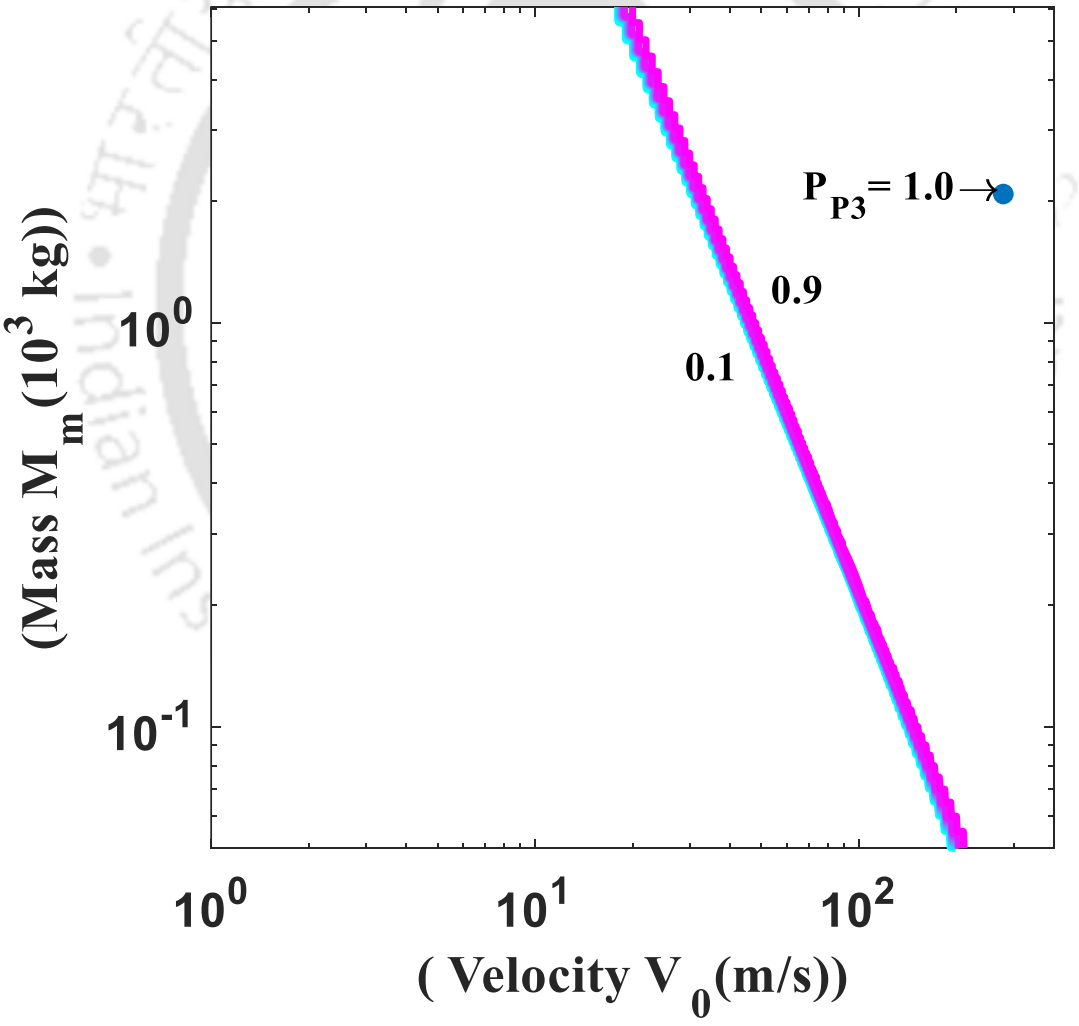

Figure 12.7 Contour plot showing the Fragility estimate for the Nuclear containment PC panel for Performance level P3

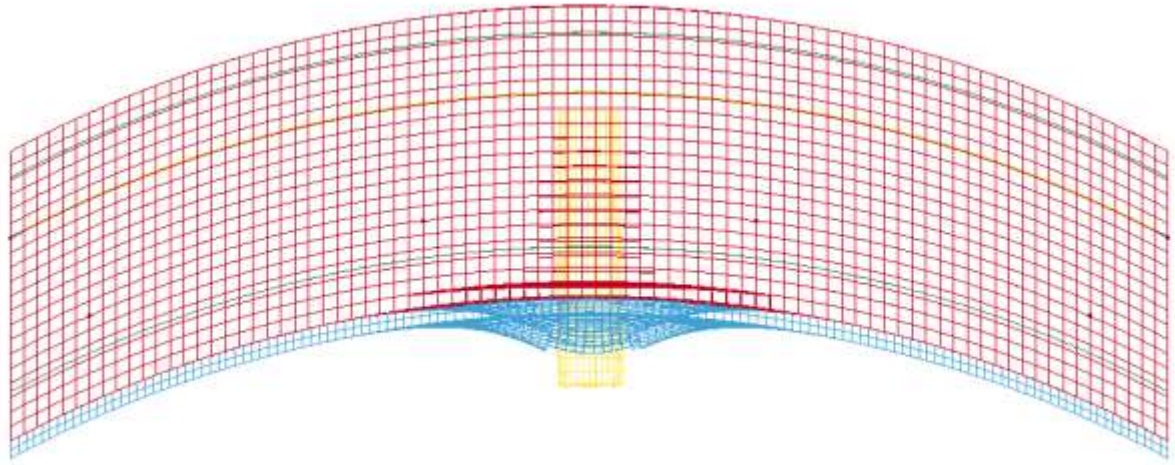

Figure 12.8 Missile impacting PC panel up to full depth, performance level-3 (P3)

12.6. Inference

In this Chapter, the development of a demand model based on kinetic energy formulation for PC panel subject to missile impact is achieved. Probabilistic demand model accounts for the dynamic interaction between the containment panel during missile impact and considers associated uncertainties. This Chapter further shows the framework to evaluate the fragility of Nuclear containment PC panel subjected to missile impact based on developed performance-based capacity models. An accurate estimate of fragility is provided in this framework. Performance and evaluation of the survival of structure for a given scenario can be determined using this performance-based fragility estimation. This research considers realistic loading and structural configurations scenarios to evaluate the response and develop the capacity and demand models. The developed models can be used to design a Nuclear containment PC panel under various impact scenarios.

CONCLUSION AND FUTURE WORK

The present work details on the possible threats upon Nuclear containment structures due to natural or man-made impact event across the world. It specifically focuses on the threat to Nuclear containment RC and PC panels subjected to missile impact. Majority of the structures are designed for static loads, at maximum quasi-static loads but the proposed work shifts the available methodology to the local damage effect based on dynamic loads which is a realistic estimate of the phenomena in case of missile collision.

The research develops a framework for performance-based analysis and design of Nuclear Containment Structures subject to missile impact which takes into the inherent uncertainty in the system properties, material and geometric configurations, as well as the interaction of the structure and the missile.

Three different performance level of the structure are quantified based on the damage occurring in the RC and PC panels subject to missile impact. Probabilistic models are developed to accurately quantify these performance levels so that the structure can be analyzed and as well as designed based on these different performance levels.

Performance-based probabilistic capacity models are developed corresponding to each performance levels. The developed probabilistic capacity models accurately estimate the capacity of the RC and PC panel at the given performance level. The developed capacity models are based on Energy-based formulation.

The probabilistic demand model is developed to estimate the demand imposed on RC and PC panel subject to missile impact. The developed demand models are based on Energy-based formulation.

The developed Performance-based capacity and demand model have the following advantages, accounting for:

- Multi-modal response of the structure,
- Transition of failure modes and their interaction
- Inherent uncertainty associated with the modelling, configuration and material properties
- The model is easy to use.
- The model incorporates the uncertainty in modeling, material properties and configuration.
- The model accounts for the increase in strength of material due to the strain rate.
- The model accounts for the effect of inertia due to dynamic loading.

These developed capacity and demand model are used to analyze the fragility (vulnerability) of any given Nuclear Containment structures subject to missile impact. The same formulation can also be used to designing Nuclear Containment structures made of RC and PC panels subject to missile impact. This provides a performance-based forwork for analysis and design of RC and PC panels of Nuclear containment structures subject to missile impact.

The present work can be extended to estimate the capacity and demand of other structural members like steel decks, columns and beams. Some impact scenarios like ship collisions, vehicle falling on slabs due to tornadoes and also like missile impact with ogive, point, hemispherical nose shapes. This achieved work can be utilized for wind-borne missiles hitting to containment structures.

Limitations of the Current Study

- This thesis focusses on impact loading of flat nose missile shape which is not the same in real world, existing conventional missiles and wind borne missiles are of pointy shape to enhance speed of the projectile and to amplify the penetration of the missile.
- Perfect rigidity of the missile is not assured in reality.

Due to the constraints in processing unit, FE models are considered coarser mesh size than usual and more of simulations could have analyzed in present study.

REFERENCES

1. Aktan, A. E., Ellingwood, B. R., & Kehoe, B. (2007). Performance-based engineering of constructed systems. Journal of structural engineering, 133(3), 311-323.
2. Amde, A. M., Mirmiran, A., & Walter, T. A. (1997). Local damage assessment of turbine missile impact on composite and multiple barriers. Nuclear engineering and design, 178(1), 145-156.
3. Amirikian, A. (1950). Design of protective structures (A new concept of structural behavior) (No. NP-3726; NavDocks P-51). Bureau of Yards and Docks.
4. Ang, A. H. S., & Tang, W. H. (2007). Probability concepts in engineering planning and design: Emphasis on application to civil and environmental engineering. Wiley.
5. Ashar, H. (2013). Containment Structures of US Nuclear Power Plants: Background, Regulations, Codes and Standards, and Other Considerations. ASME Press.
6. Steckmest, D., & Asplund, E. (2014). Design with Regard to Collision Impact-Comparison of Response between a Simplified 2DOF systemand FE analysis for Impact on a Simply Supported Elastic Beam (Master's thesis).
7. Bahar, L. Y., & Rice, J. S. (1978). Simplified derivation of the reaction-time history in aircraft impact on a nuclear power plant. Nuclear Engineering and Design, 49(3), 263–268.
8. Balomenos, G. P., & Pandey, M. D. (2017). Probabilistic finite element investigation of prestressing loss in nuclear containment wall segments. Nuclear Engineering and Design, 311, 50–59.
9. Bangash. (2011). Structures for Nuclear Facilities. In Springer (Vol. 1).
10. Becker, R. (2008, December). Fundamentals of performance-based building design. In Building Simulation (Vol. 1, No. 4, pp. 356-371). Tsinghua Press.
11. Bischoff, P. H., & Perry, S. H. (1991). Compressive behaviour of concrete at high strain rates. Materials and Structures, 24(6), 425–450.
12. Box, G. E. P., & Wilson, K. B. (1951). Experimental designs for exploring response surfaces. *Ann Math Stat*, *13*, 1-45.
13. CEB-FIP, M. (1993). 90. Design of concrete structures. CEB-FIP-Model-Code 1990. *British Standard Institution, London*.
14. CEB. (1988). Concrete Structures Under Impact and Impulsive Loading. Comite Euro-International du Beton Lausanne, Switzerland.

15. Chelapati, C. V., Kennedy, R. P., & Wall, I. B. (1972). Probabilistic assessment of aircraft hazard for nuclear power plants. Nuclear Engineering and Design, 19(2), 333–364.
16. Chen, W., Hao, H., & Chen, S. (2015). Numerical analysis of prestressed reinforced concrete beam subjected to blast loading. Materials and Design, 65, 662–674.
17. Chen, X. W., Li, X. L., Huang, F. L., Wu, H. J., & Chen, Y. Z. (2008). Normal perforation of reinforced concrete target by rigid projectile. International Journal of Impact Engineering, 35(10), 1119-1129.
18. Chen, X. W., & Li, Q. M. (2002). Deep penetration of a non-deformable projectile with different geometrical characteristics. International Journal of Impact Engineering, 27(6), 619–637.
19. Choi, S. J., Lee, S. W., & Kim, J. H. J. (2017). Impact or blast induced fire simulation of bi-directional PSC panel considering concrete confinement and spalling effect. Engineering Structures, 149, 113–130.
20. Choun, Y. S., & Park, H. K. (2015). Containment performance evaluation of prestressed concrete containment vessels with fiber reinforcement. Nuclear Engineering and Technology, 47(7), 884–894.
21. Daudeville, L., & Malécot, Y. (2011). Concrete structures under impact. European Journal of Environmental and Civil Engineering, 15(sup1), 101–140.
22. Do, T. V., Pham, T. M., & Hao, H. (2018). Numerical investigation of the behavior of precast concrete segmental columns subjected to vehicle collision. Engineering Structures, 156, 375–393.
23. Easa, S. M., & Yan, W. Y. (2019). Performance-Based Analysis in Civil Engineering: Overview of Applications. Infrastructures, 4(2), 28.
24. Fang, Q., & Wu, H. (2017). Concrete structures under projectile impact. In Concrete Structures under Projectile Impact.
25. Findlay, S. J., & Harrison, N. D. (2002). Why aircraft fail. Materials Today, 5(11), 18–25.
26. Forrestal, M. J., & Hanchak, S. J. (2002). Penetration Limit Velocity for Ogive-Nose Projectiles and Limestone Targets. Journal of Applied Mechanics, 69(November), 853.
27. Frano, R. Lo, & Forasassi, G. (2011). Preliminary evaluation of aircraft impact on a near term nuclear power plant. Nuclear Engineering and Design, 241(12), 5245–5250.
28. Gabi, B., Tov, E., & Anatoly, D. (2013). High-speed penetration dynamics: engineering models and methods. World Scientific.

29. Gardoni, P., Der Kiureghian, A., & Mosalam, K. M. (2002). Probabilistic capacity models and fragility estimates for reinforced concrete columns based on experimental observations. Journal of Engineering Mechanics, 128(10), 1024–1038.
30. Gibson, E. J. (1982). A Report from CIB Commission W60 Working with the Performance Approach to Building. Performance Concept in Building, 23-30.
31. Grisaro, H. and Dancygier, A. N. (2014) 'A Modified Energy Method to Assess the Residual Velocity of Non-Deforming Projectiles That Perforate Concrete Barriers', International Journal of Protective Structures, 5(3), pp. 307–321.
32. Gross, J. G. (1996, December). Developments in the application of the performance concept in building. In 3rd. International Symposium-Applications of the Performance Concept in Building.
33. Gu, Z. (2018, October 1). History review of nuclear reactor safety. Annals of Nuclear Energy, Vol. 120, pp. 682–690.
34. Hanchak, S. J., Forrestal, M. J., Young, E. R., & Ehrgott, J. Q. (1992). Perforation of concrete slabs with 48 MPa (7 ksi) and 140 MPa (20 ksi) unconfined compressive strengths. International Journal of Impact Engineering, 12(1), 1–7.
35. Houssin, D., Dujardin, T., Cameron, R. (2015). 2015 Technology Roadmap: Nuclear Energy.
36. Huang, X., Kwon, O. S., Bentz, E., & Tcherner, J. (2017). Evaluation of CANDU NPP containment structure subjected to aging and internal pressure increase. Nuclear Engineering and Design, 314, 82–92.
37. International Atomic Energy Agency. (2004). Design of Reactor Containment Systems for Nuclear Power Plants.
38. Iqbal, M. A., Kumar, V., & Mittal, A. K. (2019). Experimental and numerical studies on the drop impact resistance of prestressed concrete plates. International Journal of Impact Engineering, 123, 98–117.
39. IRSN. (2016). Health consequences of the Fukushima accident Summary of the epidemiological studies conducted on the inhabitants of the Fukushima Prefecture Report on the situation in March 2016 Principle of the studies in place State of progress of the on-going studies. (March), 1–13.
40. Jasawanth, G., Kumar, S., & Sharma, H. (2017). Impact testing Facility: BHISM for Performance Based Design of Reinforced Concrete (RC) Structures. Procedia Engineering.
41. Jeong, U. Y., & Tarrant, K. (2018). Wind Loading on Tall Building Structures in Consideration of Performance-Based Design. In Wind Engineering for Natural Hazards:

Modeling, Simulation, and Mitigation of Windstorm Impact on Critical Infrastructure (pp. 79-95).

42. Jiang, H., & Chorzepa, M. G. (2015). An effective numerical simulation methodology to predict the impact response of pre-stressed concrete members. Engineering Failure Analysis, 55, 63–78.
43. Jin, S., Li, Z., Lan, T., & Gong, J. (2019). Fragility analysis of prestressed concrete containment under severe accident condition. Annals of Nuclear Energy, 131, 242–256.
44. Johansson, A., & Fredberg, J. (2015). Structural Behaviour of Prestressed Concrete Beams During Impact Loading. 176.
45. Jung, R., Hwang, J., Chung, C., & Lee, J. (2015). Assessment of Impact Resistance Performance of Post-Tensioned Curved Wall using Numerical Impact Simulation.
46. Kassem, F. (2015). Reliability of reinforced concrete structures: Case of slabs subjected to impact (Doctoral dissertation).
47. Kar, A. K. (1979) 'Impactive Effects of Tornado Missiles and Aircraft', ASCE J Struct Div, 105(11), pp. 2243–2260
48. Kennedy, R. P. (1976) 'A review of procedures for the analysis and design of concrete structures to resist missile impact effects', Nuclear Engineering and Design. North-Holland, 37(2), pp. 183–203.
49. Khaji, A., Fallahdoost, S., Soroush, M. R., Movaghar, V. R., & Shuang-ming, S. (2012). Civilian casualties of Iraqi ballistic missile attack to Tehran, capital of Iran. Chinese Journal of Traumatology, 15(3), 162–165.
50. Kœchlin, P. and Potapov, S. (2009) 'Classification of soft and hard impacts—Application to aircraft crash', Nuclear Engineering and Design, 239(4), pp. 613–618.
51. Kojima, I. (1991) 'An experimental study on local behavior of reinforced concrete slabs to missile impact', Nuclear Engineering and Design, 130(2), pp. 121–132.
52. Krauthammer, T. (1998) 'Blast mitigation technologies: Developments and numerical considerations for behavior assessment and design', International Conference on Structures Under Shock and Impact, SUSI, 32, pp. 3–12.
53. Kumar, V., Iqbal, M. A. and Mittal, A. K. (2017) 'Behaviour of Prestressed Concrete under Drop Impact Loading', Procedia Engineering, 173, pp. 403–408.
54. Kumar, V. and Mittal, A. K. (2018) 'Experimental investigation of prestressed and reinforced concrete plates under falling weight impactor', Thin-Walled Structures. Elsevier, 126, pp. 106–116.

55. Lee, K., Han, S. E. and Hong, J.-W. (2013) 'Analysis of impact of large commercial aircraft on a prestressed containment building', Nuclear Engineering and Design. North-Holland, 265, pp. 431–449.
56. Li, J., Hao, H. and Wu, C. (2017) 'Numerical study of precast segmental column under blast loads', Engineering Structures. Elsevier Ltd, 134, pp. 125–137.
57. Li, Q. M., Reid, S. R., Wen, H. M., & Telford, A. R. (2005). Local impact effects of hard missiles on concrete targets. International Journal of Impact Engineering, 32(1–4), 224–284.
58. Li, Q. M., & Reid, S. R. (2004). Development of concrete impact models. Report to Magnox Electric Ltd., Report Reference: MAME. AM/0304/4500288589/JKL, Department of Mechanical, Aerospace and Civil Engineering, UMIST.
59. M.Y.H. Bangash, T. B. (2006). Explosion-Resistant Buildings. In Explosion-Resistant Buildings.
60. Myers, R. H., Montgomery, D. C., & Anderson-Cook, C. M. (1995). Response Surface Methodology: Process and Product Optimization Using Designed Experiments, John Wiley& Sons. *Inc., New York, NY*, 134-174.
61. Nachtsheim, W., & Stangenberg, F. (1983). Interpretation of results of Meppen slab tests—comparison with parametric investigations. Nuclear engineering and design, 75(2), 283-290.
62. Nour, Moataz. (2018). Fire Safety Design System between Performance-Based vs Prescriptive Design-Tools and Challenges.
63. Orbovic, N., Blahoainu, A., Sagals, G., Tarallo, F., Rambach, J. M., Huerta, A., ... & Krutzik, N. (2014). Improving Robustness Assessment Methodologies for Structures Impacted by Missiles (IRIS-2012)-Final Report (No. NEA-CSNI-R--2014-5). Organisation for Economic Co-Operation and Development.
64. Orbovic, N., Tarallo, F., Rambach, J. M., Sagals, G., & Blahoianu, A. (2015). IRIS_2012 OECD/NEA/CSNI benchmark: Numerical simulations of structural impact. Nuclear Engineering and Design, 295(October 2012), 700–715.
65. Priestley, M. J. N. (2000). Performance based seismic design. Bulletin of the New Zealand society for earthquake engineering, 33(3), 325-346.
66. Rajput, A., Jakka, R., Pruthvik, B. M., & Iqbal, M. A. (2016). Experimental Study of Plain and Reinforced Concrete Targets Subjected to Impact Loading. Procedia Engineering, 144, 124–131.

67. Rajput, A., & Iqbal, M. A. (2017). Ballistic performance of plain, reinforced and pre-stressed concrete slabs under normal impact by an ogival-nosed projectile. International Journal of Impact Engineering, 110, 57–71.
68. Ranjan, R., Banerjee, S., Singh, R. K., & Banerji, P. (2014). Local impact effects on concrete target due to missile: An empirical and numerical approach. Annals of Nuclear Energy, 68, 262–275.
69. Reid, S. R., & Wen, H. M. (2001). Predicting penetration, cone cracking, scabbing and perforation of reinforced concrete targets struck by flat-faced projectiles. *UMIST Report. Manchester: University of Manchester Institute of Science and Technology*.
70. Riera, J. D. (1968) 'On the stress analysis of structures subjected to aircraft impact forces', Nuclear Engineering and Design, 8(4), pp. 415–426.
71. Riera, J. D. (1980). A critical reappraisal of nuclear power plant safety against accidental aircraft impact. Nuclear Engineering and Design, 57(1), 193–206.
72. Sagals, G., Orbovic, N., & Blahoianu, A. (2015). Numerical Simulation of Missile Impact on Reinforced Concrete Slabs: Effect of Concrete Pre-stressing.
73. Samuely, F. J., & Hamann, C. W. (1939). Civil protection. Architectural Press.
74. Schwer, L. E. (2016). Modeling Pre and Post Tensioned Concrete. 13th International LS-DYNA Conference, Dynamore, 1–22.
75. Sehgal, B. R. (Ed.). (2011). Nuclear safety in light water reactors: severe accident phenomenology. Academic Press.
76. Sharath, R., Arumugam, D., Dhanasekaran, B., & Subash, T. R. (2017). Numerical Modeling of 'Concrete Response' to High Strain Rate Loadings. 11th European LS-DYNA Conference.
77. Sharma, H. (2012). Performance-based reliability analysis and code calibration for RC column subject to vehicle collision. Texas A&M University.
78. Sharma, H., Hurlebaus, S., & Gardoni, P. (2012). Performance-based response evaluation of reinforced concrete columns subject to vehicle impact. International Journal of Impact Engineering, 43, 52–62.
79. Shih Kwang TAY, Jing Koon POON, Roger CHAN (2016). Modeling Rebar in Reinforced Concrete for ALE Simulations. 14th International LS-DYNA Conference, Dynamore, 1–13.
80. Sugano, T., Tsubota, H., Kasai, Y., Koshika, N., Orui, S., von Riesemann, W. A., Parks, M. B. (1993). Full-scale aircraft impact test for evaluation of impact force. Nuclear Engineering and Design, 140(3), 373–385.

81. Stander, N., & Craig, K. J. (2002, May). Response surface and sensitivity-based optimization in LS-OPT: A benchmark study. In *7th International LS-DYNA Users Conference, Dearborn, MI*
82. Thai, D.-K., & Kim, S.-E. (2017). Numerical simulation of pre-stressed concrete slab subjected to moderate velocity impact loading. Engineering Failure Analysis, 79, 820–835.
83. Thai, D. K., Nguyen, D. L., & Kim, S. E. (2019). Numerical investigation on local damage of proposed RC panels under impact loading. Nuclear Engineering and Design, 341(July 2018), 377–389.
84. U.S. Department of Defense (2008) 'Structures to Resist the Effects of Accidental Explosions - UFC 3-340-02', Structures Congress 2011, (May 2005), p. 1867.
85. Walter, T. A., & Wolde-Tinsae, A. M. (1984). Turbine missile perforation of reinforced concrete. Journal of Structural Engineering, 110(10), 2439-2455.
86. Wen, H. M., & Xian, Y. X. (2015). A unified approach for concrete impact. International Journal of Impact Engineering, 77, 84–96.
87. Whittaker, A., Hamburger, R., & Mahoney, M. (2003, December). Performance-based engineering of buildings for extreme events. In AISC-SINY symposium on resisting blast and progressive collapse (pp. 55-66).
88. Winkelbauer, B. J., Bielenberg, R. W., Reid, J. D., Faller, R. K., Rosenbaugh, S. K., & Schmidt, J. D. (2016). Phase I Evaluation of Selected Concrete Material in LS-DYNA (No. TRP-03-330-16). Midwest Roadside Safety Facility.
89. Wu, Y., Crawford, J. E., & Magallanes, J. M. (2012). Performance of LS-DYNA Concrete Constitutive Models. 12th International LS-DYNA Users Conference, (1), 1–14.
90. Yamawaki, K., Kitamura, H., Tsuneki, Y., Mori, N., & Fukai, S. (2000, January). Introduction of performance-based design. In the 12th World Conference on Earthquake Engineering, Auckland (Vol. 30).
91. Zhang, T., Wu, H., Fang, Q., & Huang, T. (2017). Numerical simulations of nuclear power plant containment subjected to aircraft impact. Nuclear Engineering and Design, 320, 207–221.
92. Zhang, T., Wu, H., Huang, T., Sheng, J. H., Fang, Q., & Zhang, F. J. (2018). Penetration depth of RC panels subjected to the impact of aircraft engine missiles. Nuclear Engineering and Design, 335(March), 44–53.
93. Zhou, L., Li, J., Zhong, H., Lin, G., & Li, Z. (2018). Fragility comparison analysis of CPR1000 PWR containment subjected to internal pressure. Nuclear Engineering and Design, 330(August 2017), 250–264.